Department
of
APPLIED MATHEMATICS

LINEAR AND WEAKLY NONLINEAR PROPAGATION OF A PULSED SOUND BEAM

by

Kjell-Eivind Frøysa

Report No. 90 June 1991

UNIVERSITY OF BERGEN
Bergen, Norway

Department of Mathematics
University of Bergen
5007 Bergen

ISSN-0084-778x

LINEAR AND WEAKLY NONLINEAR PROPAGATION OF A PULSED SOUND BEAM

by

Kjell-Eivind Frøysa

Report No. 90 June 1991

ABSTRACT

The propagation of a pulsed sound beam generated by a real, plane or weakly curved sound source is investigated. The physical effects of diffraction, dissipation and nonlinearity are studied both separately and in combinations within the limitations of the linearized and the weakly nonlinear (quasilinear) version of the Khokhlov-Zabolotskaya-Kutznetsov nonlinear parabolic equation. By the presented model, calculations can be made all the way from the generating sound source and into the dissipative and diffractional farfields. Both numerical and analytical/asymptotical results are presented. Earlier and more simplified models for weakly nonlinear propagation of pulsed sound beams are analyzed and compared to the present model. The validity of the parabolic approximation for a pulsed sound beam is also studied by comparing the results from the linearized model to the results from more accurate linearized models.

Acknowledgements

This report is a slightly revised version of my dissertation for the Dr. Scient. degree in applied mathematics. I hereby want to thank my supervisors Professor Jacqueline Naze Tjøtta and Professor Sigve Tjøtta, for introducing me to a very interesting problem. I also want to thank them for all help and encouragement these years.

Dr. Scient. Jarle Berntsen has given me very useful help on the numerical algorithms used. He also let me use two new numerical integration routines before they were published.

I wish to thank Professor Magne S. Espedal for all the practical help the two first years of my Dr. Scient study, when both my supervisors had a sabbatical leave. The members of the acoustic group at the Department of Mathematics, University of Bergen the last years have made this a nice place to work. I also wish to thank them for many useful acoustical discussions.

My father-in-law, Trygve Guldbrandsen has read through this dissertation, and thereby prevented many orthographical and grammatical errors.

Last, but not least, I want to thank my wife, Kristin for her encouragement, support and patience during the work on this dissertation. I also want to thank the rest of my family and my friends for their interest and support as to this work.

Contents

List of Figures

List of Symbols

Here is a list of the most commonly used symbols in this work:

a	=	Characteristic radius of the source
c_0	=	Ambient sound speed
d	=	Focal distance
D	=	Diffusivity of the sound
$f(\mathbf{x})$	=	Onsource amplitude distribution
$f_1(x)$	=	$= f(\mathbf{x})$ when the source is axisymmetric
$F(\tau)$	=	Time dependency on the source
$F_1(\tau)$	=	Slowly varying envelope function when $F(\tau) = F_1(\tau)\sin\omega_0\tau$
$\tilde{F}(\omega)$	=	$\frac{1}{\sqrt{2\pi}}\int_{-\infty}^{\infty} F(\tau)e^{i\omega\tau}d\omega$, Fourier transform of $F(\tau)$ with respect to τ.
i	=	$\sqrt{-1}$, Imaginary unit
L_0	=	$\frac{2c_0^3}{D\omega_0^2}$, (Fast) Absorption distance
L_s	=	Slow absorption distance related to the characteristic frequency of $F_1(\tau)$
p	=	$p_0 + \epsilon p_1 + \epsilon^2 p_2 + \ldots$, Total pressure
p_0	=	Equilibrium pressure
p_1	=	Linear pressure
p_2	=	Quasilinear pressure
P_2	=	$\beta\rho_0 c_0^2 (\omega_0 a/c_0)^2$, Normalisation factor to p_2 in the figures of chapter 5
r	=	$\sqrt{\mathbf{x}^2 + z^2}$
r_0	=	$\frac{\omega_0 a^2}{2c_0}$, Rayleigh distance
t	=	Time
$U(\tau)$	=	The Heaviside function
v_0	=	Characteristic velocity on the source
$\mathbf{x}$	=	(x_1, x_2), Transverse coordinates
x	=	$\lvert\mathbf{x}\rvert$
x_1	=	Transverse coordinate
x_2	=	Transverse coordinate
z	=	Longitudinal coordinate

β = $1 + \frac{B}{2A}$, where B/A is the nonlinearity parameter of the fluid
$\delta(\tau)$ = The Dirac delta function
ϵ = $\frac{v_0}{c_0}$, Mach number
θ = $\arctan \frac{x}{z}$, Polar angle in the x, z –plane
ρ_0 = Ambient density
τ = $t - \frac{z}{c_0}$, Retarded time
ω = Fourier variable for angular frequency
ω_0 = Fastest characteristic angular frequency of $F(\tau)$

Chapter 1

Introduction

In nature, all sound signals have finite duration. In order to say if such a signal is long or short, we have to define what we mean by a long or a short signal. In most senses, we can find both long and short signals in nature. A signal which is long when considering one specific application, can also be a short signal when we consider other applications. In many applications, the long signals are modelled like an infinite long signal. Especially, it is usual to consider signals which just contain one frequency. Such signals are said to be monochromatic signals. The assumption of monochromatic signals often simplifies the mathematical model greatly. When the signal is so that the monochromatic signal does not predict the sound propagation properly, we have to consider more complex models. In this work, we will look at signals which cannot be described by monochromatic signals, and also in some cases discuss when the monochromatic theory can be used and when it cannot be used. The signals considered in this work will thus be pulsed signals or just pulses. By a pulse, we will mean a sound signal that either has a finite duration, or a sound signal that decays to zero when the time approaches plus and minus infinity.

Sound propagation is a complex interaction between different physical effects which tend to alter the signal in different ways. These effects are for instance diffraction, energy dissipation, nonlinearity, relaxation and dispersion. The study of these effects for a pulsed signal, can often be found from the knowledge of the sound propagation of a monochromatic signal. By using the Fourier analysis, we can find solutions for pulsed signals in this way. This approach can often be a good way to describe a pulsed signal. The approach also gives a physical interpretation of pulsed signals as a superposition of monochromatic signals with different frequencies. If the pulse is very broadbanded, this approach can be both unpractical and time-consuming. This is also the case when strong nonlinearity has to be studied. The generation of different frequencies by the nonlinearity is quite complicated to study in the frequency domain. By some adjustments of the algorithms, it is, however, possible to study pulses by using the frequency domain when strong nonlinearity is included. Despite this, there exist no consistent and simple models for the general case where all the above-mentioned physical effects are included, and both the geometry of the boundary and the medium where the sound propagates, are general.

The motivation for studying such pulsed signals has already been briefly mentioned. To supplement, we can say that pulsed signals have to be studied in many different applications. An area where there is a big activity at the moment, is the medical ap-

plication of destroying kidney stones. When a lithotripter destroys kidney stones, one method is to use a short pulse generated by an electrical spark with high amplitude. It is therefore important to be able to describe the combined effect of nonlinearity, diffraction and dissipation on short sound signals. The geometry of the curved sound source that is used in such litotripters is also very important. Other applications for pulsed signals are for instance seismology, underwater communication and acoustic imaging.

Pulsed sound beams can in some cases be described by the Khokhlov-Zabolotskaya-Kuznetsov (KZK) nonlinear, parabolic equation[1, 2, 3]. This equation describes propagation of sound beams in a homogeneous fluid. The sound beams have to be thin in the sence that they mainly propagate away from the sound source in one direction. This means that far from the sound source, we can find the sound wave basically near the axis indicating the main propagtion direction from the sound source. At propagation directions that are making great angles from this main direction, there is basically no sound present. The KZK-equation accounts consistently for diffraction, dissipation and nonlinearity. It cannot be used everywhere in the space, and neither for all frequencies nor for all geometries of the boundaries. The main approximation that causes these restrictions, is the so-called parabolic approximation that is performed in the derivation of the KZK-equation. For monochromatic and bifrequent sources, Naze Tjøtta and Tjøtta have analysed the validity of the parabolic approximation, both within a linear model[4] and also briefly within a weakly nonlinear model[5]. We will come back to a discussion of the validity of the KZK-equation in chapter 2 and in chapter 4. The KZK-equation has been used in the discussion of many problems of nonlinear acoustics, and especially when the sound generated by the sound source is monochromatic or bifrequent. In recent years it has also been used to describe pulsed signals within a nonlinear model.

In this work, we will study the linear and weakly nonlinear propagation of a pulsed sound beam generated by a plane or a weakly curved sound source. We will use an approximative version of the KZK-equation in this study. Diffraction, dissipation and nonlinearity will be studied within this approximation. We want to study each of these physical effects separately, and also to study the effects on the pulsed signal caused by a combination of these physical effects. The mathematical model is described in more detail in chapter 2.

When comparing the propagation of pulsed signals and of monochromatic signals, we will find that there will be some new effects in the case of pulsed signals compared to monochromatic signals. The absorption due to dissipative effects will for instance act in a different way on the different frequency components present in the pulse, because they will be damped differently. Besides the damping of the amplitude, this leads to a distortion of the pulse. In chapter 3, it is shown within a linear, one-dimensional model that for pulses with a sinusoid which oscillates inside a slowly varying envelope function, there are two different absorption distances which are important. The location of the actual observation point compared to the absorption distances, decides the actual behaviour of the pulsed signal. It is there shown that the pulsed signal at first behaves much like a monochromatic signal. Beyond both absorption distances, it is shown that the actual waveform is strictly dependent on the envelope function of the pulsed signal.

In chapter 4, the effect of diffraction is discussed within a linear, three-dimensional model. Most of the work is done for plane sound sources and in the absence of dissipative effects. The impulse response approach is discussed within the parabolic approximation

and it is there shown how a general pulsed signal can be decomposed in terms which can be interpreted by different geometrical effects. For instance, when we consider a uniform, circular piston, we can decompose the solution on the symmetry axis into one term which comes from the centre of the sound source, and one term which comes from the edge of the source. The impulse response solution is compared to earlier results by Stepanishen[6] and by Naze Tjøtta and Tjøtta[7] where no parabolic approximation is performed. In this way, the validity of the parabolic approximation is briefly studied for pulsed signals. We will see that some of the restrictions on the parabolic approximation when using a monochromatic signal, are also valid in the pulsed case when we interprete the frequencies used in the correct way. Farfield results and beam patterns will also be discussed when we use a pulsed signal. It will then be shown how the sidelodes in the beam pattern gradually disappear when we consider gradually shorter pulses. Focusing sources will then be discussed, and it will be shown how the results for plane sources are directly applicable in a weakly focused model. For instance, we find that the solution in the focal plane when using the focused source, is the same as the farfield solution when a similar unfocused sound source has been used. Finally, the combination of diffraction and absorption is discussed. It will be shown how we can combine the results when only diffraction is considered with the results when only dissipation is considered in order to get results when both effects are present.

The first correction to the linear theory due to nonlinear effects, is called the quasi-linear approximation. This is found by first solving the linearized problem. The solution of this problem then has to be substituted into the nonlinear term of the KZK-equation, and we solve this new problem. In chapter 5, this nonlinear correction is studied. Previous models[8, 9, 10, 11, 12] often treat the absorption in an ad hoc way. Also the diffraction, especially in the linear solution, is treated similarly. This means that the solutions that have been found are not uniform solutions of the KZK-equation. We will see that in some senses, these solutions will be valid far away from the source, when the dissipation has distorted the signal significantly. In this work, a Gaussian onsource amplitude distribution has been chosen because of the simplifications in the computations in this case. The model can be used all the way from the sound source, describes the combined effect of diffraction and dissipation on this signal, and is still valid when the dissipation has damped and distorted the signal. Both asymptotical and numerical results will be shown, and it will be shown by numerical examples that the previous models break down when the pulse is too short, when we are too far from the sound source and when the diffraction and the dissipation are not properly balanced.

Some of the results from this work have earlier been published in Refs. 13 and 14, and some results have been reported in Ref. 15. Besides this, a few of the linear results are direct generalisations of the results in Ref. 16.

Chapter 2

Mathematical and Physical Model

2.1. The KZK-equation

We want to describe the sound propagation from a pulsed, real sound source radiating into a homogenous, dissipative fluid. The amplitude of the sound will be so large that nonlinear effects have to be considered. As a governing equation, we start from the Khokhlov-Zabolotskaya-Kutznetsov (KZK) nonlinear parabolic equation:

$$\left(\nabla_\perp^2 - \frac{2}{c_0}\frac{\partial^2}{\partial\tau\partial z} + \frac{D}{c_0^4}\frac{\partial^3}{\partial\tau^3}\right)p = -\frac{\beta}{\rho_0 c_0^4}\frac{\partial^2}{\partial\tau^2}(p-p_0)^2. \tag{2.1}$$

Here $\nabla_\perp^2 = \frac{\partial^2}{\partial x^2} + \frac{\partial^2}{\partial y^2}$ is the transverse Laplacian, $\tau = t - z/c_0$ the retarded time, p_0, ρ_0 and c_0 the ambient pressure, density and sound speed of the medium respectively, and D the sound diffusivity of the medium. Further, $\beta = 1 + B/(2A)$ where B/A is the nonlinearity parameter of the medium. In Eq. (2.1), it is assumed that the main propagation direction is the positive z-direction and that the sound beam is narrow. This means that $\omega_0 a/c_0 \gg 1$ where ω_0 is a characteristic angular frequency of the sound and a is a characteristic radius of the source. This is referred to as the high ka condition, and means that a parabolic approximation is made. Within this restriction, Eq. (2.1) consistently accounts for diffraction (first term), absorption (third term) and nonlinearity (right hand side term). Eq. (2.1) was first derived by Khokhlov and Zabolotskaya[1] in the absence of absorption. Kutznetsov[2] included absorption in the equation. The derivations were based on slow variations of the shape of the wave both along and orthogonal to the beam axis. Absorption was introduced by linearizing the absorptional terms in the hydrodynamic equations. Naze Tjøtta and Tjøtta[3] later rederived Eq. (2.1) by using the method of multiple scales in the z-direction. They also required that diffraction, absorption and nonlinearity were taken into account in the same asymptotic order. The KZK-equation then appeared as a condition to avoid secularities. Their analysis also showed that the choice of scales made by Khokhlov and Zabolotskaya, was the only possible when all the effects were to be taken into account in the same order of magnitude. It was also shown that the impedance relation for linear plane waves $p = \rho_0 c_0 v_z$, where v_z is the z-component of the velocity of the fluid, can be used when linearizing this model. The similar result in the weakly nonlinear case is discussed in chapter 5.

The KZK-equation is a consequence of the Navier-Stoke's equation, and has therefore a damping due to dissipative effects, which is proportional to the square of the frequency.

This is a good model in fluids. In other media, this absorption law is not acceptable, and one has to adjust the absorption to behave as wanted. In sediments, for instance, there is no general agreement of how the absorption law is, but it seems like a linear dependency of frequency is more widely accepted than a square dependency. In biological tissue, it is usual to model the absorption as proportional to ω^r where r varies from tissue to tissue. The absorption law used in the KZK-equation makes this equation not causal. This effect has to be kept in mind when results are discussed later in this work. We will discuss this non-causality later, when linear propagation is studied more in detail in chapter 3 and 4.

We want to describe the propagation of a pulsed sound beam generated by a plane or weakly curved source. As mentioned above, the linear plane wave impedance relation is valid when our model is linearized. A consequence of this is that we then cannot discriminate between piston sources (where the normal velocity on the source is given), and membrane sources (where the pressure on the source is given). This is one of the reasons why there is a layer close to the source, where the model is not valid. Besides this, in the parabolic approximation, we have neglected a second derivative term with respect to z in the equation. In this way, we have thrown away the regressive waves and have to expect problems close to boundaries. Naze Tjøtta and Tjøtta[4] showed in the linear, monochromatic case, that when the sound is generated by a uniform, circular piston, this layer has a thickness of $\Delta z \approx a(\omega_0 a/c_0)^{1/3}$. We will discuss the validity of the parabolic approximation further in chapter 4.

The KZK-equation has a parabolic nature. We see this by the absence of z – derivatives of orders higher than one. We therefore just need one boundary condition. This is the pressure at $z = 0$ where the plane source embedded in a baffle is located. In the case of a weakly curved source, we assume that the source is located close to the plane $z = 0$. Because of the parabolic approximation, we can approximate the curved source by an equivalent plane source in the $z = 0$ plane. Sommerfeldt's radiation condition which ensures that no waves come back from infinity, is not needed in this case. This condition is also already used in the derivation of the KZK-equation. The boundary condition for the KZK-equation is then:

$$p(z = 0) = p_0 + \rho_0 c_0 v_0 f(\mathbf{x}) F(\tau + \frac{g(\mathbf{x})}{c_0}). \tag{2.2}$$

A derivation and a more complete discussion of this boundary condition for curved sources is found in appendix A. Here, v_0 is a characteristic value of the normal velocity on the source, $f(\mathbf{x})$ is the onsource amplitude distribution over the source, $F(\tau)$ is the time dependency on the source and $g(\mathbf{x})$ is the surface where the source is located. When considering a plane source, $g(\mathbf{x}) = 0$. When the source is a focusing, spherical cap, we can use $g(\mathbf{x}) = \frac{\mathbf{x}^2}{2d}$ where d is the focal distance. By choosing d negative, we get a defocusing, spherical cap, and by letting $d \to \infty$, we get the plane source. In order to verify the boundary condition for the focused or defocused source, we have to require that $|d|$ is of the same asymptotical order as the Rayleigh distance $\omega_0 a^2/2c_0$, or greater.

The boundary condition Eq. (2.2) is assumed separable, and is thus not the most general one. We want, however, just to study separable boundary conditions. Many of the results obtained later in this work, can be transferred directly to the more general boundary condition where $f(\mathbf{x})F(\tau + \frac{g(\mathbf{x})}{c_0})$ is replaced with $h(\mathbf{x}, \tau + \frac{g(\mathbf{x})}{c_0})$.

There is one limitation needed in Eq. (2.2). In the linear, non-dissipative case, this condition can be shown from the equations of hydrodynamics. The z-component of the equation of motion (Euler's equation) with no external forces, is then

$$\rho_0 \frac{\partial v_z}{\partial t} = -\frac{\partial p}{\partial z}. \tag{2.3}$$

In our model, the impedance relation $p = \rho_0 c_0 v_z$ is valid because we at the moment consider a linear model. We now assume that the sound generates a motion in the medium which starts from 0 and which dies out when t is increasing towards infinity. By using the impedance relation and integrating the equation from $-\infty$ to ∞ with respect to t, we get

$$\frac{\partial}{\partial z} \int_{-\infty}^{\infty} p(\mathbf{x}, z, t) dt = 0, \tag{2.4}$$

which means that

$$\int_{-\infty}^{\infty} p(\mathbf{x}, z, t) dt = C(\mathbf{x}). \tag{2.5}$$

To find the function $C(\mathbf{x})$, we consider the behaviour of the pressure when $z \to \infty$. In this case, Sommerfeldt's radiation condition, which is used in the derivation of the KZK-equation, says that $p \to 0$. This means that $C(\mathbf{x}) = 0$. Because Eq. (2.5) is valid also when $z = 0$, we have to require

$$\int_{-\infty}^{\infty} F(\tau) d\tau = 0. \tag{2.6}$$

We have thus shown that in order to be consistent with the parabolic approximation in the linear, non-dissipative case, we have to assume that the time dependency has zero mean value. This result is similar to the result found by Bakhvalov, Zhileikin and Zabolotskaya[17] for a general, periodic onsource time dependency using the KZK-equation.

In the nonlinear case, this condition can be seen from the KZK-equation directly by using a similar approach as the one indicated in Ref. 17. We first define the Fourier transform with respect to τ to be

$$\tilde{F}(\omega) = \frac{1}{\sqrt{2\pi}} \int_{-\infty}^{\infty} F(\tau) e^{i\omega\tau} d\tau. \tag{2.7}$$

We now Fourier transform the KZK-equation Eq. (2.1) and the boundary condition Eq. (2.2) with respect to τ:

$$\left(\nabla_\perp^2 + \frac{2i\omega}{c_0} \frac{\partial}{\partial z} + \frac{Di\omega^3}{c_0^4} \right) \tilde{p} = \frac{\beta\omega^2}{\rho_0 c_0^4 \sqrt{2\pi}} \tilde{p} * \tilde{p},$$
$$\tilde{p}(z = 0) = \rho_0 c_0 v_0 f(\mathbf{x}) \tilde{F}(\omega). \tag{2.8}$$

Here $\tilde{p}$ means the Fourier transform of $p - p_0$ and the asterisk denotes convolution with respect to ω:

$$g(\omega) * h(\omega) = \int_{-\infty}^{\infty} g(\omega_1) h(\omega - \omega_1) d\omega_1. \tag{2.9}$$

Eq.(2.8) should be valid for any ω. We now assume that the equation is not singular at $\omega = 0$, and look at this ω-value:

$$\begin{aligned} \nabla_\perp^2 \tilde{p} &= 0, \\ \tilde{p}(z=0) &= \rho_0 c_0 v_0 f(\mathbf{x}) \tilde{F}(0). \end{aligned} \tag{2.10}$$

This means that when $\omega = 0$, $\tilde{p}$ is a harmonic function with respect to $\mathbf{x}$. When $z = 0$, $\tilde{p}$ is proportional to $f(\mathbf{x})$. Because the source function $f(\mathbf{x})$ does not have to be harmonic, we have to require $\tilde{F}(0) = 0$ in order to be consistent. This is equivalent to Eq. (2.6). This result can also be derived from the time domain version of the KZK-equation. We then integrate the equation and the boundary condition from $-\infty$ ot ∞ with respect to τ. When using that the signal and its derivatives is zero when $\tau = \pm\infty$, we can conclude in the same way as above.

We can also explain this condition physically. The source which generates the sound is vibrating, and after the vibration, it goes back to its original position. In the case of a piston source, this means that the velocity v_p of the piston has to satisfy

$$\int_{-\infty}^{\infty} v_p(\tau) d\tau = 0. \tag{2.11}$$

We have to require a no slip condition for the fluid at the sound source when absorption is accounted for. In the absence of absorption, we must similarly have continuity in normal velocity. In both cases, this means that the normal velocity of the fluid at the piston has zero mean value. In the linear case, this leads to Eq. (2.6). It thus seems like we are limited to consider time dependencies with zero mean value in order to be consistent with the mathematical model and the physics.

We can, however, ask if this condition has to be fulfilled also when the parabolic approximation not is used, and the boundary condition on the source is of the piston type. For a plane source, this means that

$$v_z(z=0) = v_0 f(\mathbf{x}) F(\tau) \tag{2.12}$$

We can then argue in the same way and require that the total displacement of the source is zero. This will lead to the same result as above. Let us now for a moment assume that Eq. (2.6) is not fulfilled. This means, as already mentioned, that the source has another position after the generation of the pulse than it had before the pulse generation. When we calculate the change in position of the piston from before to after the pulse generation, we get, however, a very small value. Assume for instance that

$$\int_{-\infty}^{\infty} F(\tau) d\tau = 1/\omega_0, \tag{2.13}$$

where ω_0 is a characteristic angular frequency of the pulse. This is a realistic estimate of the integral for many pulses. The change in position of the piston is then $\frac{\epsilon\lambda}{2\pi}$ where $\epsilon = v_0/c_0$ is the Mach number, and λ is the wavelength of a wave of the angular frequency ω_0. To see that this displacement can be very small, we look at an example. Consider a 2 MHz sound source in water generating a pulsed signal satisfying Eq. (2.13). If we assume the Mach number to be $\epsilon = 10^{-4}$, which in the monochromatic case means 227 dB relative 1μPa, the change in position will be $1.2 \cdot 10^{-8}$m. This displacement is so small

that it hardly can be observed. For instance, the wavelength of visible light is of the order 10^{-7}m. We are thus talking of displacements of an order less than the wavelength of visible light. Therefore it seems difficult to require Eq. (2.6) when we do not have a parabolic approximation.

We have thus seen that Eq. (2.6) is a consequence of the approximations made in the mathematical model, and not a physical assumption which always has to be fulfilled. In many applications, it is, however, reasonable to expect that this integral is quite small when the sound source is not moving appart from the vibration. The numerical methods which will be used in this work, will still work if there is a zero frequency component in the generated pulse. We can, however, not expect that such a component can be properly described by the parabolic approximation. We will therefore, with one exception, only use pulses where Eq. (2.6) is fulfilled. The exception is $F(\tau) = \delta(\tau)$ when the impulse response is discussed in chapter 4. We will briefly comment this inconsistency in section 4.1 where it appears for the first time.

2.2. Quasilinear Approximation

In this work, the nonlinearity is assumed weak. We therefore use the socalled quasilinear approximation of the KZK-equation. This approximation is based on a straight forward perturbation

$$p = p_0 + \epsilon p_1 + \epsilon^2 p_2 + \cdots. \tag{2.14}$$

By inserting this into the KZK-equation and the boundary condition and solving order by order in ϵ, we get

$$\left(\nabla_\perp^2 - \frac{2}{c_0}\frac{\partial^2}{\partial\tau\partial z} + \frac{D}{c_0^4}\frac{\partial^3}{\partial\tau^3}\right) p_1 = 0, \tag{2.15a}$$

$$p_1(z=0) = \rho_0 c_0^2 f(\mathbf{x}) F(\tau + \frac{\mathbf{x}^2}{2dc_0}), \tag{2.15b}$$

and

$$\left(\nabla_\perp^2 - \frac{2}{c_0}\frac{\partial^2}{\partial\tau\partial z} + \frac{D}{c_0^4}\frac{\partial^3}{\partial\tau^3}\right) p_2 = -\frac{\beta}{\rho_0 c_0^4}\frac{\partial^2}{\partial\tau^2} p_1^2, \tag{2.16a}$$

$$p_2(z=0) = 0 \tag{2.16b}$$

in the two first orders of approximation. p_1 is thus the linear part of the solution, and p_2 is called the quasilinear part. This is the first correction to the linear solution due to nonlinear effects. In this work, nonlinearity will be studied within the quasilinear model. We have also used the boundary condition for spherical caps, and not for a general curved source, because this is the only curved source which will be considered here.

2.3. Integral Solutions

We now want to find the solutions of Eqs. (2.15) and (2.16) as multiple integrals. Of course, there are several ways of writing the solutions. In this section, we just give a general solution, and then we can start from this, and get other representations later when we seek special properties or special cases.

2.3.1. Linear Solution

We now want to solve the linear part, Eq. (2.15). We use the Fourier transform to solve the equation, and the solution is

$$p_1(\mathbf{x},z,\tau)=\frac{\rho_0 c_0}{z(2\pi)^{(3/2)}}\int_{-\infty}^{\infty}(-i\omega)\tilde{F}(\omega)e^{-i\omega\tau-\frac{D\omega^2}{2c_0^3}z}\iint_{-\infty}^{\infty}e^{\frac{i\omega|\mathbf{x}-\mathbf{x}'|^2}{2zc_0}-\frac{i\omega\mathbf{x}'^2}{2dc_0}}f(\mathbf{x}')d\mathbf{x}'d\omega. \tag{2.17}$$

Eq. (2.17) will be the starting point for the analysis of the linear part of the solution.

2.3.2. Quasilinear Solution

It is also possible to obtain an exact solution of the quasilinear part, Eq. (2.16), as a multiple integral. We then substitute Eq. (2.17) into the right hand side of Eq. (2.16), and use the Fourier transform in $\mathbf{x}$ and τ. After some calculations, we get

$$\begin{aligned}p_2=&\frac{\beta\rho_0}{16\pi^3 zc_0}\int_{-\infty}^{\infty}i\omega e^{-i\omega(\tau-\frac{\mathbf{x}^2}{2zc_0})-\frac{D\omega^2}{2c_0^3}z}\int_{-\infty}^{\infty}s(\omega-s)\tilde{F}(s)\tilde{F}(\omega-s)\int_0^z\frac{e^{\frac{Ds(\omega-s)z'}{c_0^3}}}{z'}\times\\&\iiiint_{-\infty}^{\infty}f(\mathbf{x}')f(\mathbf{x}'')\exp\left(-\frac{is\mathbf{x}\cdot\mathbf{x}'+i(\omega-s)\mathbf{x}\cdot\mathbf{x}''}{zc_0}+\right.\\&\frac{is(\omega z(1-\frac{z'}{d})-s(z-z'))\mathbf{x}'^2}{2zz'c_0\omega}+\frac{i(\omega-s)(\omega z(1-\frac{z'}{d})-(\omega-s)(z-z'))\mathbf{x}''^2}{2zz'c_0\omega}-\\&\left.\frac{is(\omega-s)(z-z')\mathbf{x}'\cdot\mathbf{x}''}{zz'c_0\omega}\right)d\mathbf{x}''d\mathbf{x}'dz'dsd\omega.\end{aligned} \tag{2.18}$$

This solution is quite complex, and it is also very difficult to solve numerically. There are other representations possible for the solution. For instance, it is possible to represent it as a sixdouble integral where the on source amplitude distributions are present through their (twodimensional) Fourier transforms. To simplify the numerical calculations, we will, however, concentrate on one special amplitude distribution where it is possible to simplify Eq. (2.18) considerably. This is the special case of a Gaussian amplitude distribution

$$f(\mathbf{x})=\exp(-\frac{\mathbf{x}^2}{a^2}). \tag{2.19}$$

In this case, the integral is reduced to three dimensions, and the numerical problems can be solved. The Gaussian source is just one special source, and cannot alone give total information about the quasilinear solution. In spite of this, it can give much information about the general mechanisms of weakly nonlinear sound propagation. The solution for the Gaussian amplitude distribution is

$$\begin{aligned}p_2=&\frac{\beta\rho_0 c_0}{4\pi}\iint_{-\infty}^{\infty}\int_0^z\omega^2 s(\omega-s)\tilde{F}(s)\tilde{F}(\omega-s)e^{-i\omega\tau-\frac{D\omega^2}{2c_0^3}z}\times\\&\frac{\exp\left(\frac{Ds(\omega-s)}{c_0^3}z'\right)}{s(\omega-s)(i\omega(1-\frac{z}{d})(1-\frac{z'}{d})-\frac{4(z-z')c_0}{a^2})-\frac{2z'c_0\omega}{a^2}(\omega(1-\frac{z}{d})+\frac{2zc_0 i}{a^2})}\times\\&\exp\left[\frac{-i\omega\mathbf{x}^2\left(s(\omega-s)(\frac{2}{a^2}+\frac{i\omega}{2dc_0}(1-\frac{z'}{d}))+\frac{z'\omega}{a^2}(\frac{2c_0 i}{a^2}-\frac{\omega}{d})\right)}{s(\omega-s)(i\omega(1-\frac{z}{d})(1-\frac{z'}{d})-\frac{4(z-z')c_0}{a^2})-\frac{2z'c_0\omega}{a^2}(\omega(1-\frac{z}{d})+\frac{2zc_0 i}{a^2})}\right]dz'dsd\omega.\end{aligned} \tag{2.20}$$

Eq. (2.20) will be the starting point of most of the analysis of the quasilinear part of the solution. We have thus formulated both the linear problem and the quasilinear problem as a multiple integral. These integrals will be studied analytically and asymptotically in the following chapters, and will also be the starting point for the numerical work.

Chapter 3

Linear One-dimensional Solution

In the next two chapters, the solution of the linearized KZK-equation is discussed. We thus consider the following equation:

$$\left(\nabla_\perp^2 - \frac{2}{c_0}\frac{\partial^2}{\partial\tau\partial z} + \frac{D}{c_0^4}\frac{\partial^3}{\partial\tau^3}\right) p_1 = 0, \tag{3.1a}$$

$$p_1(z=0) = \rho_0 c_0^2 f(\mathbf{x}) F(\tau + \frac{\mathbf{x}^2}{2dc_0}). \tag{3.1b}$$

This is the linearized, parabolic approximation. It is important to understand the effects of absorption and diffraction within this frame in order to get a good understanding of the same effects in the quasilinear case. In this chapter, we consider the very simple case where $f(\mathbf{x}) = 1$ and $d = \infty$, that is, the case of a one-dimensional motion. Absorption will then be the only effect altering the shape of the pulse. In chapter 4, we first consider the case of non absorption in order to study the effect of diffraction isolated, and finally, we will combine the results with only diffraction and with only absorption into results valid when both effects are present.

3.1. General theory

In the one-dimensional case, the KZK-equation reduces to the Burgers' equation. In this case, it is assumed that the wave propagation is in the direction of increasing z only. In the linear case, Eq. (3.1) reduces to:

$$\left(\frac{\partial^3}{\partial\tau^3} - \frac{2c_0^3}{D}\frac{\partial^2}{\partial\tau\partial z}\right) p_1 = 0, \tag{3.2a}$$

$$p_1(z=0) = \rho_0 c_0^2 F(\tau), \tag{3.2b}$$

which of course also is the linearized Burgers equation. This equation can be integrated once with respect to τ. When assuming that the pressure is zero at $\tau = -\infty$, we obtain

$$\left(\frac{\partial^2}{\partial\tau^2} - \frac{2c_0^3}{D}\frac{\partial}{\partial z}\right) p_1 = 0, \tag{3.3a}$$

$$p_1(z=0) = \rho_0 c_0^2 F(\tau). \tag{3.3b}$$

This assumption does not violate the lack of causality which was commented in chapter 2, and which will be discussed more in detail here. The time dependency $F(\tau)$ is assumed to decay to zero when $\tau \to -\infty$. This means that even with non-causality present in the model, the solution approaches 0 when τ decreases towards $-\infty$. The non-causality will in this case just give a contribution, which decays like a Gaussian function when $\tau \to -\infty$.

As earlier, this equation can be solved by Fourier transforms. We then get a solution as an integral over the frequency domain:

$$p_1 = \frac{\rho_0 c_0^2}{\sqrt{2\pi}} \int_{-\infty}^{\infty} \tilde{F}(\omega) e^{-\frac{D\omega^2 z}{2c_0^3} - i\omega\tau} d\omega. \tag{3.4}$$

It is also possible to write the solution as an integral over the time domain:

$$p_1 = \frac{\rho_0 c_0^2}{\sqrt{2\pi}} \sqrt{\frac{c_0^3}{Dz}} \int_{-\infty}^{\infty} F(\tau') e^{-\frac{(\tau-\tau')^2 c_0^3}{2zD}} d\tau'. \tag{3.5}$$

In Eq. (3.5) we clearly see the lack of causality in our model. As a special case of this causality, we can demonstrate the appearance of a signal in the medium before the generation of the same signal at the source. Consider for instance a pulseshape $F(\tau)$ that is zero when $|\tau| > T$. The integration will then be from $-T$ to T. However, for any positive z-value this integral will be nonzero for all τ-values (except possibly at isolated τ-points). This illustrates the parabolic nature of this problem.

By looking at Eq. (3.5), we can get a good first idea of how the absorption works in this case. We see that for each τ-value, the solution is a weighted average of the values of $F(\tau)$ in the neighbourhood of the actual τ-value. The distance away from the source (value of z) decides how long this averaging interval is. Often we have a pulse which contains a rapid oscillation inside a slowly varying envelope function. In this case we can expect three different behaviours of the solution depending on the value of z. When the averaging interval is smaller than half a period of the rapid oscillation, we expect the solution to be just slightly modified from the original pulseshape. When the averaging interval is greater than a period but not as long as the whole pulse, we expect a different behaviour. When the averaging interval is greater than the whole pulse, we expect still another behaviour. This leads us to define two different absorption distances, one for the rapid oscillating frequency, and one for the characteristic frequency of the envelope function. This last characteristic distance is not present in a monochromatic theory, while the first one will be the same absorption distance as defined in that theory. We come back to this later.

Eqs. (3.4) and (3.5) are both the exact solution of Eq. (3.3). They are therefore a good starting point when we want to find general properties of the influation of dissipative effects on the pulse.

Before we consider the general time dependency $F(\tau)$, we will study a special case. This result is useful when we are going to test the validity of the forthcoming results. Besides, it is instructive by itself.

3.2. Gaussian pulse

We look at the special time dependency

$$F(\tau) = e^{-\frac{\omega_0^2\tau^2}{n^2}} \sin\omega_0\tau. \tag{3.6}$$

In this case, both Eq. (3.4) and Eq. (3.5) can be evaluated analytically:

$$p_1 = \frac{\rho_0 c_0^2}{\sqrt{1+\frac{2D\omega_0^2 z}{c_0^3 n^2}}} \exp\left(-\frac{D\omega_0^2 z}{2c_0^3(1+\frac{2D\omega_0^2 z}{c_0^3 n^2})} - \frac{\omega_0^2\tau^2}{n^2(1+\frac{2D\omega_0^2 z}{c_0^3 n^2})}\right) \sin\left(\frac{\omega_0\tau}{(1+\frac{2D\omega_0^2 z}{c_0^3 n^2})}\right). \tag{3.7}$$

This expression can be used for a detailed analysis of the effect of absorption. We will in this analysis assume that $n^2/4 \gg 1$. We then see that here are two characteristic z-values. These values can be chosen as $L_0 = \frac{2c_0^3}{D\omega_0^2}$ and $L_s = \frac{c_0^3 n^2}{2D\omega_0^2}$. L_0 is the usual absorption distance for a monochromatic signal of the frequency ω_0, which here is the carrier frequency of the pulsed signal generated at the source. L_s then is the absorption distance for the angular frequency $2\omega_0/n$ which is a characteristic frequency for the envelope function $\exp\left(-\frac{\omega_0^2\tau^2}{n^2}\right)$. We thus call L_0 the fast absorption distance or just the absorption distance because it is related to the fast oscillations at a carrier frequency inside an envelope function. L_s is similary called the slow absorption distance since it is related to the slow characteristic frequency of the envelope function. For short pulses, n is not too large, and L_s is not too much greater than L_0. For longer pulses, however, these two distances are very well separated.

When $z \ll L_s$, the pulse will keep its shape, and will decay like $\exp(-z/L_0)$, just like a monochromatic signal will do. When $z = O(L_s)$, new phenomena occur. We see that the exponential decay more and more will stop, and finally, when $z \gg L_s$, this factor is just $\exp(-n^2/4)$. This means that when n is not too large, the signal can be propagated to much greater distances than a monochromatic signal. We also see that the carrier frequency is lower than ω_0 when $z = O(L_s)$ and that the envelope function is widening out. The lowering of the carrier frequency happens faster than the widening of the envelope function. This means that finally, when $z \gg L_s$, we have a pulse which contains only one oscillation. In order to observe this in an experimental situation, however, we must have a short pulse, so that $\exp(-n^2/4)$ is not too small. This stretching of the pulse will also introduce a decay of the maximum amplitude. This decay is like $1/z^{1/2}$ when $z \gg L_s$. In this region, we also have a decay like $1/z^{1/2}$ from the first factor of the solution. The total decay of the maximum amplitude is therefore $1/z$ when $z \gg L_s$. The stretching of the pulse is easily explained physically by the fact that the highest frequencies all the way are damped away when z is increasing. Because we now have a signal with just one oscillation, and it tends to be more and more lowfrequent, it has to be both stretched out and damped down.

In the numerical examples throughout this work, these Gaussian pulses will be much used. The parameter n is used to get shorter or longer pulses, and figure 3.1 shows the pulses for a selection of n-values.

Now, we will start looking in more details into the propagation of these Gaussian pulses. In Figure 3.2, we see the behaviour of this pulse when $n = 6$ and $n = 12$. We see there clearly that at first, the only effect of the absorption is to reduce the amplitude

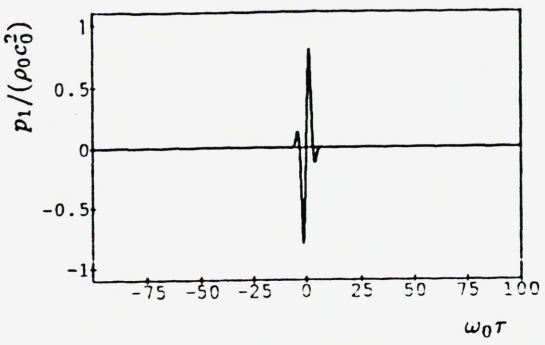

(a)

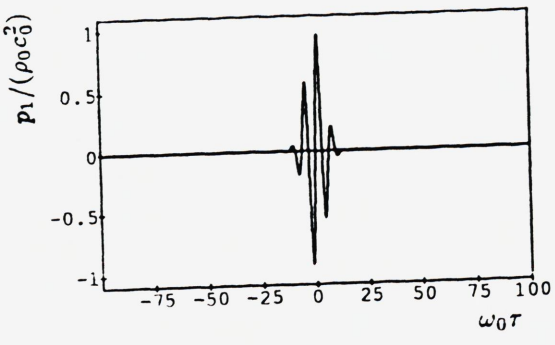

(b)

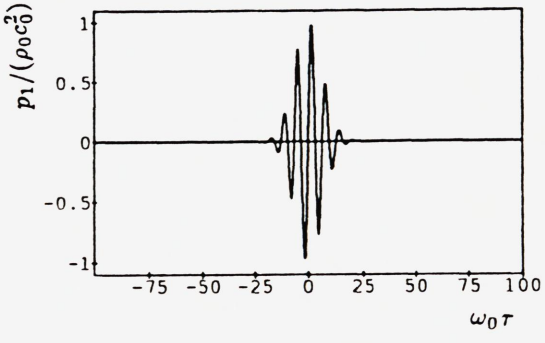

(c)

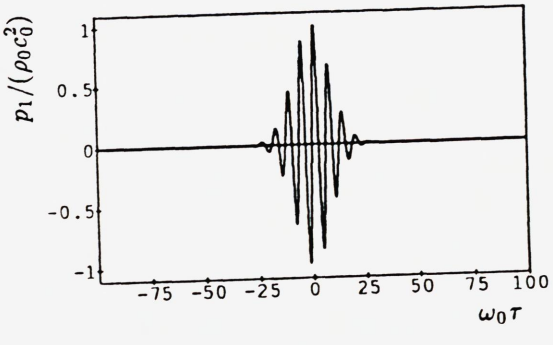

(d)

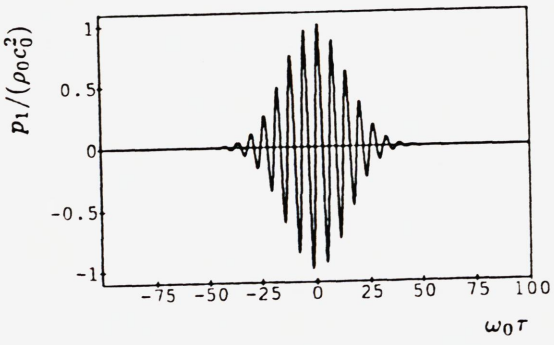

(e)

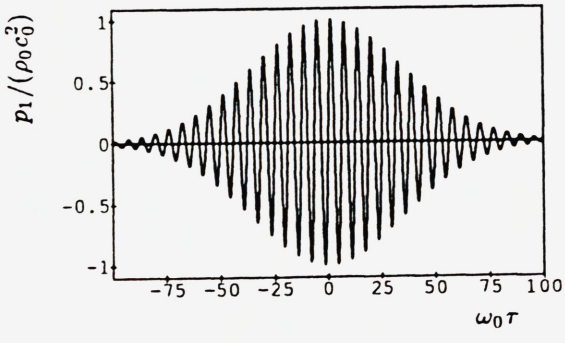

(f)

FIG. 3.1. Gaussian onsource time dependencies, $n = 3$ (a), 6 (b), 9 (c), 12 (d), 20 (e) and 50 (f).

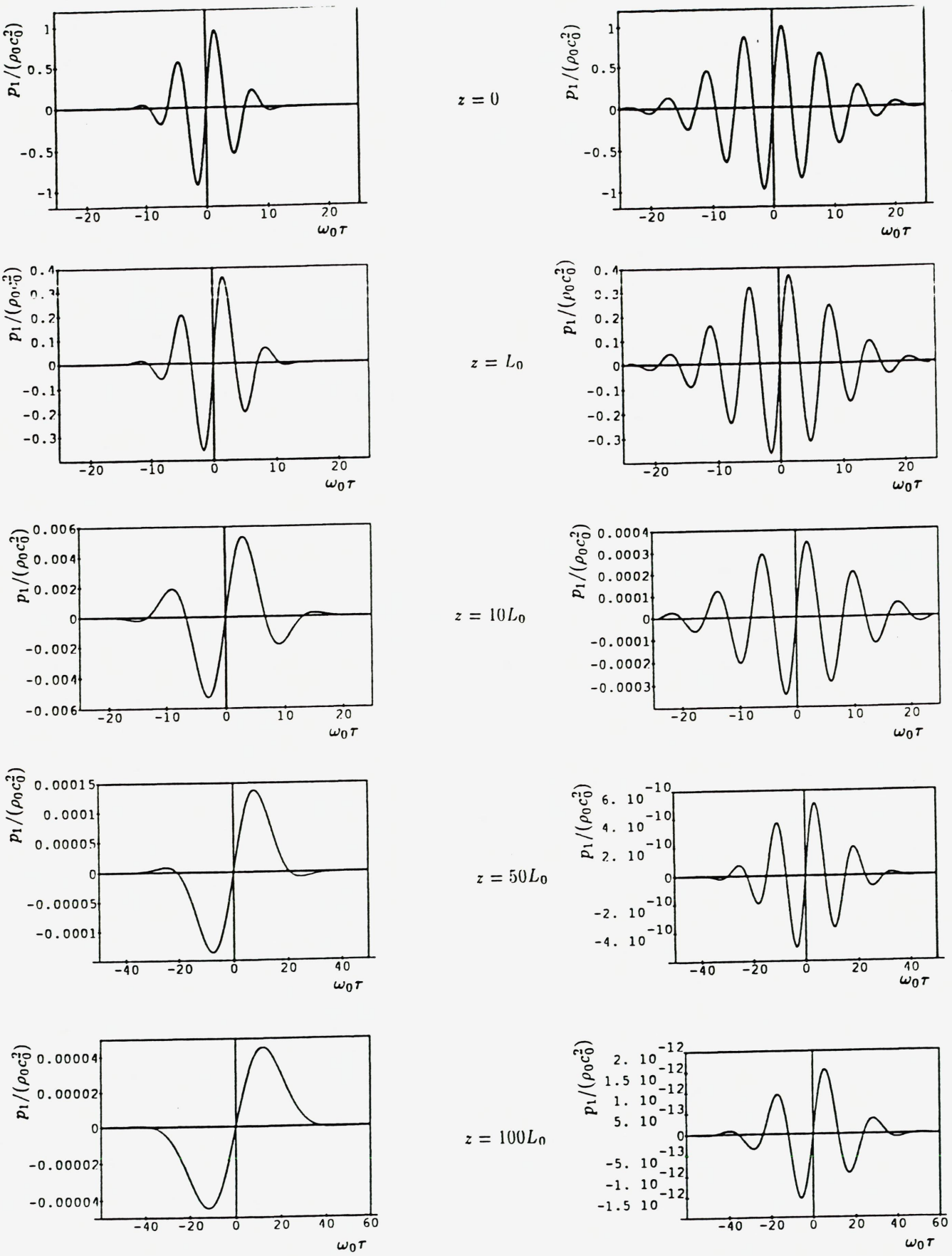

FIG. 3.2. One-dimensional propagation of Gaussian pulses.

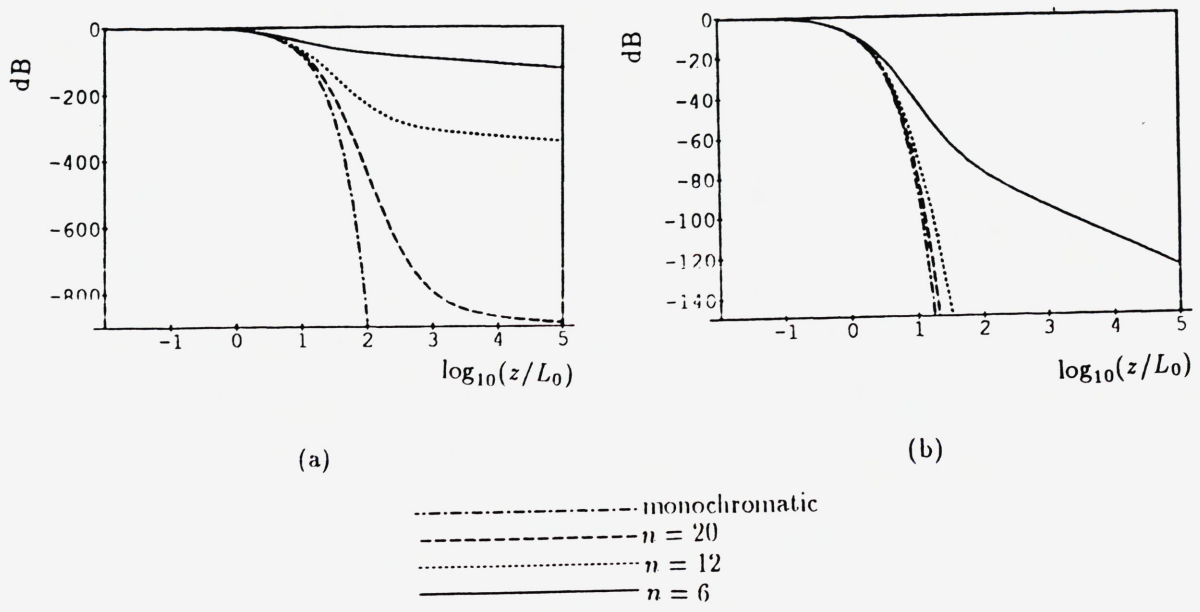

FIG. 3.3. Energy of Gaussian pulses at various distances. (a) and (b) is the same figure, but with different scaling of the vertical axis.

of the pulse according to the monochromatic absorption law. We also see that the demodulation of the pulse towards a signal containing only one oscillation, should be possible to observe when $n = 6$, but when $n = 12$ the amplitude is so small that in a practical situation it is very difficult to detect it. Else, we note that L_s is 4 times larger when $n = 12$ than when $n = 6$. The widening of the envelope function and slowing of the carrier frequency is observed earlier when $n = 6$ than when $n = 12$. This is consistent with the fact that these effects occur when $z = O(L_s)$.

In Figure 3.3 the energy in the pulse is studied for different z-values and different pulse-lengths n. In the parabolic approximation, we have assumed the plane wave impedance relation within the linear approximation. Therefore acoustic energy per time unit is proportional to p_1^2. Define therefore

$$E(z) = \int_{-\infty}^{\infty} p_1^2(z,\tau)d\tau. \tag{3.8}$$

It is possible to evaluate $E(z)$ analytically:

$$E(z) = \frac{\rho_0^2 c_0^4 n}{2\omega_0}\sqrt{\frac{\pi}{2(1+\frac{2D\omega_0^2 z}{c_0^3 n^2})}}\exp\left(-\frac{D\omega_0^2 z}{c_0^3(1+\frac{2D\omega_0^2 z}{c_0^3 n^2})}\right)\left(1-\exp\left(\frac{-n^2}{2(1+\frac{2D\omega_0^2 z}{c_0^3 n^2})}\right)\right). \tag{3.9}$$

In the figure, we plot $10\log_{10}(E(z)/E(0))$ for the different pulse-lengths. We thus get the energy in decibels relative to the energy on the source. We see that at first the pulses decay exponentially. When $z \gg L_s$ the decay is just 15dB when z is multiplied by 10. We see also that the long pulses like $n = 20$ is damped by more than 800dB before they reach this region. When $n = 6$, the 15dB damping is present when the energy is not reduced by more than about 90dB. In this case, the pulse has just lost a little more than 120dB when $z = 10^5 L_0$. This shows that small pulses can be propagated far longer than monochromatic signals or long pulses.

A similar figure where $20\log_{10}(|p_{max}(z)|/|p_{max}(0)|)$ (the maximum absolute value of the amplitude) was plotted, would give a 20dB decay and not 15dB decay when $z \gg L_s$. This shows that when we consider pulsed signals, it is not the same to study the maximum amplitude of the sound at different locations as to study the energy of the sound at the same locations. In the monochromatic case, this difference is not present. We can explain this difference of 5dB by the stretching of the pulse. Even though the amplitude decay indicates 20dB decrease, energy will be present on a larger interval on the τ-axis when z increases. Therefore the decay of energy is less than 20dB.

In the rest of this work, we will often find that the cases $z \ll L_0$ and $z \gg L_0$ have to be studied. We will call these cases the dissipative nearfield and farfield, respectively. This is done because we often will have to distinguish between these near- and farfield, and the near- and farfields generated by the diffraction. When there is no way these terms can be mixed, we will just use the words near- and farfield. It will then be seen from the context whether it is meant the dissipative or the diffractional farfield. The diffractional farfield will be specified better in chaper 4.

3.3. Broadbanded signals

We saw in 3.2 that for a Gaussian pulse, there are two important absorption distances. When we consider phenomena on the scale of the fast absorption length, the pulse behaves much like a monochromatic signal. The only effect of absorption is an exponential damping similar to the monochromatic case. When considering effects on the scale of the slow absorption length, new effects appear. The carrier frequency tends to be slowed down, and the pulse tends to stretch out on the τ-axis. The exponential damping which was present earlier, is now replaced by a 15dB decay when moving from z to $10z$.

We now consider more general pulses of the type

$$F(\tau) = F_1(\tau)\sin\omega_0\tau, \tag{3.10}$$

where $F_1(\tau)$ is a slowly varying envelope function compared to the rapid oscillations from the carrier frequency ω_0. For such pulses, we expect much of the same behaviour as for the Gaussian pulses discussed above. There are, however, also new effects which have to be discussed when considering a general pulse. These effects can be introduced by looking at the Fourier transform of the actual pulses. The Fourier transform of the Gaussian pulse is

$$\tilde{F}(\omega) = \frac{n}{2\sqrt{2}i\omega_0}\left(e^{-(\frac{n(\omega+\omega_0)}{2\omega_0})^2} - e^{-(\frac{n(\omega-\omega_0)}{2\omega_0})^2}\right). \tag{3.11}$$

In Figure 3.4 the Fourier transform of a Gaussian pulse ($n = 12$) and a pulse with a rectangular envelope function is compared. The rectangular pulse is given by

$$F_1(\tau) = \begin{cases} (-1)^n & , |\omega_0\tau| \leq n\pi \\ 0 & , |\omega_0\tau| > n\pi, \end{cases} \tag{3.12}$$

where n is an integer which specifies the number of oscillations in the pulse. The factor $(-1)^n$ is chosen so that the first oscillation of the pulse always starts with a positive

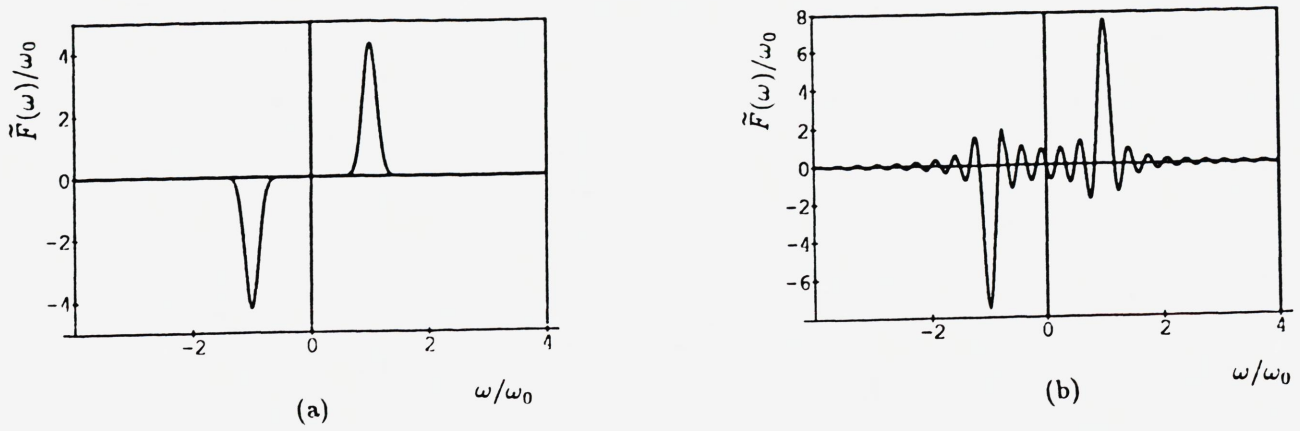

FIG. 3.4. Fourier transform of a Gaussian pulse (a) ($n = 12$) and a rectangular pulse (b) ($n = 6$).

derivative. The Fourier transform of this pulse is

$$\tilde{F}(\omega) = \frac{-2\omega_0 \sin \frac{n\pi\omega}{\omega_0}}{\sqrt{2\pi}i(\omega^2 - \omega_0^2)}. \tag{3.13}$$

We see that the Fourier transforms of the two pulses are quite different. For the Gaussian pulse, the Fourier transform is still Gaussian, and there is very little of the very low frequencies. The Fourier transform of the Gaussian pulse with $n = 6$ is similar, but the lobe is wider, and contains therefore also a little amount of the very low frequencies. This is the reason for the result above where we found that the $n = 6$ pulse is much less damped than the $n = 12$ pulse. The Fourier transform of the rectangular pulse also contains a main lobe similar to the Gaussian, but now there are also several sidelobes which are so strong that they will influence the sound field. This makes the rectangular pulses much more broadbanded than the Gaussian pulses. Of particular interest here, are the sidelobes for very low frequencies. These will contribute to the solution at much larger distances than the main lobe, according to Eq. (3.4), and will therefore dominate the sound field when $z \gg L_0$. We can therefore expect broadbanded pulses to survive much longer than more smallbanded pulses like the Gaussian. The conclusion is that the behaviour of the Fourier transform close to $\omega = 0$ will decide how far the pulse can be propagated.

In real life, the pulses used have finite duration. From the Fourier analysis it is known that such functions often have Fourier transforms containing sidelobes. The size of the sidelobes depends on the smoothness of the pulse in the start- and stopregion. The rectangular pulse has a discontinuous first derivative, and will therefore contain strong sidelobes compared to pulses which are several times continuously differentiable. The pulses used in a realistic situation will be smoother than the rectangular. We therefore

introduce a smoothed version of the rectangular pulse:

$$F_1(\tau) = \begin{cases} (-1)^n & ,0 \le \omega_0\tau < n\pi \\ (-1)^n \left(35\left(\frac{\omega_0\tau-(n+m)\pi}{m\pi}\right)^4 + 84\left(\frac{\omega_0\tau-(n+m)\pi}{m\pi}\right)^5 + \right. & \\ \left. 70\left(\frac{\omega_0\tau-(n+m)\pi}{m\pi}\right)^6 + 20\left(\frac{\omega_0\tau-(n+m)\pi}{m\pi}\right)^7\right) & ,n\pi \le \omega_0\tau \le (n+m)\pi \\ 0 & ,\omega_0\tau > (n+m)\pi \\ F_1(-\tau) & ,\omega_0\tau < 0. \end{cases} \tag{3.14}$$

In this pulse, n is the number of oscillations in the steady state region, i. e. where the envelope function is 1, and m is the number of half oscillations at each end of the pulse, where the pressure builds up to the maximum amplitude, and where it decays to zero after the pulse. The envelope function of this pulse is everywhere three times continuously differentiable, and should be a more reasonable pulse for an experimental situation. There is, however, no ringing after this pulse, which is often produced by real sound sources. The Fourier transform of this pulse is

$$\begin{aligned} \tilde{F}(\omega) = \frac{\omega_0^7}{\sqrt{2\pi\pi^7 m^7 i}} \Bigg\{ & 1680\pi m \left(60\frac{7\omega^6 + 35\omega^4\omega_0^2 + 21\omega^2\omega_0^4 + \omega_0^6}{(\omega^2-\omega_0^2)^7} - \right. \\ & \left. \frac{\pi^2 m^2(5\omega^4 + 10\omega^2\omega_0^2 + \omega_0^4)}{\omega_0^2(\omega^2-\omega_0^2)^5}\right)\left(\sin\frac{\pi n\omega}{\omega_0} + (-1)^m \sin\frac{\pi(n+m)\omega}{\omega_0}\right) \\ & -40320\left(\frac{40\omega\omega_0(\omega^2+\omega_0^2)(\omega^4+6\omega^2\omega_0^2+\omega_0^4)}{(\omega^2-\omega_0^2)^8} - \right. \\ & \left. \frac{\pi^2 m^2\omega(3\omega^4 + 10\omega^2\omega_0^2 + 3\omega_0^4)}{\omega_0(\omega^2-\omega_0^2)^6}\right) \\ & \left(\cos\frac{\pi n\omega}{\omega_0} - (-1)^m\cos\frac{\pi(n+m)\omega}{\omega_0}\right)\Bigg\}. \end{aligned} \tag{3.15}$$

In Figures 3.5 and 3.6, the rectangular pulse Eq. (3.12) and the smoothed rectangular pulse Eq. (3.14) are studied.

We see that in the rectangular pulse, there are some new effects. First, this pulse behaves much like the Gaussian. It simply just has the same exponential decay as a monochromatic wave of the same frequency as the carrier frequency of the pulse. When $z = O(L_0)$, however, we see that new effects start growing from the start and stop points of the pulse ($\tau = \pm n\pi/\omega_0$). The first and last half oscillation of the pulse now does not decay as rapidly as the rest of the pulse, which still has the exponentional decay of the monochromatic wave. When $z \gg L_0$ ($z = 10L_0$), these edge effects are the only thing left of the pulse. The rest of it is negligible compared to them. These half oscillations now also start to become wider. When $z = O(L_s) = O(n^2 L_0)$, they start to overlap, and finally, when $z \gg L_s$, they form a total signal which just includes one single oscillation. Simulations further out would have shown that the maximum amplitude of this oscillation would decay as $1/z$. The pulse would also be widened out, just like the Gaussian. However, the amplitude of the signal is now much greater than for the Gaussian pulses. We thus conclude that the transition from the signal on the source to the old age signal when $z \gg L_s$ is different and simpler for Gaussian pulses compared to more broadbanded signals. The old age signal also has a much higher amplitude for the

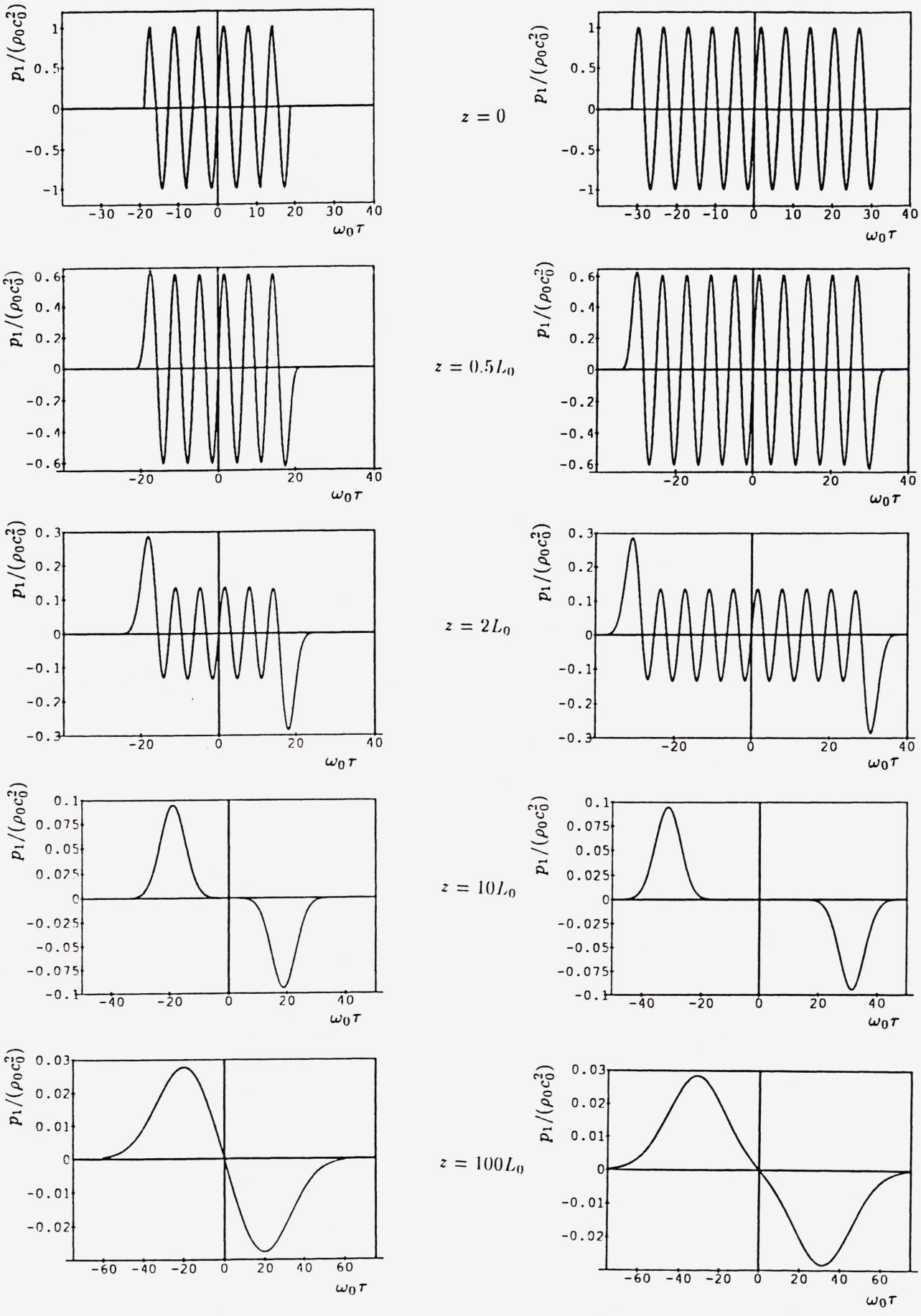

FIG. 3.5. One-dimensional propagation of rectangular pulses.

rectangular pulse than for the Gaussian pulse. This can be explained by the sidelobes of the Fourier transform, which give the very low frequencies around $\omega = 0$ a significant contribution in the sound signal.

When considering the smoothed rectangular pulse in Figure 3.6, we see a similar picture as for the rectangular pulse. This time the transition from $z = O(L_0)$ to $z \gg L_s$, however, is even more complicated. When $m = 4$, the half oscillation at each end which decayed less than the rest of the pulse for the rectangular pulse, has become two or three half oscillations. The steady state part of the pulse, where $F_1(\tau) = \pm 1$, still decays exponentially. The end effects also start to widen out when $z \gg L_0$, and we end up with one single oscillation when $z \gg L_s$. The same thing happens when $m = 8$, but this time even more oscillations survive in the start and stop region. This is not surprising because the end effects now happen on a larger time scale. Other simulations keeping the smoothness at the end (m) fixed, and varying the pulse-length (n), show similar behaviours as above. The only difference is that L_s changes its value so that the final transition to a signal with only one oscillation happens at different distances. When comparing the two pulses in Figure 3.6 at $z = 100L_0$, we see that the amplitude for $m = 8$ is much less than the amplitude for $m = 4$. We have thus seen that the end effects are at least as important as the pulse-length when discussing the pulse shape far outside the fast absorption distance L_0.

In Figure 3.7 we have compared the energy of several rectangular and smoothed rectangular pulses. All pulses have a decay like $1/z^{3/2}$ when $z \gg L_s$ (15dB loss when going from z to $10z$). The total loss of energy of the pulses is critically dependent on m, the smoothness of the pulse in the start and stop regions. A smoother function will have less effect from the start and stop regions, and it is therefore not surprising that the pulses with $m = 8$ have lost more energy when $z \gg L_s$ than the pulses with $m = 4$. The rectangular pulses $m = 0$ have lost still less energy, as expected. Common to all these pulses is that they have lost far less energy than the Gaussian pulses studied above. We also see that when $z \ll L_s$, all pulses decay similarly. This decay is similar to the decay of a monochromatic wave with angular frequency ω_0.

In real life, the difference in the Fourier transform between different pulses is critical. The behaviour of the Fourier transform around $\omega = 0$ determines how far the pulse can propagate. This behaviour is related to the sidelobes of the Fourier transform which in turn are related to the behaviour of the pulse around the turn on and turn off times. Therefore it is very easy to introduce artificial discontinuities when we are going to study a specific, physical situation by this approach. These discontinuities, which can be in the onsource time dependency $F(\tau)$, or in one of the time derivatives of it, can dominate the solution in the dissipative farfield.

3.4. Heuristic Asymptotic Results

In this section, we will try to explain some of the effects of the broadbanded signal from the integral solutions Eqs. (3.4) and (3.5). We will derive some asymptotic results valid when $z \gg L_0$. Here will be no stringent asymptotic treatment, but nevertheless, the results indicate what happens.

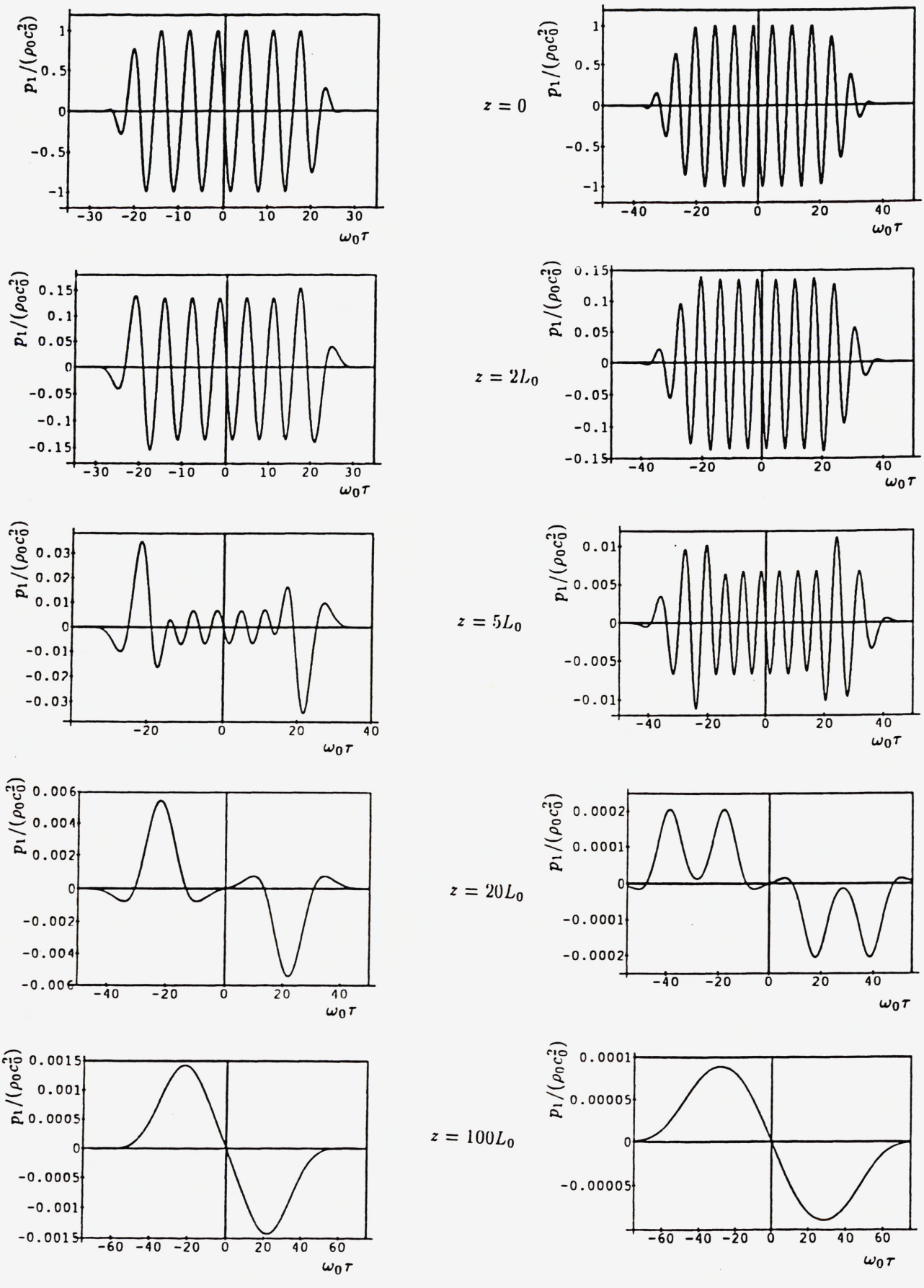

FIG. 3.6. One-dimensional propagation of smoothed rectangular pulses.

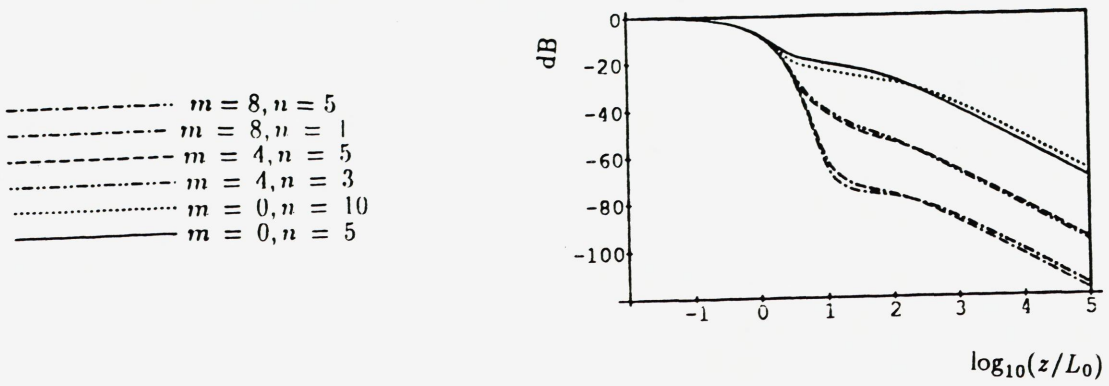

FIG. 3.7. Energy of rectangular and smoothed rectangular pulses at various distances.

3.4.1. General Results when $z \gg L_s$.

We first want to find the final shape of the pulse after all the absorption effects have been present. The analysis start with Eq. (3.4) which we repeat here:

$$p_1 = \frac{\rho_0 c_0^2}{\sqrt{2\pi}} \int_{-\infty}^{\infty} \tilde{F}(\omega) e^{-\frac{D\omega^2 z}{2c_0^3} - i\omega\tau} d\omega. \tag{3.16}$$

When $z \gg L_s$, just a small interval around $\omega = 0$ will contribute in the integral. We therefore expand $\tilde{F}(\omega)$ in a Taylor series around $\omega = 0$:

$$\begin{aligned} \tilde{F}(\omega) &= \tilde{F}(0) + \omega \tilde{F}'(0) + O(\omega^2) \\ &= \omega \tilde{F}'(0) + O(\omega^2), \end{aligned} \tag{3.17}$$

where we have used that $\tilde{F}(0) = 0$ in this model. This is according to Eq. (2.6). By introducing this, we get

$$p_1 \sim \frac{\rho_0 c_0^2 \tilde{F}'(0)}{\sqrt{2\pi}} \int_{-\infty}^{\infty} \omega e^{-\frac{D\omega^2 z}{2c_0^3} - i\omega\tau} d\omega. \tag{3.18}$$

This integral can be evaluated, and gives

$$\begin{aligned} p_1 &\sim -\rho_0 c_0^2 i \tilde{F}'(0) \left(\frac{c_0^3}{Dz}\right)^{3/2} \tau e^{-\frac{\tau^2 c_0^3}{2Dz}} \\ &= \frac{\rho_0 c_0^2}{\sqrt{2\pi}} \int_{-\infty}^{\infty} \tau_1 F(\tau_1) d\tau_1 \left(\frac{c_0^3}{Dz}\right)^{3/2} \tau e^{-\frac{\tau^2 c_0^3}{2Dz}}. \end{aligned} \tag{3.19}$$

This shows that the final pulseshape for a general pulse is one single oscillation. It also describes how this oscillation is widened out when z increases. The maximum absolute value of the amplitude of Eq. (3.19) for a fixed z is given as

$$|p_{1max}| \sim \frac{\rho_0 c_0^2}{\sqrt{2\pi}} \left| \int_{-\infty}^{\infty} \tau_1 F(\tau_1) d\tau_1 \right| \frac{c_0^3}{Dz} e^{-\frac{1}{2}}. \tag{3.20}$$

This value is obtained at the times $\tau = \pm\sqrt{\frac{Dz}{c_0^3}}$. For a general pulse, the decay in the amplitude is thus $1/z$, just as we found for the Gaussian pulse. We can also find the

energy of the signal by considering

$$E(z) = \int_{-\infty}^{\infty} p^2(z,\tau)d\tau. \tag{3.21}$$

We find here

$$E(z) \sim \frac{\rho_0^2 c_0^4}{4\sqrt{\pi}} \left(\int_{-\infty}^{\infty} \tau_1 F(\tau_1) d\tau_1 \right)^2 \left(\frac{c_0^3}{Dz} \right)^{3/2}, \tag{3.22}$$

which explains the 15dB decay found for all pulses above.

When we consider the rectangular pulse in particular, we get

$$\int_{-\infty}^{\infty} \tau_1 F(\tau_1) d\tau_1 = -\frac{2\pi n}{\omega_0^2}. \tag{3.23}$$

Inserting this in the results above, we get

$$p_1 \sim -\frac{\rho_0 c_0^2 n \sqrt{\pi}}{2} \left(\frac{2c_0^3}{D\omega_0^2 z} \right)^{3/2} \omega_0 \tau e^{-\frac{\tau^2 c_0^3}{2Dz}} \tag{3.24}$$

for the final time signal. The maximum amplitude is

$$|p_{1max}| \sim \rho_0 c_0^2 n \sqrt{\frac{\pi}{2}} \frac{2c_0^3}{D\omega_0^2 z} e^{-\frac{1}{2}}, \tag{3.25}$$

and the energy can be written

$$E(z)/E(0) \sim \frac{n\sqrt{\pi}}{2\sqrt{2}} \left(\frac{2c_0^3}{D\omega_0^2 z} \right)^{3/2}. \tag{3.26}$$

This shows that the energy loss relative to the source energy is less for long rectangular pulses than for short rectangular pulses. This is opposite to what is the case for Gaussian pulses. The maximum amplitude for the pulse is also dependent on the pulse-length in the sense that it is greater for a long pulse than for a short pulse. The fact that the amplitude when $z \gg L_s$ is greater for a long pulse than for a short pulse, is again the opposite of the case for a Gaussian pulse.

For the smoothed rectangular pulse, we get

$$\begin{aligned} \int_{-\infty}^{\infty} \tau_1 F(\tau_1) d\tau_1 = & \frac{40320(1-(-1)^m)(40-3\pi^2 m^2)}{\omega_0^2 \pi^7 m^7} \\ & + \frac{1680\pi^2 m(60-\pi^2 m^2)(n+(-1)^m(m+n))}{\omega_0^2 \pi^7 m^7}. \end{aligned} \tag{3.27}$$

When m is an even number, this expression reduces to

$$\int_{-\infty}^{\infty} \tau_1 F(\tau_1) d\tau_1 = \frac{1680(60-\pi^2 m^2)(2n+m)}{\omega_0^2 \pi^5 m^6}, \tag{3.28}$$

and when m is odd, it reduces to

$$\int_{-\infty}^{\infty} \tau_1 F(\tau_1) d\tau_1 = \frac{1680(1920-204\pi^2 m^2+\pi^4 m^4)}{\omega_0^2 \pi^7 m^7}. \tag{3.29}$$

This last expression is interesting because it shows that the amplitude of the pulse when $z \gg L_s$ does not depend on the pulse-length n, but only on the edge effects m when m is an odd number. When m is even, however, the amplitude also depends on n. Numerical results not shown here confirm this result. This again shows how critically dependent the solution is on the behaviour of the pulse in the start and stop region when $z \gg L_s$.

We concentrate on the case when m is even. In that case, we get the time signal as

$$p_1 \sim \frac{\rho_0 c_0^2 420(2n+m)(60-\pi^2 m^2)}{\pi^{11/2} m^6} \left(\frac{2c_0^3}{D\omega_0^2 z}\right)^{3/2} \omega_0 \tau e^{-\frac{\tau^2 c_0^3}{2Dz}}, \tag{3.30}$$

the maximum amplitude as

$$|p_{1max}| \sim \frac{\rho_0 c_0^2 420\sqrt{2}(2n+m)|60-\pi^2 m^2|}{\pi^{11/2} m^6} \frac{2c_0^3}{D\omega_0^2 z} e^{-\frac{1}{2}}, \tag{3.31}$$

and the energy as

$$\begin{aligned} E(z)/E(0) \sim\ & 352800(2n+m)^2(60-m^2\pi^2)^2\left(\frac{2c_0^3}{D\omega_0^2 z}\right)^{3/2} \times \\ & \left(\sqrt{2\pi}\left(\pi^{11} m^{12} n + \frac{521\pi^{11} m^{13}}{1287} + 315\pi^5 m^7 - \frac{1575}{2}\pi^3 m^5 - \right.\right. \\ & \left.\left. 4167450\pi m^3 + \frac{256496625m}{\pi} - \frac{2128376250}{\pi^3 m}\right)\right)^{-1}. \end{aligned} \tag{3.32}$$

All these formulas show that the pulse is more critically dependent on the end effects m than on the pulse-length n. This is also what was shown in numerical examples above.

In Figure 3.8, we have compared the energy loss in dB and the time signal calculated numerically with the asymptotic formulas derived above for the rectangular and the smoothed rectangular pulses. We see that for the shortest pulse ($n = 5$, $m = 0$), the asymptotic formula is valid for smallest z-values. This can be explained by L_s, which is larger when the pulse is longer. We see also that the asymptotic formulas describe the energy loss very well when $z \gg L_s$. The difference in L_s for the different pulses is also illustrated in the plots of the pulse shape in the farfield. We see that for a rectangular ($n = 5$) and a smoothed rectangular ($n = 5, m = 4$) pulse, the asymptotic formula describes the pulse fairly well when $z = 500L_0$, but with the longer pulse $n = 5, m = 8$, it is not equally well described before $z = 2000L_0$.

We conclude this section with two more general remarks. In the derivations above, it is assumed that $\tilde{F}(0) = 0$ but that $\tilde{F}'(0) \neq 0$. The result for instance in Eq. (3.19) is strictly dependent on that. Instead of this, if we assume that $\tilde{F}^{(j)}(0) = 0$ for $j = 0, \ldots, k-1$ and $\tilde{F}^{(k)}(0) \neq 0$, Eq. (3.19) would have become

$$\begin{aligned} p_1 &\sim \rho_0 c_0^2 i^k \tilde{F}^{(k)}(0) \sqrt{\frac{c_0^3}{Dz}} \frac{\partial^k}{\partial \tau^k} e^{-\frac{\tau^2 c_0^3}{2Dz}} \\ &= \frac{\rho_0 c_0^2 (-1)^k}{\sqrt{2\pi}} \sqrt{\frac{c_0^3}{Dz}} \int_{-\infty}^{\infty} \tau_1^k F(\tau_1) d\tau_1 \frac{\partial^k}{\partial \tau^k} e^{-\frac{\tau^2 c_0^3}{2Dz}}. \end{aligned} \tag{3.33}$$

This equation is valid for any positive integer value of k. It is also valid for the case $k = 0$, which is shown inconsistent with the parabolic approximation in the three dimensional model.

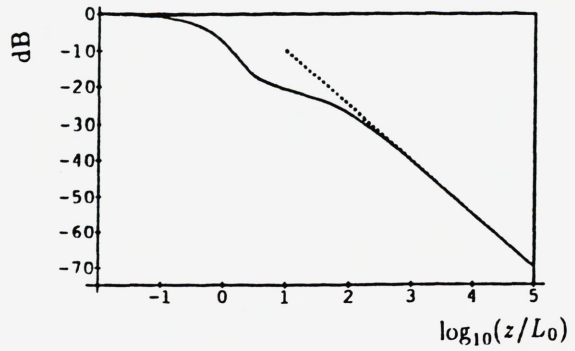

$n = 5,\ m = 0$

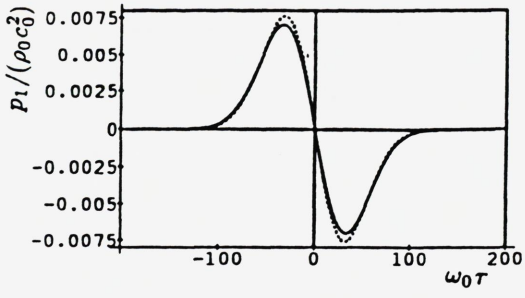

$n = 5,\ m = 0,\ z = 500L_0$

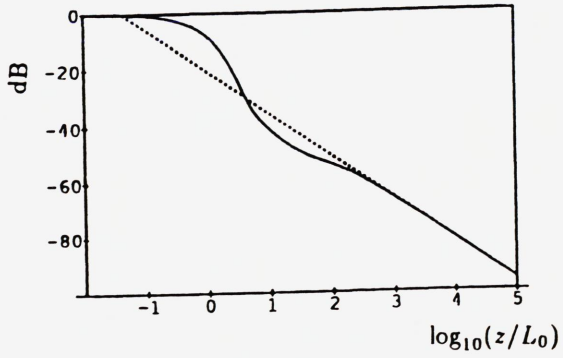

$n = 5,\ m = 4$

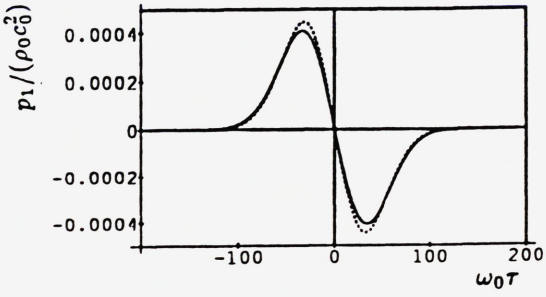

$n = 5,\ m = 4,\ z = 500L_0$

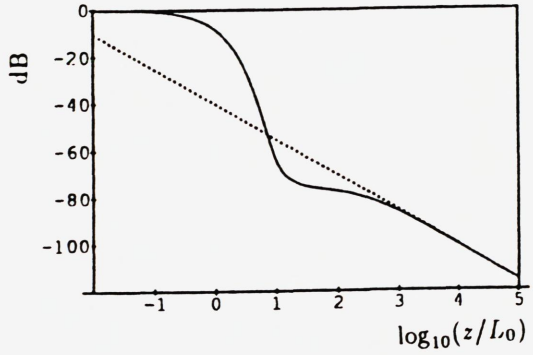

$n = 5,\ m = 8$

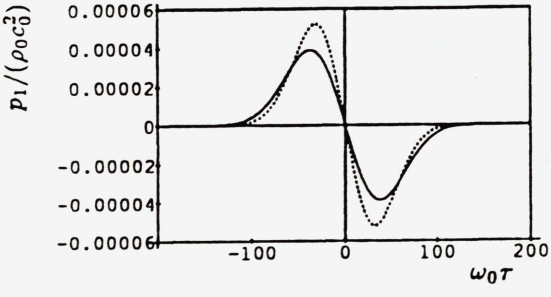

$n = 5,\ m = 8,\ z = 500L_0$

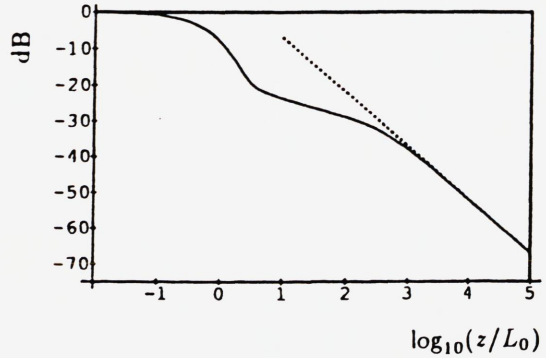

$n = 10,\ m = 0$ (a)

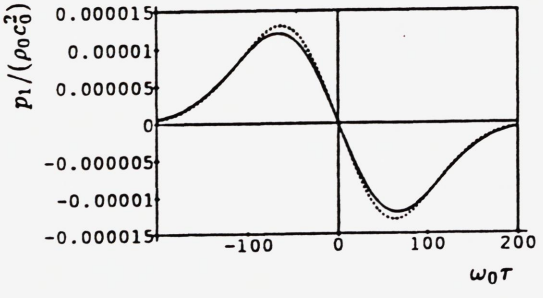

(b) $n = 5,\ m = 8,\ z = 2000L_0$

FIG. 3.8. Comparison between the asymptotic farfield formulas (···) and a numerical solution (—), for energy (a) and waveform (b) when using a rectangular and a smoothed rectangular pulse.

Another interesting discussion is the discussion of different absorption laws. In the model discussed here, the absorption lengths are inversly proportional to the frequency squared. As mentioned earlier, this is a good model for sound waves in water. For waves in other media, like sediments or biological tissue, the absorption law is different. We therefore consider a generalisation of Eq. (3.4), where we have a general frequency law $A(\omega)$ where $A(-\omega) = A(\omega)$:

$$p_1 = \frac{\rho_0 c_0^2}{\sqrt{2\pi}} \int_{-\infty}^{\infty} \tilde{F}(\omega) e^{-A(\omega)z - i\omega\tau} d\omega. \tag{3.34}$$

We now define $a(\tau, z)$ as the inverse Fourier transform of $e^{-A(\omega)z}$:

$$a(\tau, z) = \frac{1}{\sqrt{2\pi}} \int_{-\infty}^{\infty} e^{-A(\omega)z - i\omega\tau} d\tau. \tag{3.35}$$

The pressure can now be written as an integral over the time domain:

$$p_1 = \frac{\rho_0 c_0^2}{\sqrt{2\pi}} \int_{-\infty}^{\infty} F(\tau_1) a(\tau - \tau_1, z) d\tau_1. \tag{3.36}$$

We can proceed like above, and get a generalisation of Eq. (3.33):

$$\begin{aligned} p_1 &= \rho_0 c_0^2 i^k \tilde{F}^{(k)}(0) \frac{\partial^k}{\partial \tau^k} a(\tau, z) \\ &= \frac{\rho_0 c_0^2 (-1)^k}{\sqrt{2\pi}} \int_{-\infty}^{\infty} \tau_1^k F(\tau_1) d\tau_1 \frac{\partial^k}{\partial \tau^k} a(\tau, z). \end{aligned} \tag{3.37}$$

For many absorption laws, the function $a(\tau, z)$ cannot be found analytically. There is, however, one important case where it can be found analytically:

$$A(\omega) = \alpha_0 |\omega|. \tag{3.38}$$

As stated earlier, this is a commonly used absorption law for sound waves in sediments. We now get

$$a(\tau, z) = \frac{2\alpha_0 z}{\sqrt{2\pi}(\alpha_0^2 z^2 + \tau^2)}. \tag{3.39}$$

In this case, Eq. (3.19) which describes the solution for $z \gg L_s$, $\tilde{F}(0) = 0$ and $\tilde{F}'(0) \neq 0$ will be

$$p_1 \sim \frac{\rho_0 c_0^2 2\alpha_0 z \tau}{\pi(\alpha_0^2 z^2 + \tau^2)^2} \int_{-\infty}^{\infty} \tau_1 F(\tau_1) d\tau_1. \tag{3.40}$$

The maximum amplitude of this expression decays like $1/z^2$, unlike Eq. (3.19) where the decay is $1/z$. This shows that the solution in this region is also critically dependent on the absorption law used.

3.4.2. Asymptotic Results for Rectangular Pulses.

We will now derive some more specific farfield asymptotic formulas for the rectangular pulses. These formulas will have a larger region of validity than the formulas derived above.

When considering the Fourier transform of the rectangular pulse, we see that close to $\omega = 0$ it behaves like a sinusoid. The idea is therefore to keep the sinus functions in the Fourier transform and approximate the rest of the Fourier transform. In this way, we should get a solution valid in the farfield, and hopefully a more general solution than the one obtained by linearizing all of $\tilde{F}(\omega)$. The Fourier transform of the rectangular pulse is given by Eq. (3.13) which we repeat here:

$$\tilde{F}(\omega) = \frac{-2\omega_0 \sin \frac{n\pi\omega}{\omega_0}}{\sqrt{2\pi}i(\omega^2 - \omega_0^2)}. \tag{3.41}$$

We now approximate $\tilde{F}(\omega)$ by

$$\tilde{F}(\omega) \sim \frac{2 \sin \frac{n\pi\omega}{\omega_0}}{\sqrt{2\pi}i\omega_0}. \tag{3.42}$$

By introducing this into Eq. (3.4), we get

$$p_1 \sim \frac{\rho_0 c_0^2}{2\pi i \omega_0} \int_{-\infty}^{\infty} \sin\left(\frac{n\pi\omega}{\omega_0}\right) e^{-\frac{D\omega^2 z}{2c_0^3} - i\omega\tau} d\omega, \tag{3.43}$$

which can be evaluated analytically:

$$p_1 \sim \rho_0 c_0^2 \sqrt{\frac{c_0^3}{2\pi D\omega_0^2 z}} \left(e^{-\frac{(\tau + \frac{n\pi}{\omega_0})^2 c_0^3}{2Dz}} - e^{-\frac{(\tau - \frac{n\pi}{\omega_0})^2 c_0^3}{2Dz}} \right). \tag{3.44}$$

We see that this equation describes the half oscillation earlier referred to as start and stop effects. Therefore this equation is expected to be valid when $z \gg L_0$, i.e. when the rapid oscillations following the monochromatic exponential decay, are damped away. The energy loss can be found by squaring and integrating this solution:

$$E(z)/E(0) \sim \frac{1}{\sqrt{2\pi}\pi n} \left(1 - e^{-\frac{\pi^2 n^2 c_0^3}{D\omega_0^2 z}} \right) \sqrt{\frac{2c_0^3}{D\omega_0^2 z}}. \tag{3.45}$$

In Figure 3.9, we compare the asymptotic solution Eq. (3.44) with a numerical solution. We see that both for $n = 6$ and $n = 10$, the solution is quite good when $z = 10L_0$ or greater. It describes the end effects in this region quite well, but does not include the rapid oscillations still present when $z = 5L_0$.

These calculations can also be made in the case of a smoothed rectangular pulse. The difference is that we would have to expand the non-sinusoidal part of the Fourier transform by a Taylor series around $\omega = 0$ and keep terms up to second order in order to get a solution with the same validity as the solution derived above for the rectangular pulse.

3.5. General Asymptotic results

In this section, we will derive some approximative solutions of Eqs. (3.4) and (3.5) by using asymptotic methods.

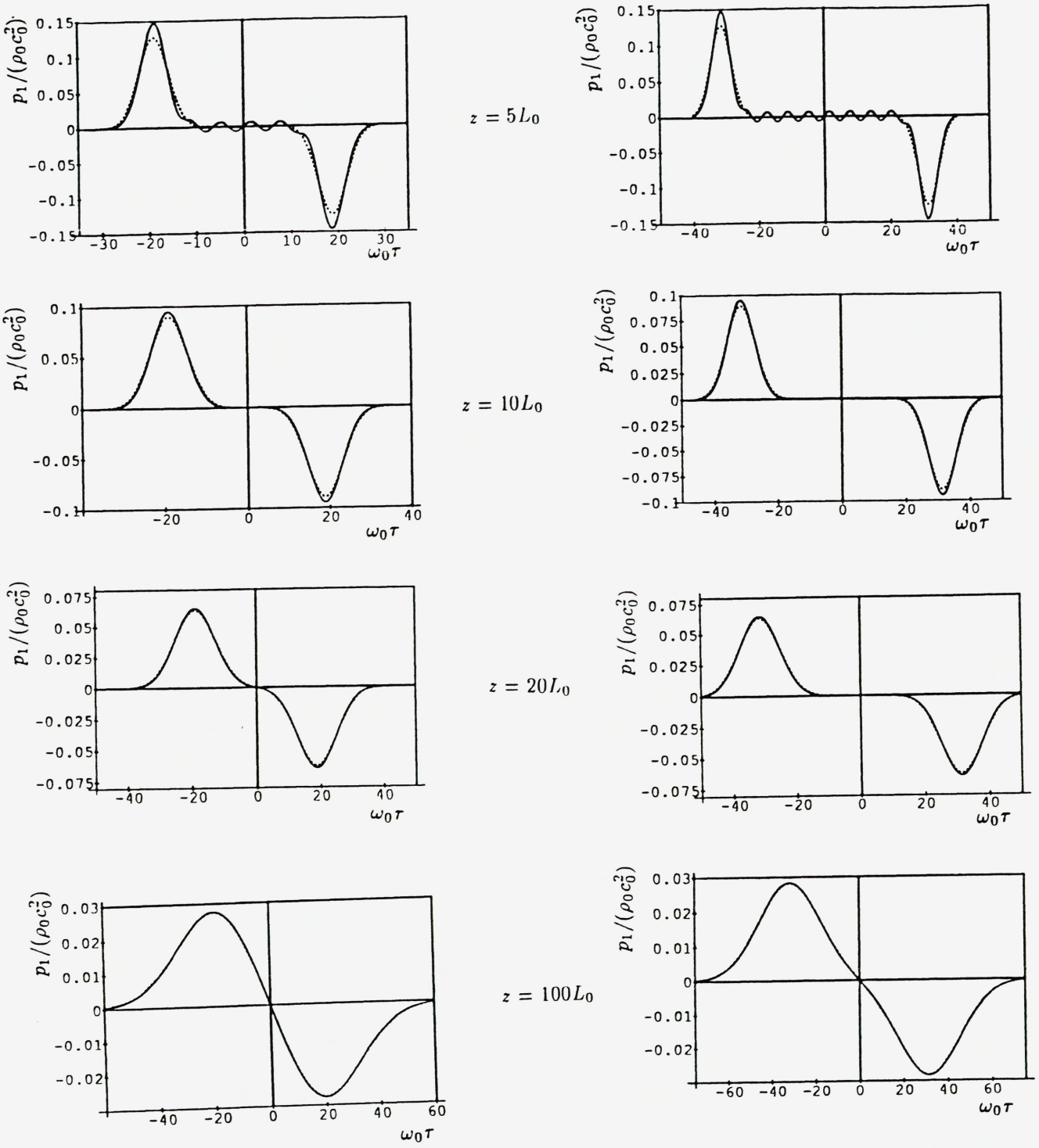

FIG. 3.9. Comparison between the numerical solution (—) and the improved asymptotic farfield formula ($\cdots$) for the waveform when using a rectangular pulse.

3.5.1. Farfield results

First, we want to obtain a solution valid when $z \gg L_s$, and to compare it with the solution found above. This process will be divided into two sub-cases.

One characteristic frequency:

First we will consider the case when we cannot separate out two different characteristic times. This means that the signal cannot be written as an envelope function with a carrier frequency inside. The analysis starts from the frequency domain solution Eq. (3.4). Let ω_0 be the characteristic frequency of the source signal $F(\tau)$. We now introduce the following non-dimensional variables:

$$\begin{aligned} \omega &= \omega_0 \overline{\omega}, \\ \tau &= \overline{\tau}/\omega_0, \\ z &= \tfrac{2c_0^3}{D\omega_0^2}\overline{z} = L_0\overline{z}, \\ \widetilde{F}(\omega) &= \widetilde{\overline{F}}(\overline{\omega})/\omega_0. \end{aligned} \tag{3.46}$$

z is thus scaled to the fast absorption distance, and we want a solution when $\overline{z}$ is large. Now, we have to scale the fraction $\overline{\tau}/\overline{z}$. It seems most physical to assume this fraction bounded (and generally not zero) because we know that the pulse stretches out in this region. We therefore first use this scaling. Eq. (3.4) can then be written:

$$p_1 = \frac{\rho_0 c_0^2}{\sqrt{2\pi}} \int_{-\infty}^{\infty} \widetilde{\overline{F}}(\overline{\omega}) e^{\overline{z}(-\overline{\omega}^2 - i\overline{\omega}\overline{\tau}/\overline{z})} d\overline{\omega}. \tag{3.47}$$

$\widetilde{\overline{F}}$ is now a function that is varying on the scale (1) and the rest of the integrand is a rapidly varying function when $\overline{z} \to \infty$. In order to find asymptotical expansions when $\overline{z} \to \infty$, we can use the method of steepest descent. The saddle point will be at $\overline{\omega} = -i\overline{\tau}/(2\overline{z})$. When assuming $\widetilde{\overline{F}}$ analytical and having proper conditions at infinity, we can deform the contour and obtain the asymptotic expansion:

$$p_1 \sim \rho_0 c_0^2 \left\{ \frac{1}{\sqrt{2\overline{z}}} \widetilde{\overline{F}}(-\frac{i\overline{\tau}}{2\overline{z}}) e^{-\frac{\overline{\tau}^2}{4\overline{z}}} + O((1/\overline{z})^{3/2}) \right\}. \tag{3.48}$$

In dimensional variables Eq. (3.48) will be

$$p_1 \sim \rho_0 c_0^2 \left\{ \sqrt{\frac{c_0^3}{Dz}} \widetilde{F}(-\frac{i\tau c_0^3}{zD}) e^{-\frac{\tau^2 c_0^3}{2Dz}} + O((\frac{2c_0^3}{D\omega_0^2 z})^{3/2}) \right\}. \tag{3.49}$$

We see that all pulses will be damped like $1/\sqrt{z}$ in this region. Besides this damping, we see that the Fourier transform may contain factors that together with the exponential factor reduce the amplitude of the signal. By Taylor expanding the Fourier transform term around 0, we get the general solutions derived in section 3.4.1. Eq. (3.49) can thus be seen as a generalisation of Eq. (3.19) to also cover pulses where $\widetilde{F}'(0) = 0$ or alternatively as a generalisation of Eq. (3.33).

Eq. (3.48) was derived under the assumption that $\overline{\tau}/\overline{z}$ is finite when $\overline{z} \to \infty$. If we scale this fraction to approach zero instead, we must take the factor $e^{-i\overline{\omega}\overline{\tau}}$ out of the rapidly varying part of the integrand. By using the method of steepest descent in this case, we obtain Eq. (3.48) with $\overline{\tau} = 0$. Thus we see that the first scaling of $\overline{\tau}/\overline{z}$ leads to a result that is more general. Finally, if we let $\overline{\tau}/\overline{z} \to \infty$ when $\overline{z} \to \infty$ we get a solution that is growing when $\overline{z}$ is growing, which is clearly unphysical. This is understandable when we see what this scaling means physically.

It is also possible to derive Eq. (3.49) by using the time domain solution Eq. (3.5). We then use the same scalings as above and the theory in chapter 4.6 in Bleistein and Handelsman[18] about small parameter expansions of integrals. In order to obtain Eq. (3.49) in this way, we have to assume either that $\overline{F}(\overline{\tau})$ has finite support or that $\overline{F}(\overline{\tau}) = o(\exp(-|\overline{\tau}|))$ when $|\overline{\tau}| \to \infty$. This is no great physical restriction since the signals used in real situations always can be assumed to have finite support.

Two characteristic frequencies:

The other sub-case to be considered is the case where the source signal contains two characteristic frequencies. We call the fast frequency ω_0 and the slow frequency γ. We also introduce the parameter $n = \omega_0/\gamma$. A large n thus says that this is a long pulse in the sense that it contains many oscillations inside a slowly varying envelope function, and a small n similarly indicates a short pulse in the same sense. It is convenient to write

$$F(\tau) = F_1(\tau)e^{i\omega_0\tau}, \tag{3.50}$$

where $F_1(\tau)$ is the slowly varying envelope function. We can get physically acceptable results by taking real or imaginary part of this expression, and eventually require that the mean value in time of the resulting pulse is zero. The Fourier transforms of these functions are connected in the following way:

$$\tilde{F}(\omega) = \tilde{F}_1(\omega + \omega_0). \tag{3.51}$$

By introducing this into Eq. (3.4) and making the substitution $\omega' = \omega + \omega_0$, we get

$$p_1 = \frac{\rho_0 c_0^2}{\sqrt{2\pi}} e^{-\frac{D\omega_0^2 z}{2c_0^3} + i\omega_0\tau} \int_{-\infty}^{\infty} \tilde{F}_1(\omega') e^{-\frac{D\omega'^2 z}{2c_0^3} + \frac{D\omega_0\omega' z}{c_0^3} - i\omega'\tau} d\omega'. \tag{3.52}$$

The main contribution to $\tilde{F}_1(\omega')$ is now around $\omega' = 0$ with a bandwith of $\omega_0/n = \gamma$. To proceed, we have to introduce new non-dimensional variables with the important thing in mind that now the frequency γ is the important characteristic frequency in the integral. We thus introduce the following variables:

$$\begin{aligned} \omega' &= (\omega_0/n)\overline{\omega}_1, \\ \tau &= (n/\omega_0)\overline{\tau}_1, \\ z &= \frac{2c_0^3 n^2}{D\omega_0^2}\overline{z}_1 = L_s\overline{z}_1, \\ \tilde{F}_1(\omega') &= (n/\omega_0)\tilde{\overline{F}}_1(\overline{\omega}_1). \end{aligned} \tag{3.53}$$

In these variables, Eq. (3.52) can be written

$$p_1 = \frac{\rho_0 c_0^2}{\sqrt{2\pi}} e^{-n^2\overline{z}_1 + in\overline{\tau}_1} \int_{-\infty}^{\infty} \widetilde{\overline{F}}_1(\overline{\omega}_1) e^{-\overline{\omega}_1^2\overline{z}_1 + 2n\overline{\omega}_1\overline{z}_1 - i\overline{\omega}_1\overline{\tau}_1} d\overline{\omega}_1. \tag{3.54}$$

Again we assume that $\overline{\tau}_1/\overline{z}_1$ is bounded (of order one) as $\overline{z}_1 \to \infty$. The argumentation for this is the same as above, and the results with other scalings are similar to the results obtained above. We therefore write Eq. (3.54) in this way:

$$p_1 = \frac{\rho_0 c_0^2}{\sqrt{2\pi}} e^{-n^2\overline{z}_1 + in\overline{\tau}_1} \int_{-\infty}^{\infty} \widetilde{\overline{F}}_1(\overline{\omega}_1) e^{\overline{z}_1(-\overline{\omega}_1^2 + 2n\overline{\omega}_1 - i\overline{\omega}_1\overline{\tau}_1/\overline{z}_1)} d\overline{\omega}_1. \tag{3.55}$$

Now, we are looking for asymptotic expansions valid when $\overline{z}_1 \to \infty$. With the above-mentioned scaling of $\overline{\tau}_1/\overline{z}_1$, we have an integrand where $\widetilde{\overline{F}}_1$ is varying on the scale (1) and the other factors are varying rapidly. We can thus use the method of steepest descent if we require $\widetilde{\overline{F}}_1$ to be analytical and to decrease properly at infinity:

$$p_1 \sim \rho_0 c_0^2 \left\{ \frac{1}{\sqrt{2\overline{z}_1}} e^{-\frac{\overline{\tau}_1^2}{4\overline{z}_1}} \widetilde{\overline{F}}_1(n - \frac{i\overline{\tau}_1}{2\overline{z}_1}) + O((1/\overline{z}_1)^{3/2}) \right\}. \tag{3.56}$$

In dimensional variables, this is the same as Eq. (3.49) except that the error now is $O((\frac{2c_0^3 n^2}{D\omega_0^2 z})^{3/2})$. That means that z has to be chosen much greater than the slow absorption distances L_s if we want to justify the use of Eq. (3.49). It is also possible to derive this result from the time domain solution Eq. (3.5) just like above.

We can now ask why we had to consider this last sub-case at all. Why not just do the first step and let that include both sub-cases? Then the solution should also have a greater validity region in this last sub-case, than we found above. The reason is that when we used the method of steepest descent in the first sub-case Eq. (3.47), we assumed that $\widetilde{\overline{F}}$ is varying on the scale (1). When we have two characteristic frequencies, this is not correct any longer. The main contribution to $\widetilde{\overline{F}}$ is still around ± 1, but we have a bandwith of $\overline{\omega} = 1/n$ which will be the fastest scale that $\widetilde{\overline{F}}$ is varying according to. We therefore have to scale ω like above in order to use the method of steepest descent.

We now insert the Gaussian pulse Eq. (3.6) into Eq. (3.49):

$$p_1 \sim \frac{\rho_0 c_0^2}{\sqrt{\frac{2zD\omega_0^2}{c_0^3 n^2}}} e^{-n^2/4} e^{-\frac{\tau^2 c_0^3}{2Dz}(1 - \frac{c_0^3 n^2}{2zD\omega_0^2})} \sin\left(\omega_0 \tau / (\frac{2zD\omega_0^2}{c_0^3 n^2})\right). \tag{3.57}$$

This can also be obtained from the exact solution Eq. (3.7) by expanding the exponents and denomonator in powers of $1/z$ and keeping one or two terms in each case. A look at the two formulas shows that this last formula is valid when z is large compared to the slow absorption distance. This is precisely what could be expected from the analysis above.

3.5.2. Nearfield results

We now want to obtain a solution valid within the slow absorption distance. Again we will start from the frequency domain solution. The non-dimensional variables Eq. (3.53)

are chosen, and we end up with Eq. (3.54). Here we write that equation like

$$p_1 = \frac{\rho_0 c_0^2}{\sqrt{2\pi}} e^{-n^2\overline{z}_1 + in\overline{\tau}_1} \int_{-\infty}^{\infty} \widetilde{\overline{F}}_1(\overline{\omega}_1) e^{2n\overline{z}_1\overline{\omega}_1 - i\overline{\omega}_1\overline{\tau}_1} e^{-\overline{\omega}_1^2\overline{z}_1} d\overline{\omega}_1. \tag{3.58}$$

We now want an asymptotic expression valid for small $\overline{z}_1$-values. We assume, however, that $n\overline{z}_1$ remains finite. In order to get the situation $1 \gg \overline{z}_1 = O(1/n)$ that is suggested here, we have to assume n large, i.e. a long pulse. In physical variables, this means $\frac{2c_0^3 n^2}{D\omega_0^2} \gg z = O(\frac{2c_0^3 n}{D\omega_0^2})$. With this assumption, the last factor in the integrand of Eq. (3.58) will be slowly varying, while the rest of the integrand will vary on the scale (1) and faster. We can thus use the theory of expansion of integrals containing a small parameter again. In this way, we get:

$$p_1 \sim \frac{\rho_0 c_0^2}{\sqrt{2\pi}} \left\{ e^{-n^2\overline{z}_1 + in\overline{\tau}_1} \int_{-\infty}^{\infty} \widetilde{\overline{F}}_1(\overline{\omega}_1) e^{-i\overline{\omega}_1(\overline{\tau}_1 + 2n\overline{z}_1 i)} d\overline{\omega}_1 + O(\overline{z}_1) \right\}. \tag{3.59}$$

This expression can be evaluated:

$$p_1 \sim \rho_0 c_0^2 \left\{ e^{-n^2\overline{z}_1} \overline{F}_1(\overline{\tau}_1 + 2in\overline{z}_1) e^{in\overline{\tau}_1} + O(\overline{z}_1) \right\}. \tag{3.60}$$

In order to justify Eq. (3.60), we have to require that $\widetilde{\overline{F}}_1(\overline{\omega}_1)$ has finite support or that it decays faster than exponentially when $|\overline{\omega}_1| \to \infty$. In physically variables, Eq. (3.60) will be

$$p_1 \sim \rho_0 c_0^2 \left\{ e^{-\frac{D\omega_0^2 z}{2c_0^3}} F_1(\tau + \frac{i\omega_0 z D}{c_0^3}) e^{i\omega_0\tau} + O(\frac{D\omega_0^2 z}{2c_0^3 n^2}) \right\}. \tag{3.61}$$

We now just note that Eq. (3.61) also can be derived by using the time domain formulation and the method of steepest descent.

By following the analysis above strictly, we find that Eq. (3.61) is just valid between the fast and the slow absorption distance. By inserting a Gaussian pulse in that equation, we get

$$p_1 \sim \rho_0 c_0^2 e^{-\frac{D\omega_0^2 z}{2c_0^3}(1 - \frac{2D\omega_0^2 z}{c_0^3 n^2})} e^{-\frac{\omega_0^2\tau^2}{n^2}} \sin\left(\omega_0\tau(1 - \frac{2D\omega_0^2 z}{c_0^3 n^2})\right). \tag{3.62}$$

Thus we see that for a Gaussian pulse, the solution is valid all the way from the source and until we approach the slow absorption distance.

Now, how interesting is Eq. (3.61)? In order to use the method of steepest descent in the time domain formulation, we have to assume that the envelope function $F_1(\tau)$ is an entire function (or at least that it is analytical except at isolated poles and then look at the contributions from the residues). It is difficult to avoid this assumption because we want to evaluate $F_1(\tau + \frac{i\omega_0 z D}{c_0^3})$ which has to be given a useful value. An alternative way to compute this expression, is to go through the Fourier Transform. This is what we did when we derived Eq. (3.61). However, it doesn't seem like this way of computing $F_1(\tau + \frac{i\omega_0 z D}{c_0^3})$ gives so much, since the integral we must solve when going through the Fourier transform often will be divergent when applied to an F_1 that is not analytical. An example of this is to let F_1 be a stepfunction. This means that it can be difficult to use the solution Eq. (3.61) for many pulseshapes, for instance when we have an envelope function with finite support. A method to avoid this difficulty, is to find

an entire function that it almost such a function for the interesting τ-values. For the stepfunction which is 1 when $|\tau| < 1$ and 0 elsewhere, we can among other functions use $\exp(-\tau^{2m})$ where m is a positive integer which is chosen large enough. An alternative to this, can be just to neglect the imaginary part of the argument of F. In this way, we have to expect that the expression breaks down a little bit before the expression above. We see, however, that the expression obtained in this way has the exponential damping that is expected in the nearfield.

Summing up, we have derived two asymptotic formulas for one-dimensional, pulsed sound propagation. Beyond the slow absorption distance we got

$$p_1 \sim \rho_0 c_0^2 \sqrt{\frac{c_0^3}{Dz}} \tilde{F}(-\frac{i\tau c_0^3}{zD}) e^{-\frac{\tau^2 c_0^3}{2Dz}}. \tag{3.63}$$

The validity of this formula is ensured by requiring that $F(\tau)$ has finite support or decays more rapidly than exponentially as $|\tau| \to \infty$. It is also assumed that z/τ remains finite when $z \to \infty$. Within the slow absorption distance, we got

$$p_1 \sim \rho_0 c_0^2 e^{-\frac{\omega_0^2 zD}{2c_0^3}} F_1(\tau + \frac{i\omega_0 zD}{c_0^3}) e^{i\omega_0 \tau}, \tag{3.64}$$

when we assumed that $F(\tau) = F_1(\tau) e^{i\omega_0 \tau}$. In order to use this formula, we have to require an entire (analytical everywhere) $F(\tau)$ which decays fast at infinity. Alternatively, we can require that $\tilde{F}(\omega)$ has finite support or decays more rapidly than exponentially as $|\omega| \to \infty$. The ratio z/τ is then assumed to go to zero when $z \to 0$.

3.6. General Remarks

We have now discussed the one-dimensional propagation of a pulsed signal. One of the conclusions was that when z is of the order of the slow absorption distance ($z = O(L_s)$) or greater, the signal is strictly dependent on the actual pulse generated. The important thing is the smoothness of the envelope function, or alternatively, the behaviour of $\tilde{F}(\omega)$ when $\omega \approx 0$. In real life, the signals often must be expected to be narrowbanded in the sense that it (almost) contains no such low frequencies. Then, in the farfield the signal is damped by the exponential factor $\exp(-\frac{D\omega_1^2 z}{2c_0^3})$ where ω_1 is the smallest characteristic frequency present in the signal. This is the case for instance for long Gaussian signals. The 20dB decay of amplitude when z is increased by a factor of 10, then does not show up until the whole signal is damped so much that it in practice totally has been damped away.

It is now natural to ask why so much space is used on a sub-case which is perhaps of no direct physical interest. One reason for this is that these results in some cases will be directly applicable also in the linear, threedimensional case. It is therefore important to understand the dissipative effects especially in the dissipative nearfield, and also in the dissipative farfield. Besides this and the academical interest, we will find that in the quasilinear solution discussed in chapter 5, lowfrequent signals will be generated. Also we will see that in the dissipative farfield, we often can assume that they propagate linearly. Therefore, the analysis for $z \gg L_0$ above is applicable when we want to explain some phenomena in the quasilinear solution.

Chapter 4

Linear Three-dimensional Solution

In this chapter, we will study the linear, three-dimensional sound propagation. In literature, there are many works on this topic, and much is known about it. We will first neglect the dissipative effects and study the diffraction isolated. The study is first for a plane source. Focusing effects will then be built into the results. Afterwards, we will study the combination of diffraction and dissipation. We will then try to combine the results from chapter 3 with the results obtained here.

In the study of the effects of diffraction in the pulsed sound propagation, there are several ways to proceed. We have chosen first to use the impulse response approach. The advantage of this is that we can get a good qualitative understanding of the mechanisms in this way. We are also able to discuss the validity of the parabolic approximation in the pulsed case when we use this approach.

4.1. Impulse Response

Consider now

$$\left(\nabla_\perp^2 - \frac{2}{c_0}\frac{\partial^2}{\partial\tau\partial z}\right) p_1 = 0,$$
$$p_1(z=0) = \rho_0 c_0^2 f(\mathbf{x})\delta(\tau), \tag{4.1}$$

where $\delta(\tau)$ is the Dirac delta function. The solution of this problem will be denoted p_δ. Once we have found p_δ, we can find the solution for a general time dependency $F(\tau)$ through the convolution

$$p_1(\mathbf{x}, z, \tau) = \int_{-\infty}^{\infty} p_\delta(\mathbf{x}, z, \tau_1) F(\tau - \tau_1) d\tau_1. \tag{4.2}$$

As stated in chapter 2, the time dependency used here is not consistent with the parabolic approximation. Anyway, we can do the calculations and get reasonable results from it. We can also show that the waveform obtained when convolving the impulse response with the actual onsource time dependency, is the correct solution of the parabolic equation. Therefore we will use the impulse response even if it actually corresponds to an inconsistent situation.

The impulse response p_δ can now be found from the general solution of the linear parabolic equation Eq. (2.17) by inserting $\widetilde{F}(\omega) = 1/\sqrt{2\pi}$:

$$p_\delta(\mathbf{x}, z, \tau) = \frac{\rho_0 c_0}{4\pi^2 z} \int_{-\infty}^{\infty} (-i\omega) e^{-i\omega\tau} \iint_{-\infty}^{\infty} e^{\frac{i\omega|\mathbf{x}-\mathbf{x}'|^2}{2zc_0}} f(\mathbf{x}') d\mathbf{x}' d\omega. \tag{4.3}$$

It is now possible to evaluate the ω-integral:

$$\begin{aligned} p_\delta &= \frac{\rho_0 c_0}{2\pi z} \frac{\partial}{\partial \tau} \iint_{-\infty}^{\infty} \delta(\tau - \frac{|\mathbf{x}-\mathbf{x}'|^2}{2zc_0}) f(\mathbf{x}') d\mathbf{x}' \\ &= \frac{\rho_0 c_0}{2\pi z} \iint_{-\infty}^{\infty} \delta'(\tau - \frac{|\mathbf{x}-\mathbf{x}'|^2}{2zc_0}) f(\mathbf{x}') d\mathbf{x}'. \end{aligned} \tag{4.4}$$

Eq. (4.4) is a good starting point for analysing the impulse response from a general, plane source which radiates into a non-dissipative, homogeneous medium.

4.1.1. Axisymmetric Source

We now assume that the source is axisymmetric, i. e. $f(\mathbf{x}) = f_1(x)$ where $x = |\mathbf{x}|$. This simplifies the integrals above. We will first look at the solution on the acoustical axis, i.e. when $x = 0$. Eq. (4.4) then simplifies into

$$p_\delta = \frac{\rho_0 c_0}{z} \frac{\partial}{\partial \tau} \int_0^{\infty} f_1(x') \delta(\tau - \frac{x'^2}{2zc_0}) x' dx'. \tag{4.5}$$

According to chapter 8 in Jones[19], it is valid to make the substitution $s = \frac{x'^2}{2zc_0}$. We are then able to evalute the integral, and finally we get

$$p_\delta = \rho_0 c_0^2 \left\{ \delta(\tau) f_1(0) + U(\tau) \sqrt{\frac{zc_0}{2\tau}} f_1'(\sqrt{2zc_0\tau}) + \Delta\delta(\tau - \frac{a^2}{2zc_0}) \right\}, \tag{4.6}$$

where $U(\tau)$ is the Heaviside function which is 0 for negative τ-values and 1 for positive t-values. It is assumed that $f_1(x)$ is continuous except at the edge of the source ($x = a$). Δ is the jump of the function $f_1(x)$ at this point. We can account for a source with more than one discontinuity by just adding one term of this type for each discontinuity. The result is therefore quite general.

The physical meaning of Eq. (4.6) is discussed by Naze Tjøtta and Tjøtta[7], and in the case of a uniform source by Stepanishen[6]. They considered the case where there was no parabolic approximation. In order to see that physical interpretation, we first consider the uniform, circular source:

$$f_1(x) = \begin{cases} 1 \ , \ x \leq a \\ 0 \ , \ x > a. \end{cases} \tag{4.7}$$

Then $f_1'(x) = 0$ and $\Delta = -1$. The impulse response is now

$$p_\delta = \rho_0 c_0^2 \left(\delta(\tau) - \delta(\tau - \frac{a^2}{2zc_0}) \right). \tag{4.8}$$

This result was also obtained and discussed by Daltveit[20] by a more direct approach. When we look at the arrival times, we see that the first term is the contribution from the centre of the source. The arrival time of the second term indicates that it comes from the edge of the source. Because of the parabolic approximation, this arrival time is different from the physical one. This is discussed in more detail in section 4.2. By convolving the impulse response with a real pulse $F(\tau)$, we find that there is one signal coming from the centre of the source, and one signal coming from the edge of the source. We refer to the first pulse as the main contribution and to the second pulse as the replica pulse. The main contribution is equal to the signal on the source and the replica pulse is the negative of this signal. More generally, we see that there is one replica pulse for each discontinuity in radial direction of the source $f_1(x)$. When $f_1'(x) \neq 0$, there is also a wake present in the signal. Both the wake and the replica pulse(s) move faster in z-direction than the main contribution. However, the main contribution is always in front of them. For a more detailed study of these effects, we refer to Naze Tjøtta and Tjøtta[7].

Consider now the solution when $x > 0$, that is, outside the acoustical axis. We then start with Eq. (4.3) which now can be simplified further. We get

$$p_\delta = \frac{\rho_0 c_0}{2\pi z}\frac{\partial}{\partial \tau}\int_{-\infty}^{\infty} e^{-i\omega\tau}\int_0^{\infty} e^{\frac{i\omega}{2zc_0}(x^2+x'^2)} J_0\left(\frac{\omega x x'}{zc_0}\right) f_1(x') x' dx' d\omega. \tag{4.9}$$

The ω-integral is basically the Fourier transform of the Bessel function J_0. This can be found in Ref. 21. Finally we get

$$p_\delta = \frac{\rho_0 c_0^2}{\pi}\frac{\partial}{\partial \tau}\left\{U(\tau)\int_{-2x\sqrt{2zc_0\tau}}^{2x\sqrt{2zc_0\tau}} \frac{f_1(\sqrt{v+x^2+2zc_0\tau})dv}{\sqrt{8x^2zc_0\tau - v^2}}\right\}. \tag{4.10}$$

We will not discuss Eq. (4.10) in general, but instead study two specific axisymmetric sources in more detail. These sources, the uniform source mentioned above, and the Gaussian source, are kind of opposite sources. By this it is meant that the uniform source has a discontinuity which generates a replica pulse on the acoustical axis. There is no wake generated there. The Gaussian source is, on the other hand, very smooth. There are no replica pulses present there, and the wake is generated by a very smooth source. We thus have discussed two limiting cases when we have discussed these two sources. Many axisymmetric sources used in a practical situation can be seen as a source somewhere in between these two sources.

The impulse response from the uniform piston is found also outside the acoustical axis by Stepanishen[6] when there is no parabolic approximation. We introduce the uniform piston in Eq. (4.10). The resulting integral can be evaluated, and we thus solve the impulse response problem for a uniform source in the parabolic approximation.

When $x < a$, we get:

$$p_\delta = \rho_0 c_0^2 \left(\delta(\tau) + \Phi_\delta\right), \tag{4.11a}$$

where

$$\Phi_\delta = \begin{cases} \frac{-(2zc_0\tau + a^2 - x^2)}{2\pi\tau\sqrt{8x^2zc_0\tau - (2zc_0\tau - a^2 + x^2)^2}}, & \frac{(x-a)^2}{2zc_0} < \tau < \frac{(x+a)^2}{2zc_0} \\ 0, & \text{elsewhere.} \end{cases} \tag{4.11b}$$

When $x = a$, we get

$$p_\delta = \rho_0 c_0^2 \left((1/2)\delta(\tau) + \Phi_\delta\right), \tag{4.12a}$$

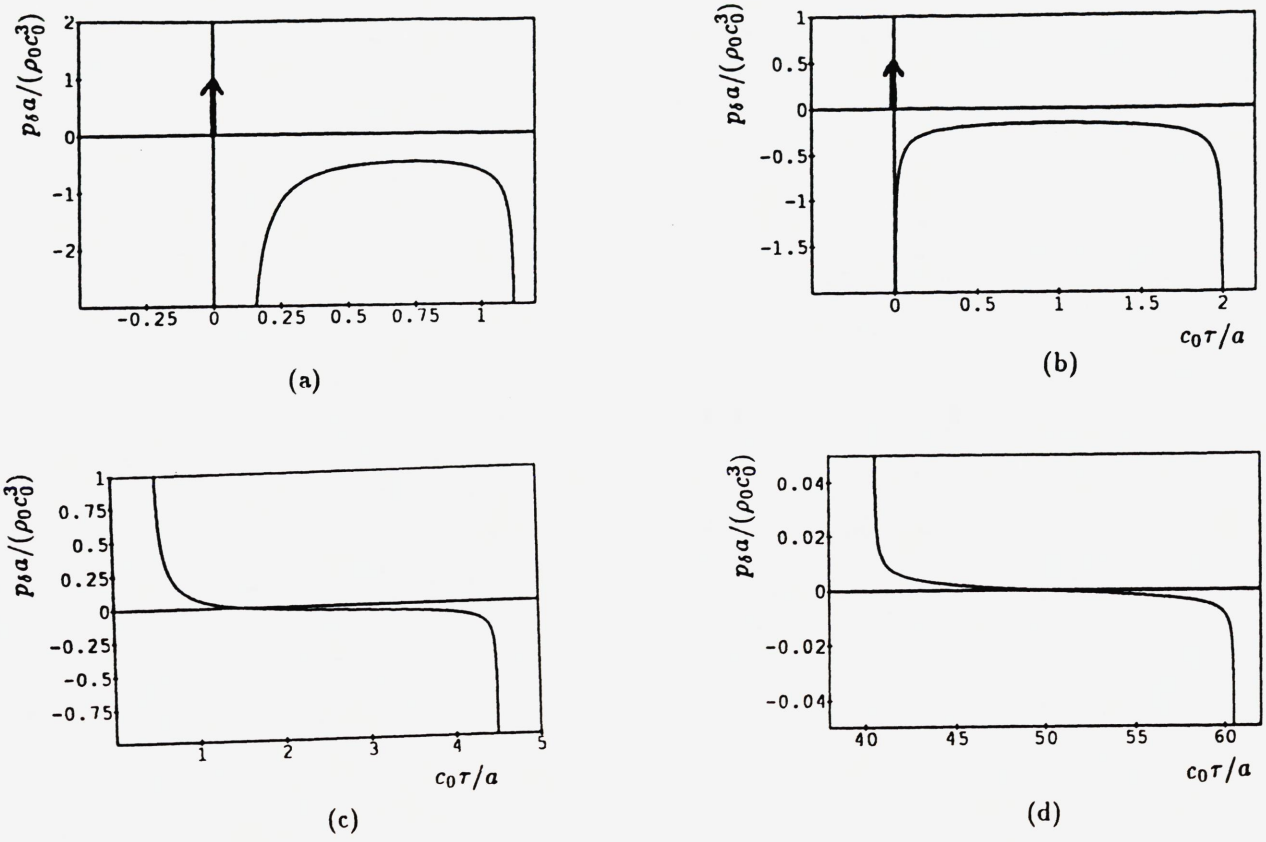

FIG. 4.1. Impulse response from a uniform, circular source. $z = a$, $x = 0.5a$ (a), $x = a$ (b), $x = 2a$ (c) and $x = 10a$ (d).

where

$$\Phi_\delta = \begin{cases} -\frac{1}{\pi}\sqrt{\frac{zc_0}{8\tau a^2 - 4zc_0\tau^2}} & , 0 < \tau < \frac{2a^2}{zc_0} \\ 0 & , \text{elsewhere.} \end{cases} \tag{4.12b}$$

When $x > a$, we get

$$p_\delta = \rho_0 c_0^2 \Phi_\delta, \tag{4.13a}$$

where

$$\Phi_\delta = \begin{cases} \frac{-(2zc_0\tau + a^2 - x^2)}{2\pi\tau\sqrt{8x^2zc_0\tau - (2zc_0\tau - a^2 + x^2)^2}} & , \frac{(x-a)^2}{2zc_0} < \tau < \frac{(x+a)^2}{2zc_0} \\ 0 & , \text{elsewhere.} \end{cases} \tag{4.13b}$$

Eqs. (4.11),(4.12) and (4.13) give a qualitatively good understanding of the pulsed sound propagation. In Figure 4.1, the impulse response is plotted in the different cases. We see that as long as the observation point is ahead of the piston ($x < a$), we first will get a pulse similar to the pulse on the source. This is the same as the main contribution on the acoustical axis. The replica pulse which was present on the acoustical axis, is now replaced by a wake. This wake is for a small x just a smeared version of the replica pulse. However, the larger x is, the more dominant is this smearing. The delta function representing the replica pulse on the acoustical axis, more and more splits up into two negative peaks when x is increasing. This indicates that when x increases, we get the superposition of two smeared versions of the replica pulse.

The case $x > a$ is often more interesting from an experimental point of view than the $x < a$ case. Now we see that the main contribution is gone. This is not surprising because we no longer are just in front of the source. When we look at the first and the

last arrival time of the signal, we find that within the parabolic approximation, these are the arrival times for the signal generated at $t = 0$ at the nearest and the furthest point of the source respectively. Physically this seems very reasonable. We also see that the impulse response now has a large positive peak at the earliest arrival point, and a large negative peak at the latest arrival point. This indicates that for a general pulse, the signal will consist of one smeared version of the original pulse located on the τ-axis at the arrival time from the nearest edge of the piston, and a similar pulse at the arrival point from the furthest edge of the piston. This second pulse has opposite sign compared to the first one. Whether these pulses overlap or not, is decided by the length of the two pulses and the difference between the two arrival times.

We will also consider the impulse response from the Gaussian source. We then again start with Eq. (4.10), and use the Gaussian source Eq. (2.19). After the substitution $u = v/(a^2)$, we get the following integral:

$$p_\delta = \frac{\rho_0 c_0^2}{\pi} e^{-(\frac{x}{a})^2} \frac{\partial}{\partial \tau} \left\{ U(\tau) e^{-\frac{2zc_0\tau}{a^2}} \int_{-\frac{2x\sqrt{2zc_0\tau}}{a^2}}^{\frac{2x\sqrt{2zc_0\tau}}{a^2}} \frac{e^{-u}du}{\sqrt{(\frac{2x\sqrt{2zc_0\tau}}{a^2})^2 - u^2}} \right\}. \tag{4.14}$$

This integral can be evaluated. Consider the integral representation of the modified Bessel function $I_0(z)$ (for example page 571 in Ref.22):

$$I_0(z) = \frac{1}{\pi} \int_0^\pi e^{z\cos t} dt. \tag{4.15}$$

By the substitution $u = -z\cos t$, this integral will be

$$I_0(z) = \frac{1}{\pi} \int_{-z}^{z} \frac{e^{-u}du}{\sqrt{z^2 - u^2}}. \tag{4.16}$$

By using this result, we find that the impulse response from a Gaussian source is

$$p_\delta = \rho_0 c_0^2 e^{-(\frac{x}{a})^2} \left\{ \delta(\tau) + U(\tau) \frac{\partial}{\partial \tau} \left[e^{-\frac{2zc_0\tau}{a^2}} I_0(\frac{2x\sqrt{2zc_0\tau}}{a^2}) \right] \right\}. \tag{4.17}$$

On the acoustical axis, this shows, in agreement with Eq. (4.6), that the signal consists of the main contribution, and a wake generated by the non-uniformness of the Gaussian source. Most of the wake contribution in the impulse response is when $\tau < \frac{a^2}{2zc_0}$. When we leave the acoustical axis, we see from figure 4.2 that the wake changes its nature. We see that the wake more and more dominates the main contribution. The main contribution will now not come from the centre of the source, but from the point on the source closest to the observation point. The arrival times of the most important parts of the wake, are around the arrival time from the signal generated at the centre of the source. This is in agreement with the physics where we have to assume that most of the sound is generated in the region of the source where $x \lesssim a$. The actual shape of the wake will change when we go far outside the acoustical axis. Close to the source, we see that it looks much like the negative of a smeared version of the generated pulse. Later on, we see that the wake contribution in the impulse response will have one whole cycle. Therefore it will look more like the negative of a smeared version of the time derivative of the generated pulse. How dominant this smearing is, depends on the actual observation point.

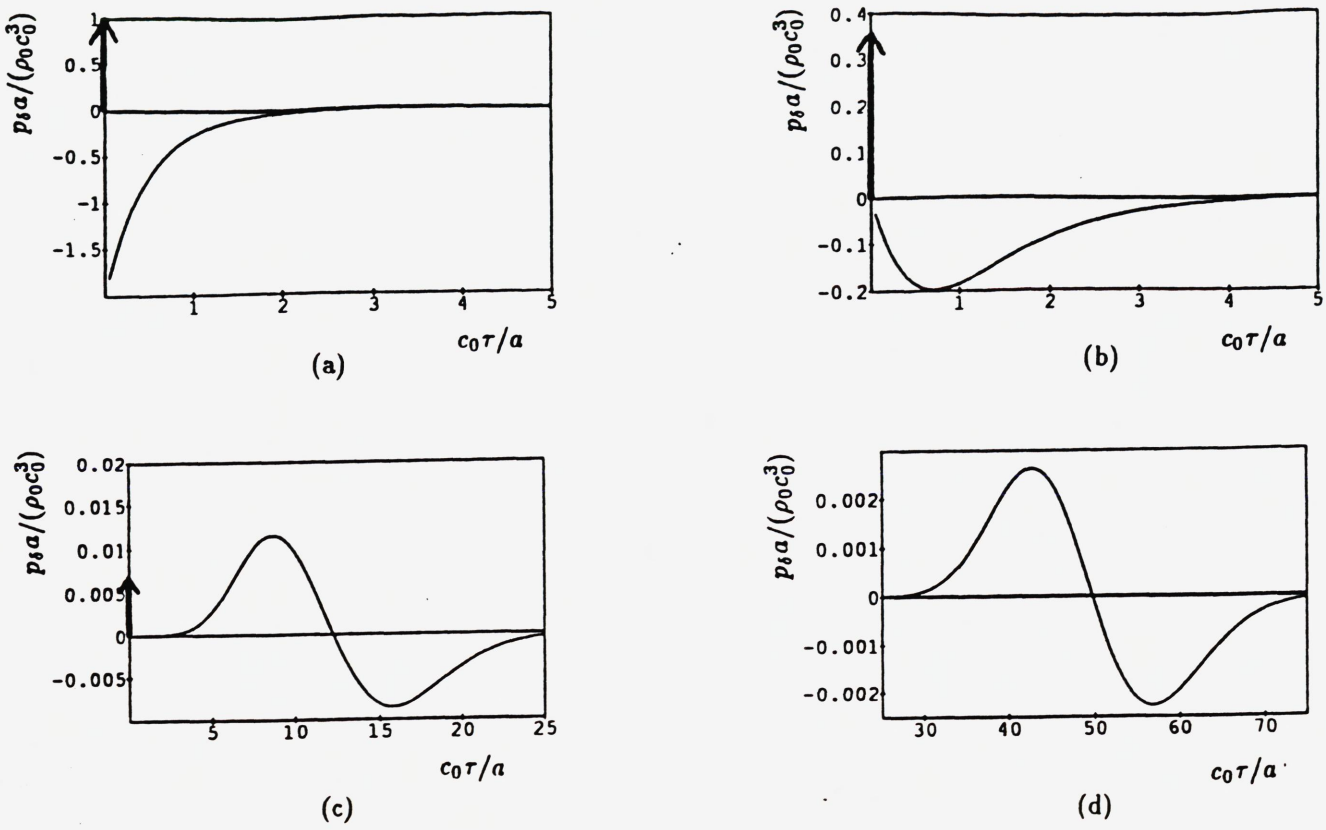

FIG. 4.2. Impulse response from a Gaussian source. $z = a$, $x = 0$ (a), $x = a$ (b), $x = 5a$ (c) and $x = 10a$ (d).

4.1.2. Separable Source

We will now consider another type of sources where it is possible to reduce the general integral representation to a single integral. These are separable sources where

$$f(\mathbf{x}) = f_1(x_1)f_2(x_2), \tag{4.18}$$

and where $\mathbf{x} = (x_1, x_2)$. Among these sources, we can mention the uniform, rectangular sources. We now introduce the general separable source into Eq. (4.4):

$$p_\delta = \frac{\rho_0 c_0}{2\pi z}\frac{\partial}{\partial \tau}\int_{-\infty}^{\infty} f_1(x_1')\int_{-\infty}^{\infty} f_2(x_2')\delta(\tau - \frac{(x_1 - x_1')^2}{2zc_0} - \frac{(x_2 - x_2')^2}{2zc_0})dx_2'dx_1'. \tag{4.19}$$

We split the inner integral into an integral from $-\infty$ to x_2 and an integral from x_2 to ∞. We can then, again according to Ref. 19, substitute $x_2' = x_2 \pm \sqrt{2zc_0 s}$ where $+$ is for the integral from x_2 to ∞ and $-$ for the other integral. Finally, we get

$$p_\delta = \frac{\rho_0 c_0}{2\pi}\sqrt{\frac{c_0}{2z}}\frac{\partial}{\partial \tau}U(\tau)\int_{x_1-\sqrt{2zc_0\tau}}^{x_1+\sqrt{2zc_0\tau}} \frac{f_1(x_1')}{\sqrt{\tau - \frac{(x_1-x_1')^2}{2zc_0}}} \times$$

$$\left(f_2(x_2 - \sqrt{2zc_0\tau - (x_1 - x_1')^2}) + f_2(x_2 + \sqrt{2zc_0\tau - (x_1 - x_1')^2})\right) dx_1'. \tag{4.20}$$

Eq. (4.20) provides a good starting point for a discussion of the impulse response from a separable source. We can for instance mention that for a uniform, rectangular piston, Eq. (4.20) can be evaluated analytically.

4.2. On the Validity of the Parabolic Approximation

It has already been briefly mentioned that the parabolic approximation is not uniformly valid as a solution of the physical problem we are considering. When deriving the parabolic approximation, we neglect a second derivative with respect to z. This means that we have to expect problems when this second derivative is large. This is the case close to the sound source where we thus have to expect problems. A consequence of the parabolic approximation is that the beam almost behaves as a plane wave which propagates in the positive z-direction. Regressive waves are discarded, and this means again that we have to expect problems close to boundaries. Because the beam almost is a plane wave propagating in the positive z-direction, we also have to expect problems at large angles from the positive z–axis. Much is known about the validity of the parabolic approximation when using a monochromatic signal. To summarize, the parabolic approximation breaks down very close to the source, and in the farfield at large angles from the acoustical axis. For the uniform piston, the critical value is $z = O(a(ka)^{1/3})$ or greater for the parabolic approximation to be valid in the nearfield[4]. In the farfield, the limitation on the angle from the acoustical axis is often taken to be $\theta < 20°$. We will now discuss briefly the validity of the linear, parabolic approximation when using a pulsed signal and a non-dissipative medium. As a part of this discussion, we will also make comments on the critical values in the monochromatic solution. An exact model for the impulse response is

$$\left(\nabla^2 - \frac{1}{c_0^2}\frac{\partial^2}{\partial t^2}\right) p_1 = 0, \tag{4.21a}$$

with the boundary conditions

$$v_{1,z}(z=0) = v_0 f(\mathbf{x})\delta(t), \tag{4.21b}$$

$$\lim_{r\to\infty} r\left(\frac{\partial p_1}{\partial t} + c_0\frac{\partial p_1}{\partial r}\right) = 0, \tag{4.21c}$$

$$rp_1 \text{ is bounded when } r \to \infty \tag{4.21d}$$

where $r = \sqrt{\mathbf{x}^2 + z^2}$, $z > 0$ and Eqs. (4.21c) and (4.21d) are Sommerfeld's radiation condition. This problem is studied by Stepanishen[6] for uniform sources, and with special emphasis on uniform circular sources. Naze Tjøtta and Tjøtta[7] discussed the problem further, and also for non-uniform sources. We will now compare the results in these works with the present results for the impulse response in the parabolic approximation. The comparison will give some information about the validity of the parabolic approximation in the pulsed case.

We first study the solution on the acoustical axis for an axisymmetric source. In the parabolic approximation, Eq. (4.6) is the solution of that problem. For Eq. (4.21), we find the solution in Ref. 7:

$$p_\delta = \rho_0 c_0^2 \left\{ \delta(\tau) f_1(0) + U(\tau)\frac{c_0^2\tau + zc_0}{\sqrt{c_0^2\tau^2 + 2zc_0\tau}} f_1'(\sqrt{c_0^2\tau^2 + 2zc_0\tau}) \right.$$
$$\left. + \Delta\delta\left(\tau + \frac{z}{c_0}(1 - \sqrt{1 + \frac{a^2}{z^2}})\right)\right\}. \tag{4.22}$$

We see here that the main contributions are identical in the two solutions. The replica pulse and the wake are a bit changed by the parabolic approximation. We first consider the replica pulse.

In the wave equation, the arrival time of the replica pulse is exactly the travel time from the discontinuity of the source which generates the replica pulse. This arrival time is $\tau = -\frac{z}{c_0}(1-\sqrt{1+\frac{a^2}{z^2}})$. In the parabolic approximation, the arrival time is approximated by $\tau = \frac{a^2}{2zc_0}$. We get this expression by expanding the square root in the exact expression in powers of $(a/z)^2$ and just keep the leading order. This means that we have to expect problems with the parabolic approximation very close to the sound source, i. e. when $z < a$. We can, however, say more. Assume now that the largest, characteristic, angular frequency of the pulse is ω_0. We then know how fast the pulse oscillates. The maximum acceptable misplacement of the replica pulse in the parabolic approximation has to be specified. It is natural to specify it as a fraction of an oscillation with ω_0 as angular frequency. The maximum misplacement is here required to be one fourth of a whole cycle. The difference between the arrival time of the parabolic and the exact replica pulse, therefore has to be less than $\pi/(2\omega_0)$. We thus have:

$$\left|\tau - \frac{a^2}{2zc_0} - \left(\tau + \frac{z}{c_0}(1-\sqrt{1+\frac{a^2}{z^2}})\right)\right| < \frac{\pi}{2\omega_0}. \tag{4.23}$$

We now expand the square root, and keep the leading order only. Then, we get the following restriction on z:

$$z > a\left(\frac{\omega_0 a}{c_0}\right)^{1/3}\left(\frac{1}{4\pi}\right)^{1/3}. \tag{4.24}$$

This means that z has to be of the order $a\left(\frac{\omega_0 a}{c_0}\right)^{1/3}$ or larger if we want to use the parabolic approximation. This result is similar to the result found by Naze Tjøtta and Tjøtta[4] for a monochromatic sound beam.

The validity of the parabolic approximation for the wake is more difficult to estimate in details. In order to give a precise estimate, we have to consider a specific sound source. This will not be done here. We just observe that the wake in the impulse response of the parabolic approximation is equal to the wake where there is no parabolic approximation if $z \gg c_0\tau$. In some sense, this means that the parabolic approximation breaks down close to the source.

For a Gaussian source, we find the solution of Eq. (4.21) from the results by Naze Tjøtta and Tjøtta in Ref. 7:

$$p_\delta = \rho_0 c_0^2 e^{-(\frac{x}{a})^2}\left\{\delta(\tau) + U(\tau)\frac{\partial}{\partial\tau}\left[e^{-\frac{c_0^2\tau^2+2zc_0\tau}{a^2}} I_0\left(\frac{2x\sqrt{c_0^2\tau^2+2zc_0\tau}}{a^2}\right)\right]\right\}. \tag{4.25}$$

We see that in order to go from this solution to the solution where a parabolic approximation is performed, Eq. (4.17), we have to assume that $z \gg c_0\tau$. This is the same assumption that was made above for the wake on the acoustical axis for a general, axisymmetric source. The precise limitations on the parabolic approximation when using a Gaussian source, will not be considered.

From the results by Stepanishen[6], we can find the impulse response for a uniform piston.
When $x < a$, we get:

$$p_\delta = \rho_0 c_0^2 \left(\delta(\tau) + \Phi_\delta\right), \tag{4.26a}$$

where

$$\Phi_\delta = \begin{cases} -\frac{(c_0^2\tau + zc_0)\left(1 - \frac{x^2-a^2}{c_0^2\tau^2+2zc_0\tau}\right)}{\pi\sqrt{4x^2(c_0^2\tau^2+2zc_0\tau)-(c_0^2\tau^2+2zc_0\tau-a^2+x^2)^2}} & \text{, when} \\ -\frac{z}{c_0}\left(1-\sqrt{1+\frac{(x-a)^2}{z^2}}\right) < \tau < -\frac{z}{c_0}\left(1-\sqrt{1+\frac{(x+a)^2}{z^2}}\right) & \text{and} \\ 0 & \text{, elsewhere.} \end{cases} \tag{4.26b}$$

When $x > a$, we get

$$p_\delta = \rho_0 c_0^2 \Phi_\delta, \tag{4.27}$$

where Φ_δ is defined as above. There are two differences between this solution and the parabolic approximation. One difference is that $z \gg c_0\tau$ is assumed in the parabolic approximation. This is the approximation that we have found several places in this section. The other difference is that the first and the last arrival time for Φ_δ are different in the two cases. We will consider these arrival times closer and thereby find a largest angle where the parabolic approximation is valid in the farfield. The idea used here is the same as the one used in the discussion of the replica pulse on the acoustical axis. Let now the first and the last arrival times in the exact model be denoted τ_{e1} and τ_{e2} respectively. The similar arrival times in the parabolic approximation are called τ_{p1} and τ_{p2}. In the farfield, the impulse response has large spikes close to τ_1 and τ_2. Assume now that the centre of generated signal $F(\tau)$ is located at $\tau = 0$. This is the case for all signals studied numerically in this work. The received signal will then contain a smeared version of $F(\tau)$ centred at the first arrival time τ_1, and a smeared version of the negative of $F(\tau)$ centred at the last arrival time τ_2. The most important thing in order to obtaining a physically correct solution when using the parabolic approximation, is to consider the difference $\tau_2 - \tau_1$. If this difference is about the same in the parabolic approximation as it is without, the parabolic approximation will predict quite well the received signal. Therefore we now study the expression

$$\Delta\tau = |\tau_{2e} - \tau_{1e} - (\tau_{2p} - \tau_{1p})|. \tag{4.28}$$

When $\Delta\tau$ is small, the parabolic approximation is fairly good. By inserting the different arrival times, and expanding the square roots in τ_{e1} and τ_{e2}, we find

$$\Delta\tau \sim \frac{xa}{z^3 c_0}\left(x^2 + a^2\right) \approx \frac{x^3 a}{z^3 c_0} = \frac{a\tan^3\theta}{c_0}, \tag{4.29}$$

where we have assumed that $x \gg a$ as will be the case outside the acoustical axis in the farfield. In order to accept the parabolic approximation, we will require that the relative misplacement between the two pulses is less than a fourth of a wavelength of the

fastest characteristic variation of the signal. As usual, we call the angular frequency of this variation ω_0. We thus have to require that

$$\Delta\tau < \frac{\pi}{2\omega_0}. \tag{4.30}$$

By inserting the expression for $\Delta\tau$, we get

$$\tan\theta < \left(\frac{\pi c_0}{2\omega_0 a}\right)^{1/3} = \left(\frac{\pi}{2k_0 a}\right)^{1/3}, \tag{4.31}$$

where $k_0 = \omega_0/c_0$ is the wave number corresponding to the angular frequency ω_0. We thus see that the maximum angle from the acoustical axis where the parabolic approximation is valid, depends on the highest characteristic ka-value. This is perhaps a bit surprising. When we consider a monochromatic signal, it is usual to assume that the maximum angle where the parabolic approximation is acceptable is about 20° regardless of what ka-value that is used. This estimate is, however, just a rough first estimate, and an analysis equal to the one done here, will show that the maximum angle depends on ka also in that case. We will briefly show this.

The directivity when using a monochromatic signal and a uniform piston is

$$D_e(\theta) = \left|\frac{2\mathrm{J}_1(ka\tan\theta)}{ka\sin\theta}\right|, \tag{4.32}$$

when using the parabolic approximation, and

$$D_e(\theta) = \left|\frac{2\mathrm{J}_1(ka\sin\theta)}{ka\sin\theta}\right| \tag{4.33}$$

without the parabolic approximation. We can now for instance require that the misplacement of the sidelobes in the parabolic approximation has to be less than a fourth of a sidelobe. This leads to the following approximative equation for the maximum angle that is accepted:

$$\tan\theta = \sin\theta + \frac{3}{4ka}. \tag{4.34}$$

It is easily shown that when ka increases, the maximum angle decreases. For $ka = 50$, this gives a maximum angle of 17.7°, while for $ka = 100$, the maximum angle is 14.0°. These values are close to the values obtained from Eq. (4.31) for the maximum angle in the pulsed case. In figure 4.3, we compare the farfield directivity with and without the parabolic approximation for the monochromatic case. We see there illustrated that the parabolic approximation is valid for larger angles when ka is decreased. We also see that the angle where it breaks down is reasonably well estimated by the analysis above.

4.3. Farfield Results

In this section, we will consider the farfield solution of the pulsed, non-dissipative sound propagation from a plane source. To some extent, this topic has already been discussed in section 4.1. Here, we will focus on this problem more in detail, and thereby find both qualitative and quantitative results. We divide the discussion into two parts, the solution on the acoustical axis, and the solution outside the acoustical axis.

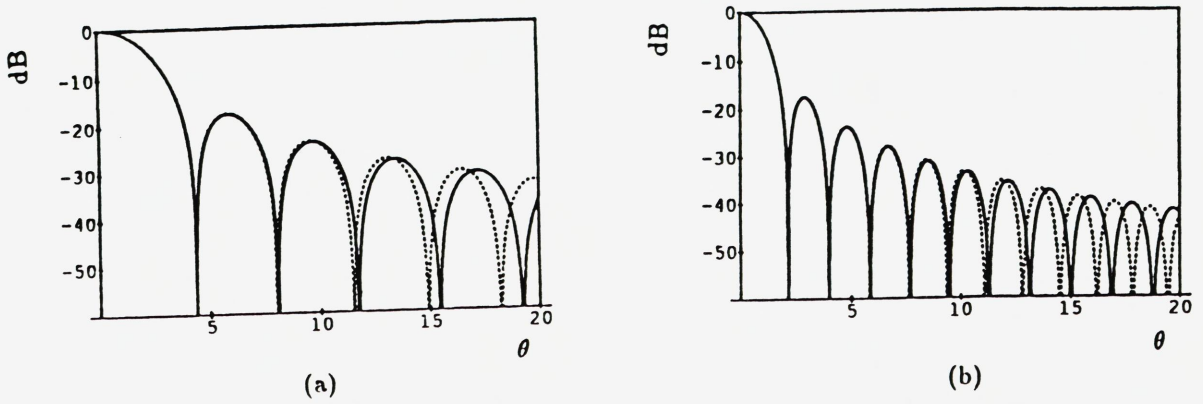

FIG. 4.3. Comparison of the directivity with the parabolic approximation ($\cdots$) and without the parabolic approximation (—) when using a uniform piston and a monochromatic signal. $ka = 50$ (a), 100 (b).

4.3.1. Results on the Acoustical Axis

We can get the solution for a general source by convolving Eq. (4.4) with the desired pulseshape $F(\tau)$:

$$p_1(\mathbf{x}, z, \tau) = \frac{\rho_0 c_0}{2\pi z} \iint_{-\infty}^{\infty} f(\mathbf{x}_1) F'(\tau - \frac{(\mathbf{x} - \mathbf{x}_1)^2}{2zc_0}) d\mathbf{x}_1. \tag{4.35}$$

The solution on the acoustical axis is now

$$p_1(0, z, \tau) = \frac{\rho_0 c_0}{2\pi z} \iint_{-\infty}^{\infty} f(\mathbf{x}_1) F'(\tau - \frac{\mathbf{x}_1^2}{2zc_0}) d\mathbf{x}_1. \tag{4.36}$$

Assume that the characteristic radius of $f(\mathbf{x})$ is a and the highest characteristic frequency of $F(\tau)$ is ω_0. A characteristic value for $\frac{\mathbf{x}_1^2}{2zc_0}$ is then $\frac{a^2}{2zc_0}$. When $\frac{\mathbf{x}_1^2}{2zc_0}$ is much larger than this value, the contribution to the integral is negligible because of the factor $f(\mathbf{x}_1)$. On the other hand, the change of $F'(\tau - \frac{\mathbf{x}_1^2}{2zc_0})$ is negligible when the argument changes by an amount much less than $1/\omega_0$. These considerations enable us to neglect $\frac{\mathbf{x}_1^2}{2zc_0}$ in the argument of F when $z \gg \frac{\omega_0 a^2}{2c_0} = r_0$. We thus get

$$p_1(0, z, \tau) \sim \frac{\rho_0 c_0}{2\pi z} F'(\tau) \iint_{-\infty}^{\infty} f(\mathbf{x}_1) d\mathbf{x}_1 \quad , z \gg r_0. \tag{4.37}$$

This means that the pulseshape on the acoustical axis in the farfield is the time derivative of the time dependency on the source. Thus the pulse received in the farfield can be quite different from the pulse generated on the source. This also introduces some restrictions on the choice of $F(\tau)$ in order to keep contact with the physics. We have to require that the function $F(\tau)$ is smooth. If we for instance used some cycles of a sinus as $F(\tau)$, the solution in the farfield would have approached a discontinuous function. This would have implied that diffraction could generate a kind of a shock wave, which of course is quite unphysical. The smoothness condition required here, is also related to the fact that if a sound pulse is too broadbanded, it can be impossible to generate it by a transducer.

Figure 4.4 shows that for Gaussian pulses and a uniform, circular piston, the farfield formula can be used when $z \gtrsim 2r_0$. This is the case both for a relatively long Gaussian pulse ($n = 12$) and for a very short pulse ($n = 3$).

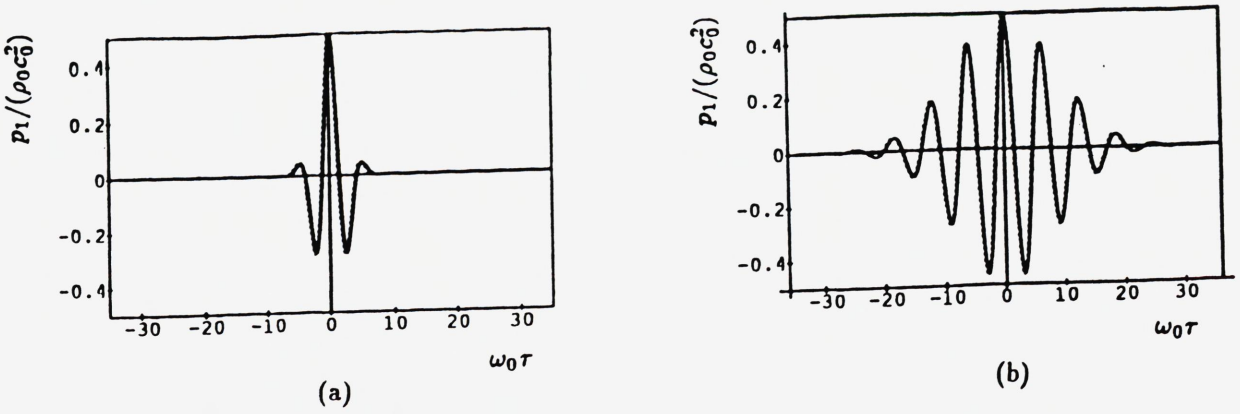

FIG. 4.4. Comparison between exact solution (—) and farfield solution ($\cdots$) for Gaussian pulses ($n = 3$ and $n = 12$) when the source is uniform circular and $z = 2r_0$ and $x = 0$.

4.3.2. Results Outside the Acoustical Axis

In the discussion of the impulse response, the actual shape of the signal outside the acoustical axis in the farfield of a uniform, circular piston was briefly discussed. Here, we will consider the directivity of the pulsed beam, and discuss how it changes when the pulse gets shorter. The directivity can be defined in two different ways. Either we can look at the maximum amplitude of the sound field different places on a circle with centre at the origin in the $x - z$-plane, or we can alternatively consider the energy in a similar way. In the monochromatic case, these two approaches give the same result when we consider the directivity plot (beam pattern) in decibels. In Ref. 16, the directivity was defined from the maximum amplitude. It was there shown, using the exponential pulse described below in Eq. (4.42), that the main lobe tended to be narrower, and the side lobes smaller when the pulse was shorter. Here, we will discuss the directivity from the energy of the signal. In all the plots, the energy on the acoustical axis is defined to be 0dB. We have thus plotted

$$E(r,\theta) = 10 \log_{10} \frac{\int_{-\infty}^{\infty} p^2(r \sin\theta, r\cos\theta, \tau) d\tau}{\int_{-\infty}^{\infty} p^2(x=0, r, \tau) d\tau} \tag{4.38}$$

as a function of θ.

The pulses used in the numerical calculations have Gaussian envelope functions. In figure 4.5, we have discussed how soon the respective farfield radiations of different pulses are established. We see that both for a relatively short pulse ($n = 6$) and for a longer pulse ($n = 20$), the farfield is almost established when $r = 2r_0$. In the dips between the lobes, this is not true. Elsewhere, the farfield seems to be established. At $r = 5r_0$ and $r = 20r_0$, we see that the field is almost identical, and except between the lobes, also equal to the field at $r = 2r_0$. The same conclusion is obtained when considering other pulse-lengths.

In figure 4.6, the effect of different pulse-lengths in the farfield is discussed. We see that when the pulse gets shorter, the sidelobes tend to be smaller, and finally, they tend to disappear. We see also that the main lobe is almost equal for the different pulses except the shortest one. These effects can be explained by considering the frequency domain. The longest pulse has the most narrow frequency band around $\omega = \omega_0$. Therefore, it will be most equal to the monochromatic signal. When the pulse is shorter, and thereby the

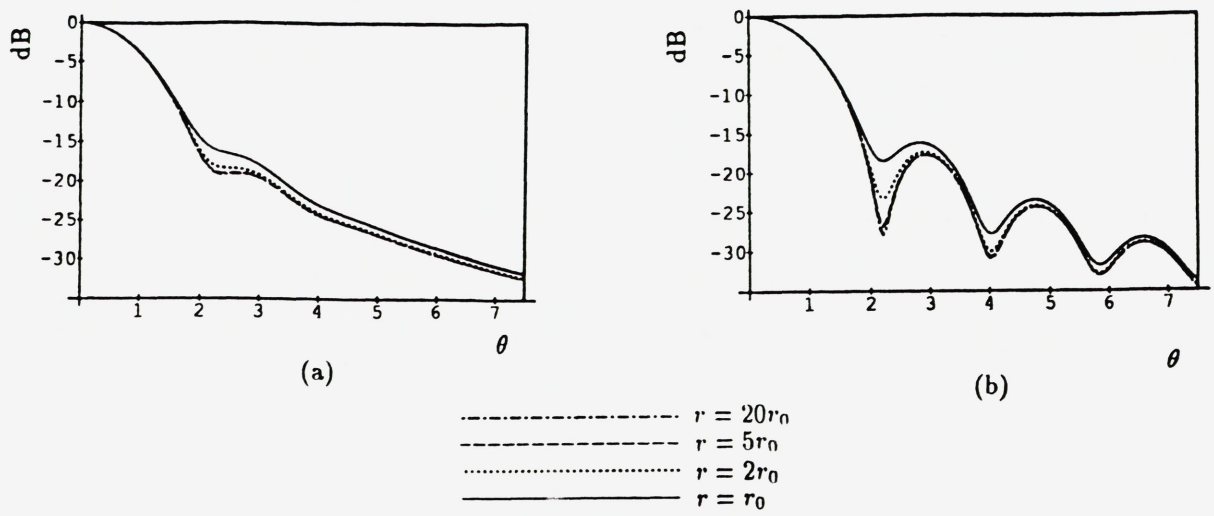

FIG. 4.5. Beam pattern for Gaussian pulses $n = 6$ (a) and $n = 20$ (b) at various distances. $\omega_0 a/c_0 = 100$.

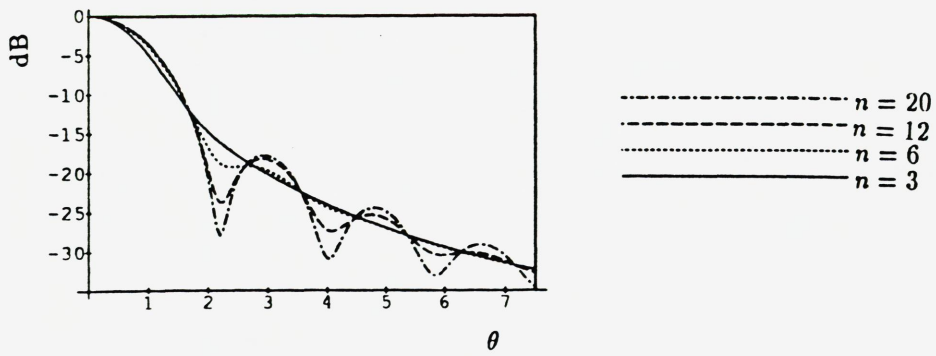

FIG. 4.6. Beam pattern for various Gaussian pulses at the range $r = 20r_0$. $\omega_0 a/c_0 = 100$.

frequency band longer, the cancellation between the sidelobes in the beam pattern, which is total in the monochromatic signal, is not as dominant any longer. This is because the signal now increasingly consists of different frequencies. These different frequencies have different beam patterns, with different zero points. The superposition of all these signals then tends to remove the sidelobes. When $n = 3$, which is the smallest pulse considered, the pulse is so small, and the frequency band so wide, that it is perhaps wiser to compare it to the time derivative of the impulse response, and expect something not far from that.

4.3.3. A Special Case

We have now discussed the directivity of a pulsed sound beam. The actual shape of the signal received in the farfield has, however, just been briefly considered. We will not have a discussion of the shape of the signals. Instead, we will consider a special case where it is possible to get analytical farfield solutions also outside the acoustical axis. Then, when considering actual pulses, this can be an alternative to other methods, and often this will be quite a fast way to obtain actual waveforms numerically. We consider here a general, but bounded, axisymmetric source. That means that $f_1(x) = 0$ when $x > a$. This is just a mathematical restriction. In real situations, we of course always have bounded sources. By convolving the actual time dependency with Eq. (4.9), we get

$$p_1 = \frac{\rho_0 c_0}{\sqrt{2\pi z}} \int_0^a f(x')x' \int_{-\infty}^{\infty} (-i\omega)\tilde{F}(\omega)e^{-i\omega(\tau - \frac{x^2+x'^2}{2zc_0})} J_0(\frac{\omega x x'}{zc_0}) d\omega dx'. \tag{4.39}$$

We are now able to integrate the ω-integral for a class of pulses which will be described below. Afterwards, we can evaluate the x'-integral within a farfield approximation.

We will now describe the class of pulses for which we can perform these calculations. Consider first the class of functions $F(\tau)$ where $\tilde{F}(\omega)$ is a rational function in ω and with all the poles outside the real ω-axis. We will mention some of the functions from this class. A very simple one is $F(\tau) = e^{-\gamma|\tau|}$. We note first that this function is not differentiable at $\tau = 0$. Two smooth functions from this class are $F(\tau) = (1 + \gamma|\tau|)e^{-\gamma|\tau|}$ and $F(\tau) = 2e^{-\gamma|\tau|} - e^{-2\gamma|\tau|}$. These functions do not satisfy Eq. (2.6), and therefore they do not have a consistent time dependency within the parabolic approximation. We can, however, multiply these functions by $\sin\omega_0\tau$ and still be within the class. In this way we get functions with zero mean value. It is possible to build a function with zero mean value and with an envelope function which is differentiable arbitrarily many times in a similar way. We can also build up other desired envelope functions, for instance envelope functions which are almost equal to one for a long τ-interval. This means that quite a few realistic pulses can be modelled with functions from this class. To summarize, the class of time dependencies we will work with, is the class of functions $F(\tau)$ where $\tilde{F}(\omega)$ is a rational function in ω and with all the poles outside the real ω-axis. Besides this, the functions have to satisfy Eq. (2.6).

With $F(\tau)$ in this class, we can integrate the ω-integral by residue calculations from the complex analysis for many of the interesting τ-values. Let now ω_u denote the locations where $\tilde{F}$ has poles in the upper half plane of the complex plane, and let the poles be of order n_u respectively. We also define ω_l and n_l in the similar way for the lower half plane. The residue calculation then gives

For $x \geq a$ and $\tau \leq \frac{(x-a)^2}{2zc_0}$ or
for $x \leq a$ and $\tau \leq 0$:

$$p_1 = \frac{\rho_0 c_0}{\sqrt{2\pi z}} \frac{\partial}{\partial \tau} \int_0^a f(x') x' \sum_{\omega_u} \left\{ \frac{2\pi i}{(n_u - 1)!} \times \right.$$
$$\left. \frac{\partial^{n_u - 1}}{\partial \omega^{n_u - 1}} \left[\tilde{F}(\omega)(\omega - \omega_u)^{n_u} e^{-i\omega(\tau - \frac{x^2 + x'^2}{2zc_0})} J_0(\frac{\omega x x'}{zc_0}) \right]_{\omega = \omega_u} \right\} dx'. \qquad (4.40a)$$

For $\tau \geq \frac{(x+a)^2}{2zc_0}$ we get

$$p_1 = \frac{\rho_0 c_0}{\sqrt{2\pi z}} \frac{\partial}{\partial \tau} \int_0^a f(x') x' \sum_{\omega_l} \left\{ \frac{2\pi i}{(n_l - 1)!} \times \right.$$
$$\left. \frac{\partial^{n_l - 1}}{\partial \omega^{n_l - 1}} \left[\tilde{F}(\omega)(\omega - \omega_l)^{n_l} e^{-i\omega(\tau - \frac{x^2 + x'^2}{2zc_0})} J_0(\frac{\omega x x'}{zc_0}) \right]_{\omega = \omega_l} \right\} dx'. \qquad (4.40b)$$

We see that there is an interval in τ which is not covered by these formulas. For this interval, it has not been possible to use the same calculations because of the more complex behaviour of J_0 at infinity. If we split up this function in Hankel functions, we can do the calculations, but besides the contributions from the residues, we get a contribution as an integral along a branch cut. This integral contribution is just as difficult to evaluate as the whole ω-integral. We are thus led to numerical evaluations of the ω-integral in this interval.

Eqs. (4.40) are exact expressions for the acoustic pressure within the parabolic approximation. Now we will make a farfield approximation of these equations. We argue similarly as in the beginning of the section, and say that when $z \gg r_0$ and x/z is bounded, we can neglect the term $\frac{x'^2}{2zc_0}$ in the exponents of the expressions. When introducing the Hankel transform of order zero, $\hat{f}$, of f:

$$\hat{f}(k) = \int_0^\infty f(x) J_0(kx) x dx,$$

we can evaluate the x'-integral. The farfield expression valid when $z \gg r_0$ and x/z is bounded, is then:
For $x \geq a$ and $\tau \leq \frac{(x-a)^2}{2zc_0}$ or
for $x \leq a$ and $\tau \leq 0$:

$$p_1 \sim \frac{\rho_0 c_0}{\sqrt{2\pi z}} \frac{\partial}{\partial \tau} \sum_{\omega_u} \frac{2\pi i}{(n_u - 1)!} \left\{ \frac{\partial^{n_u - 1}}{\partial \omega^{n_u - 1}} \left[\tilde{F}(\omega)(\omega - \omega_u)^{n_u} e^{-i\omega(\tau - \frac{x^2}{2zc_0})} \hat{f}(\frac{\omega x}{zc_0}) \right] \right\}_{\omega = \omega_u}. \qquad (4.41a)$$

For $\tau \geq \frac{(x+a)^2}{2zc_0}$ we get

$$p_1 \sim \frac{\rho_0 c_0}{\sqrt{2\pi z}} \frac{\partial}{\partial \tau} \sum_{\omega_l} \frac{-2\pi i}{(n_l - 1)!} \left\{ \frac{\partial^{n_l - 1}}{\partial \omega^{n_l - 1}} \left[\tilde{F}(\omega)(\omega - \omega_l)^{n_l} e^{-i\omega(\tau - \frac{x^2}{2zc_0})} \hat{f}(\frac{\omega x}{zc_0}) \right] \right\}_{\omega = \omega_l}. \qquad (4.41b)$$

We will now look at an example of the use of Eq. (4.41). We consider the pulse

$$F(\tau) = e^{-\gamma|\tau|} \sin \omega_0 \tau. \qquad (4.42)$$

We note that this pulse is inside the above-mentioned class, and that it is continuously differentiable once with respect to τ. The Fourier transform of $F(\tau)$ is given by

$$\tilde{F}(\omega) = \frac{4i\gamma\omega_0\omega}{\sqrt{2\pi}((\omega+\omega_0)^2+\gamma^2)((\omega-\omega_0)^2+\gamma^2)}. \tag{4.43}$$

We get two values of ω_u, namely $\omega_u = \pm\omega_0 + i\gamma$. n_u is 1 in both cases. Similarly, we get $\omega_l = \pm\omega_0 - i\gamma$ and $n_l = 1$. By inserting this into Eq. (4.41), we get
For $x \geq a$ and $\tau \leq \frac{(x-a)^2}{2zc_0}$ or
for $x \leq a$ and $\tau \leq 0$:

$$p_1 \sim \frac{\rho_0 c_0}{z}\frac{\partial}{\partial\tau}\mathrm{Re}\left\{ie^{-i\omega_0(\tau-\frac{x^2}{2zc_0})}e^{\gamma(\tau-\frac{x^2}{2zc_0})}\hat{f}(\frac{(\omega_0+i\gamma)x}{zc_0})\right\}. \tag{4.44a}$$

For $\tau \geq \frac{(x+a)^2}{2zc_0}$ we get

$$p_1 \sim \frac{\rho_0 c_0}{z}\frac{\partial}{\partial\tau}\mathrm{Re}\left\{ie^{-i\omega_0(\tau-\frac{x^2}{2zc_0})}e^{-\gamma(\tau-\frac{x^2}{2zc_0})}\hat{f}(\frac{(\omega_0-i\gamma)x}{zc_0})\right\}. \tag{4.44b}$$

The results from this analysis are a good starting-point when considering pulsed farfield solutions. The solution for many τ-values does not contain any integral. Therefore, we can get numerical results very fast for these τ-values.

Finally in this section, we note that the two τ-values which appear in the solution above, are the same as the τ-values appearing in the impulse response for a uniform piston. The physical interpretation is also similar. We have to expect this, because the envelope function contains functions of the type $\exp(-\gamma|\tau|)$ which has a discontinuous derivative in $\tau = 0$. This must be expected to leave a trace in the solution of the problem.

4.4. Focusing Effects

We now want to study the effects of focusing the source. The discussion will be within the parabolic approximation. It will be shown that the results for a plane source are directly applicable in the focused case through a transformation.

In order to discriminate between the unfocused and the focused solution, we introduce for the moment the notation p_u for the unfocused solution and the notation p_d for the focused solution. We have from Eq. (4.35) that

$$p_u(\mathbf{x},z,\tau) = \frac{\rho_0 c_0}{2\pi z}\iint_{-\infty}^{\infty} f(\mathbf{x}_1)F'(\tau-\frac{(\mathbf{x}-\mathbf{x}_1)^2}{2zc_0})d\mathbf{x}_1 \tag{4.45}$$

is a general solution of the unfocused problem. The focused problem can be formulated mathematically like

$$(\nabla_\perp^2 - \frac{2}{c_0}\frac{\partial^2}{\partial\tau\partial z})p_d = 0,$$

$$p_d(z=0) = \rho_0 c_0^2 f(\mathbf{x})F(\tau+\frac{\mathbf{x}^2}{2dc_0}). \tag{4.46}$$

The focused source is here replaced by an equivalent plane source. As shown in appendix A, this is consistent within the parabolic approximation only. Also, we have

to assume that the focal distance d is of the same asymptotical order as the Rayleigh distance defined from the largest characteristic frequency of the signal $F(\tau)$. Comparisons between experimental results for long pulses and this theory for monochromatic signals have, however, verified that this model still works with focal distances within the Rayleigh distance.

This problem can be solved in the same way as the unfocused problem:

$$p_d(\mathbf{x}, z, \tau) = \frac{\rho_0 c_0}{2\pi z} \iint_{-\infty}^{\infty} f(\mathbf{x}_1) F'(\tau + \frac{\mathbf{x}_1^2}{2dc_0} - \frac{(\mathbf{x} - \mathbf{x}_1)^2}{2zc_0}) d\mathbf{x}_1. \tag{4.47}$$

We can interpret this as the introduction of a new retarded time $\tau + \frac{\mathbf{x}_1^2}{2dc_0}$. The physical meaning of this time is quite clear. $\tau = t - z/c_0$ is a retarded time that is adjusting for the distance z from the plane $z = 0$ to the observation point. The new retarded time instead is adjusting for the distance from the curved surface where the source is located to the observation point. In order to connect this solution to the solution when using a plane source, p_u, we introduce the new variables

$$\begin{aligned} \frac{1}{z_d} &= \frac{1}{z} - \frac{1}{d}, \\ \frac{\mathbf{x}_d}{z_d} &= \frac{\mathbf{x}}{z}, \\ \tau_d - \frac{\mathbf{x}_d^2}{2z_d c_0} &= \tau - \frac{\mathbf{x}^2}{2zc_0}. \end{aligned} \tag{4.48}$$

We can now write the solution when using the focused source, p_d, as

$$\begin{aligned} p_d(\mathbf{x}, z, \tau) &= \frac{\rho_0 c_0}{2\pi z} \iint_{-\infty}^{\infty} f(\mathbf{x}_1) F'(\tau_d - \frac{(\mathbf{x}_d - \mathbf{x}_1)^2}{2z_d c_0}) d\mathbf{x}_1 \\ &= \frac{z_d}{z} p_u(\mathbf{x}_d, z_d, \tau_d). \end{aligned} \tag{4.49}$$

This is a rather significant result. It says that the sound pressure from a focused source can be found when we know the sound pressure from the similar plane source. All we then have to do is to transform the result according to Eqs. (4.48) and (4.49). We see that Eq. (4.48) transforms the z-value according to the lens formula of optics. The other transformations are just to adjust the width of the pulsed beam and the arrival time in order to fit the new geometry.

This result leads us to some general results concerning focusing. We can see that the solution in the focal plane ($z = d$) will be like the farfield solution in the unfocused case. On the axis, the solution in focus in this way is found as

$$p_d(\mathbf{0}, d, \tau) = \frac{\rho_0 c_0}{2\pi d} F'(\tau) \iint_{-\infty}^{\infty} f(\mathbf{x}_1) d\mathbf{x}_1. \tag{4.50}$$

We see here that the amplitude in focus depends on three factors: the generating source, the generated pulse, and the focal distance. The gain of a focused source is defined as the ratio between the maximum amplitude in focus and the maximum amplitude on the source. When using a monochromatic signal, this gain is $G = r_0/d$ when $\iint_{-\infty}^{\infty} f(\mathbf{x}_1) d\mathbf{x}_1 = \pi a^2$. A similar definition for the gain when using a pulsed signal now gives

$$G = \frac{a^2 \sup_\tau (|F'(\tau)|)}{2dc_0 \sup_\tau (|F(\tau)|)} \tag{4.51}$$

when we again assume $\iint_{-\infty}^{\infty} f(\mathbf{x}_1)d\mathbf{x}_1 = \pi a^2$. Thus the new effect coming from the pulsed signal is that if the time dependency on the source $F(\tau)$ has rapid variations so that $F'(\tau)$ is large, the gain can be larger for a pulsed signal than for a similar monochromatic signal. This can be the case for instance when $F(\tau)$ increases more rapidly to a maximum value than it decreases from this value to zero again.

When applying the transformation for $z > d$, we get a problem. In this case $z_d < 0$ and we have to get the non-focused result at a negative z-value. This is of course not a physical solution for the non-focused problem. Therefore, in many results for the plane source, it is assumed that $z > 0$ without saying this explicitly. When applying the result to an integral solution, there usually are no problems. Many analytical and asymptotical results, however, have to be modified in order to be used for negative z-values. An example of this, is the impulse response solution from an axisymmetric source on the acoustical axis Eq. (4.6). The extended solution valid for z positive or negative, is

$$p_u = \rho_0 c_0^2 \left\{ \delta(\tau) f_1(0) + U(\tau z)\sqrt{\frac{zc_0}{2\tau}} f_1'(\sqrt{2zc_0\tau}) + \Delta\delta(\tau - \frac{a^2}{2zc_0}) \right\}, \tag{4.52}$$

where we recall that U is the heaviside function. The impulse response solution on the acoustical axis for a focused, axisymmetric source is then

$$p_d = \frac{\rho_0 c_0^2}{1-\frac{z}{d}} \left\{ \delta(\tau) f_1(0) + U(\tau(1-\frac{z}{d}))\sqrt{\frac{zc_0}{2\tau(1-\frac{z}{d})}} f_1'(\sqrt{\frac{2zc_0\tau}{(1-\frac{z}{d})}}) + \right.$$
$$\left. \Delta\delta(\tau - \frac{a^2(1-\frac{z}{d})}{2zc_0}) \right\}. \tag{4.53}$$

This result shows how the solution is extended to be valid also after the focal point. We see that the replica pulse arrives before the main contribution when $z > d$. The signs of the two pulses are now reversed, so that the replica pulse is equal to the generated pulse on the source, and the main contribution is the negative of this signal. In this sense, the replica pulse and the main contribution have changed roles when $z > d$. Also, the wake will arrive before the main contribution and not after as it did before focus and in the unfocused case. The presence of the wake before the main contribution can give an interesting effect. If the discontinuity Δ at the edge of the source is small, the signal received beyond the focal distance, will essentially consist of the wake and the main contribution. As mentioned above, the wake appears first, and can therefore in some cases be a kind of precursor for the main contribution. Another interesting aspect of the solution, is the lack of causality beyond the focal distance when having an infinite source like for instance the Gaussian source. This is a special case of non-causality coming from geometry and not from the dissipative effects of the media. Dissipative effects are neglected in this discussion. In fact, this non-causality is caused by the precursor, which in this case is infinitely long on the τ-axis. When looking at the focused boundary condition, it is not surprising that we get this effect. Strictly speaking we have a non-causal boundary condition when the source is infinite, because the time delay is increasing towards infinity when $\mathbf{x}$ is growing. This effect is just theoretical, because we always have a bounded source in a practical situation, and because it comes from the approximations done when modelling a focused source, and not from the physics present. Finally, we note that when $z \to \infty$ we get the unfocused solution at $z = -d$. When the focal point

is in the nearfield and the source is a uniform piston, this solution has the same structure as the nearfield solution at $z = d$. The amplitude is now damped and the replica pulse arrives first. This means that the replica pulse and the main contribution have changed roles, as mentioned above.

4.5. Effects of Absorption

We have now discussed the effects of absorption and diffraction separately for the linear sound field. In this section, we want to combine some of the results, and thereby get results for linear sound propagation including both diffraction and absorption.

The solution of this problem is generally given by Eq. (2.17):

$$p_1(\mathbf{x}, z, \tau) = \frac{\rho_0 c_0}{z(2\pi)^{(3/2)}} \int_{-\infty}^{\infty} (-i\omega)\tilde{F}(\omega) e^{-i\omega\tau - \frac{D\omega^2}{2c_0^3}z} \iint_{-\infty}^{\infty} e^{\frac{i\omega|\mathbf{x}-\mathbf{x}'|^2}{2zc_0} - \frac{i\omega \mathbf{x}'^2}{2dc_0}} f(\mathbf{x}') d\mathbf{x}' d\omega. \tag{4.54}$$

If we call the solution with no absorption p_u and the solution including absorption p_a, we can rewrite Eq. (4.54):

$$p_a = \sqrt{\frac{c_0^3}{2\pi D z}} \int_{-\infty}^{\infty} p_u(\tau_1) e^{-\frac{(\tau-\tau_1)^2 c_0^3}{2Dz}} d\tau_1. \tag{4.55}$$

We can thus get the solution with absorption by convolving the solution with no absorption with a Gaussian function in time. This is an alternative way to the integration in frequency domain to get the solution in the dissipative case. Eq. (4.55) will now be used to find some general properties.

We will first consider the dissipative solution on the acoustical axis in the diffractional farfield. The non-dissipative solution is given by Eq. (4.37):

$$p_u(\mathbf{0}, z, \tau) \sim \frac{\rho_0 c_0}{2\pi z} F'(\tau) \iint_{-\infty}^{\infty} f(\mathbf{x}_1) d\mathbf{x}_1 \quad , z \gg r_0. \tag{4.56}$$

By introducing this into Eq. (4.55), we get a problem similar to the one-dimensional problem discussed in chapter 3:

$$p_a = \frac{\rho_0 c_0}{2\pi z} \sqrt{\frac{c_0^3}{2\pi D z}} \iint_{-\infty}^{\infty} f(\mathbf{x}_1) d\mathbf{x}_1 \int_{-\infty}^{\infty} F'(\tau_1) e^{-\frac{(\tau-\tau_1)^2 c_0^3}{2Dz}} d\tau_1. \tag{4.57}$$

This can be analysed in the same way as the one-dimensional problem, and we get fast and slow absorption distances just like there. The only difference is that the final waveform Eq. (3.33) will now be proportional to $\exp\left(-\frac{\tau^2 c_0^3}{2Dz}\right)$ differentiated one more time than in the one-dimensional solution Eq. (3.33). This is because we are working with $F'(\tau)$ instead of with $F(\tau)$. In addition to the decay in the solution caused by dissipative effects and discussed in chapter 3, we get a decay like z^{-1} from the spherical spreading, as expected.

The beam pattern in the diffractional farfield, is studied numerically. Figure 4.7 shows the beam pattern when using Gaussian pulses. We see that for the relative long pulse ($n = 20$), the absorption does not alter the directivity significantly if the absorption distance L_0 is less than or approximately equal to the distance between the source and

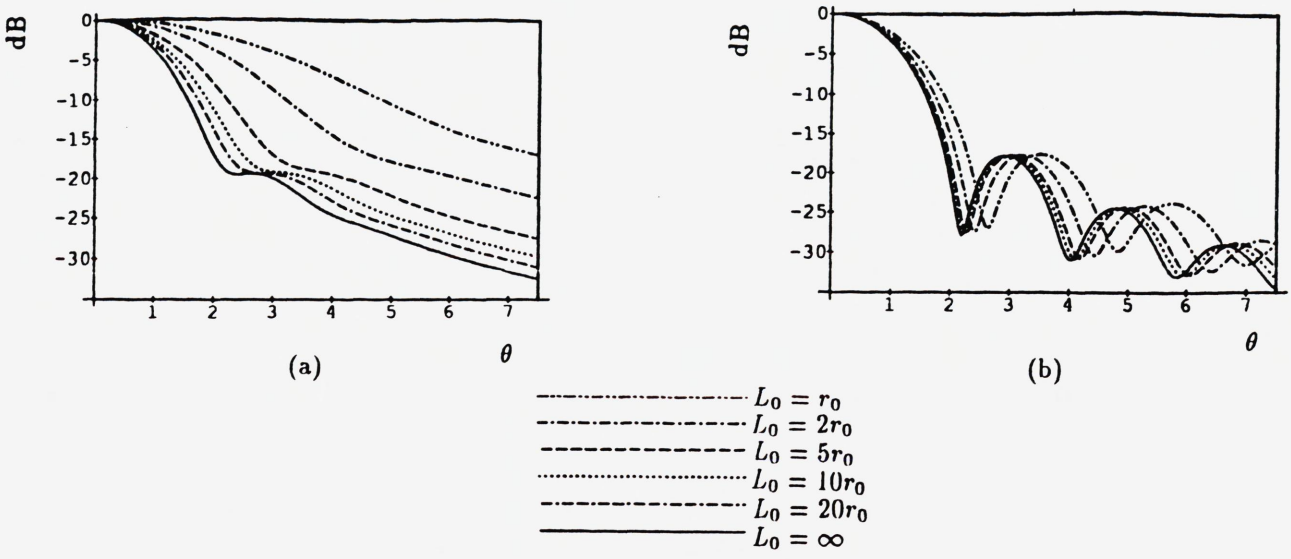

FIG. 4.7. Beam pattern for Gaussian pulses, uniform source, $\omega_0 a/c_0 = 100$, $r = 20r_0$, $n = 6$ (a) and $n = 20$ (b) and for different absorption distances.

the observation point. When the absorption is stronger, we see that the beam pattern is widened out. This tendency will be stronger the stronger the absorption is. Numerical calculations not shown here show the same phenomenon when the observation point is $r = 2r_0$. When the pulse is shorter ($n = 6$), we see the same tendency to a widening of the beam pattern. The difference now is that the widening appears with larger absorption distances (weaker absorption) than it did with the long pulse.

Qualitatively, the widening of the beam pattern is easily explained. When the absorption is significant for the signal, it filters away the high frequencies. We therefore end up with a more low-frequent signal than the original one. A more low-frequent signal has a wider beam pattern. Therefore, the effect shown in figure 4.7 is in agreement with physics.

We also found that the short pulse started widening with weaker absorption than the long pulse. We can explain this in the same way. The short signal has a large bandwidth in the frequency domain. The highest significant frequencies are therefore higher in the short pulse than in the long pulse. This means that the filtering towards a low-frequent signal starts closer to the source, and the beam pattern is widening more out.

We will finally mention another direct application of the theory of chapter 3. The impulse response on the acoustical axis from a general axisymmetric source is given by Eq. (4.6) in the non-dissipativ case:

$$p_{\delta,u} = \rho_0 c_0^2 \left\{ \delta(\tau) f_1(0) + U(\tau) \sqrt{\frac{zc_0}{2\tau}} f_1'(\sqrt{2zc_0\tau}) + \Delta\delta(\tau - \frac{a^2}{2zc_0}) \right\}. \tag{4.58}$$

As discussed earlier, this gives a main contribution, a wake and/or replica pulses. We get the similar impulse response in the dissipative case by using Eq. (4.55):

$$p_{\delta,a} = \rho_0 c_0^2 \sqrt{\frac{c_0^3}{2\pi D z}} \left\{ f_1(0) e^{-\frac{\tau^2 c_0^3}{2Dz}} \right.$$

$$+\int_0^\infty \sqrt{\frac{zc_0}{2\tau_1}} f_1'(\sqrt{2zc_0\tau_1}) e^{-\frac{(\tau-\tau_1)^2 c_0^3}{2Dz}} d\tau_1 + \Delta e^{-\frac{(\tau-\frac{a^2}{2zc_0})^2 c_0^3}{2Dz}} \Bigg\}. \qquad (4.59)$$

We see that the delta functions indicating the main contribution and the replica pulse(s) now are replaced by Gaussian functions. The wake contribution is now an integral. The integral defining the wake, has the same structure as the one-dimensional problem. If the integrand is finite in all the region of integration, we therefore can use the same methods as in chapter 3 to study the wake. When we will consider one specific pulse, we convolve Eq. (4.59) with the desired waveform $F(\tau)$. The main contribution and the replica pulse will then become problems identical to the one-dimensional. In addition, we get the contribution to the wake. If the source is a uniform circular piston, there is no wake contribution. Therefore the whole solution can be analysed by the methods of chapter 3. We thus see that the ideas used there, and the conclusions found about the dissipative sound propagation, in many cases are directly applicable to three-dimensional problems.

Chapter 5

Quasilinear Solution

In this chapter, we will discuss the quasilinear problem Eq. (2.16). We approach the problem by first looking at the one-dimensional solution. Afterwards, we will consider more realistic problems.

5.1. One-dimensional Solution

We now neglect the Laplacian in Eq. (2.16) in order to study the one-dimensional problem:

$$\left(-\frac{2}{c_0}\frac{\partial^2}{\partial\tau\partial z}+\frac{D}{c_0^4}\frac{\partial^3}{\partial\tau^3}\right)p_2=-\frac{\beta}{\rho_0 c_0^4}\frac{\partial^2}{\partial\tau^2}p_1^2, \tag{5.1a}$$

$$p_2(z=0)=0, \tag{5.1b}$$

where p_1 is the solution of the linear problem Eq. (3.2). This equation can be integrated once with respect to τ. When we assume that the pressure perturbation $p-p_0$ is zero when $\tau=-\infty$, the resulting equation is

$$\left(\frac{\partial}{\partial z}-\frac{D}{2c_0^3}\frac{\partial^2}{\partial\tau^2}\right)p_2=\frac{\beta}{2\rho_0 c_0^3}\frac{\partial}{\partial\tau}p_1^2, \tag{5.2a}$$

$$p_2(z=0)=0. \tag{5.2b}$$

This assumption has already been used and commented other places in this work. We will divide the one-dimensional discussion into two parts: the discussion of the non-dissipative problem, and the discussion of the dissipative problem.

5.1.1. Non-dissipative Problem

We now let $D=0$ in Eq. (5.2). The linear solution p_1 is then just

$$p_1(\tau,z)=\rho_0 c_0^2 F(\tau), \tag{5.3}$$

and Eq. (5.2) reduces to

$$\frac{\partial p_2}{\partial z}=\frac{\beta\rho_0 c_0}{2}\frac{\partial}{\partial\tau}F^2(\tau), \tag{5.4a}$$

$$p_2(z=0)=0, \tag{5.4b}$$

which gives

$$p_2(\tau, z) = \frac{\beta \rho_0 c_0 z}{2} \frac{\partial}{\partial \tau} F^2(\tau). \tag{5.5}$$

This equation describes the first correction due to nonlinearity when we have removed all effects of diffraction and dissipation, and studied the nonlinearity isolated. We will study Eq. (5.5) more closely because it contains some information which can be useful when considering more complex models afterwards.

The complete solution for the weakly nonlinear sound propagation can be written

$$p = p_0 + \epsilon p_1 + \epsilon^2 p_2 + \cdots. \tag{5.6}$$

In the one-dimensional, non-dissipative case, this can be written as

$$p = p_0 + \rho_0 c_0 v_0 \left(F(\tau) + \frac{\epsilon \beta z}{2 c_0} \frac{\partial}{\partial \tau} F^2(\tau) + \cdots \right). \tag{5.7}$$

Let now ω_0 be a the highest characteristic frequency of $F(\tau)$, and define $\overline{\tau} = \omega_0 \tau$ and $\overline{F}(\overline{\tau}) = F(\tau)$. We then get

$$p = p_0 + \rho_0 c_0 v_0 \left(\overline{F}(\overline{\tau}) + \frac{z}{2 z_s} \frac{\partial}{\partial \overline{\tau}} \overline{F}^2(\overline{\tau}) + \cdots \right), \tag{5.8}$$

where $z_s = \frac{1}{\epsilon \beta \omega_0}$ is the shock formation distance for a plane wave with angular frequency ω_0. We note here that the asymptotic expansion for p is secular in z. Therefore we cannot describe the generation of shock waves by direct use of Eq. (5.8).

If we have a monochromatic model $F(\tau) = \sin \omega_0 \tau$, Eq. (5.5) gives a contribution to the second harmonics $2\omega_0$, as expected. Also, if $F(\tau)$ consists of two frequencies, Eq. (5.5) gives a contribution to the second harmonic of each frequency, and also a contribution to the sum- and difference frequencies of the two frequencies. This is just a very simple version of the mechanism in the parametric array. When we have a general, pulsed signal, we can think of that as a superposition of many frequencies. We therefore expect the quasilinear solution to contain a contribution to the second harmonics of each frequency, and sum and difference frequencies between all frequencies present. Adding all of these together, we get Eq. (5.5). If we look at the Fourier transform of Eq. (5.5), we find that this is exactly what happens. We now look more closely at the special case where $F(\tau) = F_1(\tau) \sin \omega_0 \tau$ and where $F_1(\tau)$ varies slowly with τ compared to the sinusoid. The Fourier transform will then be large close to $\omega = \pm \omega_0$ compared to the value other places. By arguing in the frequency domain again, we expect Eq. (5.5) to contain some very low frequencies and some frequencies close to $\omega = \pm 2\omega_0$. When inserting the described time dependency in Eq. (5.5), we get

$$p_2(\tau, z) = \frac{\beta \rho_0 c_0 z}{4} \left(\frac{\partial}{\partial \tau} F_1^2(\tau) - \left(\frac{\partial}{\partial \tau} F_1^2(\tau) \right) \cos 2\omega_0 \tau + 2\omega_0 F_1^2(\tau) \sin 2\omega_0 \tau \right). \tag{5.9}$$

Thus we see that the first term is the lowfrequency term due to difference frequencies. It has the same structure as the whole time dependency of Eq. (5.5). The two last terms are due to sum frequencies and second harmonics. We note that if the envelope function is strictly band limited with $\tilde{F}_1(\omega) = 0$ when $|\omega| > C < \omega_0$, the linear signal will

have no frequency components close to $\omega = 0$. The quasilinear solution will, however, have frequency components arbitrarily close to $\omega = 0$ if the envelope function has such components. These low frequency components are of special interest when looking at the dissipative solution. We will come back to that discussion later.

In the expressions above, the time derivative of the time dependency squared, $F^2(\tau)$, is present. This is a new indication of the fact that a waveform generated in a real situation has to be sufficiently smooth. A waveform which includes a discontinuity will for instance have delta functions in the quasilinear solution. So here again we have to remember that a waveform generated by a transducer cannot be too broadbanded, and thus has to be a smooth function.

We can now ask if it is possible to measure the quasilinear pressure directly. It is clear that the signal present is a sum of the linear and the quasilinear solution. In order to measure the quasilinear solution directly, we must have one of two: The linear solution is so small compared to the quasilinear solution that all we see is the quasilinear solution. This happens for instance when the absorption has damped away the linear solution while the quasilinear solution still is present. This is the case when we consider the dissipative farfield. Secondly, the linear solution can be so narrowbanded that the linear and the quasilinear solutions are separated in the spectrum. Then we can separate out just the quasilinear solution. If none of these conditions are fullfilled, we have to use more indirect methods. We can for instance compute the linear plus the quasilinear solution and compare the sum to the measured signal. Alternatively, we can increase the amplitude of the signal on the source, and see what differences there are in the measured signal except an amplitude increament. From this information, it should be possible to get some facts about the quasilinear solution. However, we all the time have to be aware of any higher order effects which can be present in the solution.

5.1.2. Dissipative Problem

We now consider the dissipative problem Eq. (5.2). The linear solution p_1 is now given by Eq. (3.4):

$$p_1(\tau, z) = \frac{\rho_0 c_0^2}{\sqrt{2\pi}} \int_{-\infty}^{\infty} \tilde{F}(\omega) e^{-\frac{D\omega^2 z}{2c_0^3} - i\omega\tau} d\omega. \tag{5.10}$$

When introducing this into Eq. (5.2), we can solve the equation by Fourier transformation methods:

$$p_2(\tau, z) = \frac{\beta\rho_0 c_0^4}{4\pi D} \int_{-\infty}^{\infty} (-i\omega) e^{-i\omega\tau - \frac{D\omega^2 z}{2c_0^3}} \int_{-\infty}^{\infty} \tilde{F}(s)\tilde{F}(\omega - s) \frac{e^{\frac{Ds(\omega-s)z}{c_0^3}} - 1}{s(\omega - s)} ds d\omega. \tag{5.11}$$

This equation cannot generally be solved analytically. We are therefore led to numerical computations. But some comments can be made based on the present form of the solution. The integration is over the $\omega - s$ plane. When $\tilde{F}(\omega)$ is considerably different from zero in the neighbourhood of $\omega = \pm\omega_0$ only, the factor $\tilde{F}(s)\tilde{F}(\omega - s)$ is considerably different from zero only close to $(\omega, s) = (2\omega_0, \omega_0)$, $(\omega, s) = (-2\omega_0, -\omega_0)$, $(\omega, s) = (0, \omega_0)$ and $(\omega, s) = (0, -\omega_0)$. The two first regions are contributions to the analog to the second harmonic and sum frequency terms as defined above, and the two last ones are contributions to the analog to the difference frequency. From the factor $e^{-\frac{D\omega^2 z}{2c_0^3}}$ in the

integrand, we see that the low frequency contributions are much less attenuated by the dissipative effects than the rest of the solution. Therefore, we have to expect that in a large z limit, these lowfrequent terms are the only ones surviving. From a physical point of view, this seems reasonable. We come back to this phenomenon in the discussion of the three-dimensional, dissipative farfield in section 5.4.

The quasilinear solution Eq. (5.11) can be related very closely to the linear solution. Consider the solution of the linear, one-dimensional problem with the boundary condition $\rho_0 c_0^2 F(\tau)$, Eq. (3.4). This solution is for the moment denoted $L[F(\tau)]$. When using the fact the $\tilde{F}(0) = 0$, we can split the integral in Eq. (5.11) into two converging integrals if we assume that $\tilde{F}(\omega)$ is differentiable at $\omega = 0$. Eq. (5.11) can now be rewritten to the form

$$p_2 = \frac{\beta c_0^2}{2D}\frac{\partial}{\partial \tau}\left(L[(\int_{-\infty}^{\tau} F(\tau')d\tau')^2] - \frac{1}{\rho_0 c_0^2}(L[\int_{-\infty}^{\tau} F(\tau')d\tau'])^2\right). \tag{5.12}$$

This means that in the one-dimensional case, we can use the linear solution directly to construct the quasilinear solution.

We also see from the integrand that when z increases, the region where $s(\omega - s)$ is positive contributes more and more to the solution compared to the region where $s(\omega - s)$ is negative when looking at a fixed ω. We thus have to expect different behaviours from the parts of the solution coming from the different regions. For a bifrequent source, this leads to different behaviour of the difference frequency compared to the sum frequency. This is discussed in Ref. 23 where for instance difference in directivity is discussed for a three-dimensional model using a Gaussian source.

We now mention briefly what differences that appear in the quasilinear solution if we use other absorption laws than the square dependency of frequency used implicitly above. We change the absorption law in an ad hoc manner by changing $\frac{D\omega^2}{2c_0^3}$ to $A(\omega)$, just like we did in the linear case in section 3.4.1. The substitution has to take place both in the linear solution substituted into the right hand side of the differential equation, and in the expression accounting for the absorption in the quasilinear sound field directly. As a result, we get

$$p_2 = \frac{\beta \rho_0 c_0}{4\pi}\int_{-\infty}^{\infty}(-i\omega)e^{-i\omega\tau - A(\omega)z}\int_{-\infty}^{\infty}\tilde{F}(s)\tilde{F}(\omega - s)\frac{e^{(A(\omega)-A(s)-A(\omega-s))z} - 1}{A(\omega) - A(s) - A(\omega - s)}dsd\omega. \tag{5.13}$$

This solution can have different properties from those of the solution using the square frequency law. In particular, in the solution using the square frequency law, the sign of $s(\omega - s)$ plays an important role. Now, it will be the sign of $A(\omega) - A(s) - A(\omega - s)$ that is important.

In the linear solution of the parabolic equation, the plane wave impedance relation $p_1 = \rho_0 c_0 v_1$ is consistently assumed where v is the velocity, and $v = v_1 + \epsilon v_2 + \cdots$. This means that we cannot discriminate between a piston source where the normal velocity is given, and a membrane source where the pressure is given at $z = 0$. In the quasilinear approximation, we will get different quasilinear solutions if we put $v_2(z = 0) = 0$ instead of $p_2(z = 0) = 0$. $v_2(z = 0) = 0$ is here the boundary condition for a piston problem, and the elsewhere used $p_2(z = 0) = 0$ is a membrane problem. The difference between these two solutions is discussed by Naze Tjøtta, TenCate and Tjøtta[24] for bifrequent sources in relation to the scattering of sound by sound. They show that within the parabolic

approximation, the relation between the normal velocity v_2 and the pressure p_2 is given by

$$v_2 - \frac{p_2}{\rho_0 c_0} = -\frac{1}{\rho_0}\int^{\tau} \frac{\partial p_1(\tau_1)}{\partial z} d\tau_1. \tag{5.14}$$

By introducing the linear solution of the one-dimensional, pulsed problem and setting $z = 0$, we get

$$v_2(z=0) - \frac{p_2(z=0)}{\rho_0 c_0} = -\frac{D}{2c_0}\frac{\partial F(\tau)}{\partial \tau}. \tag{5.15}$$

We thus get the quasilinear problem for the piston source by solving the following problem:

$$\left(\frac{\partial}{\partial z} - \frac{D}{2c_0^3}\frac{\partial^2}{\partial \tau^2}\right) p_2 = \frac{\beta}{2\rho_0 c_0^3}\frac{\partial}{\partial \tau} p_1^2, \tag{5.16a}$$

$$p_2(z=0) = \frac{\rho_0 D}{2}\frac{\partial F(\tau)}{\partial \tau}. \tag{5.16b}$$

Let us for the moment denote the quasilinear solution of the membrane problem p_{2m} and the quasilinear solution for the piston problem p_{2p}. The solution of the piston problem is then

$$p_{2p} = p_{2m} + \frac{\rho_0 D}{2}\int_{-\infty}^{\infty} (-i\omega)\tilde{F}(\omega) e^{-\frac{D\omega^2 z}{2c_0^3} - i\omega\tau} d\omega. \tag{5.17}$$

We thus see that the correction term is of the same type as the linear solution, but with the time derivative of the time dependency on the source instead of just the time dependency. If the highest characteristic frequency of $F(\tau)$ is ω_0, the correction term is of the order α_0/k_0 times the order of the linear solution. α_0 is here the absorption coeffisient and k_0 the wavenumber for the angular frequency ω_0. In the derivation of the KZK-equation, the factor α_0/k_0, which is proportional to the Stokes number, is assumed to be of the same asymptotical order as the Mach number[3]. Except close to the source, we can therefore expect the correction term to be small compared to p_{2p}, just as in Ref. 24.

5.2. Three-dimensional, Non-dissipative Solution

We now proceed to the discussion of pulsed, three-dimensional, quasilinear sound propagation. In this section we consider the non-dissipative case, and in the two following sections we discuss the dissipative case. The computation of the quasilinear field is greatly simplified when we consider a Gaussian source. For this reason, most of the work in this chapter is based on this source. We now start with a discussion of the solution for a Gaussian source. Afterwards we give some considerations for general sources.

5.2.1. Gaussian Source

We now study the quasilinear sound field generated by a pulsed Gaussian source which radiates into a lossless medium. The solution of that problem can be found by letting $D = 0$ in Eq. (2.20):

$$p_2 = \frac{\beta\rho_0 c_0}{4\pi}\iint_{-\infty}^{\infty}\int_0^z \omega^2 s(\omega - s)\tilde{F}(s)\tilde{F}(\omega - s) e^{-i\omega\tau} \times$$

$$\frac{1}{s(\omega-s)(i\omega(1-\frac{z}{d})(1-\frac{z'}{d})-\frac{4(z-z')c_0}{a^2})-\frac{2z'c_0\omega}{a^2}(\omega(1-\frac{z}{d})+\frac{2zc_0i}{a^2})}\times \tag{5.18}$$
$$\exp\left[\frac{-i\omega\mathbf{x}^2\left(s(\omega-s)(\frac{2}{a^2}+\frac{i\omega}{2dc_0}(1-\frac{z'}{d}))+\frac{z'\omega}{a^2}(\frac{2c_0i}{a^2}-\frac{\omega}{d})\right)}{s(\omega-s)(i\omega(1-\frac{z}{d})(1-\frac{z'}{d})-\frac{4(z-z')c_0}{a^2})-\frac{2z'c_0\omega}{a^2}(\omega(1-\frac{z}{d})+\frac{2zc_0i}{a^2})}\right]dz'dsd\omega.$$

The z'-integral can be evaluated, giving the exponential integral E_1. Consider now the solution on the acoustical axis ($\mathbf{x}=\mathbf{0}$). In this case, the integration greatly simplifies, and gives

$$p_2=\frac{\beta\rho_0c_0}{4\pi}\iint_{-\infty}^{\infty}\omega^2s(\omega-s)\tilde{F}(s)\tilde{F}(\omega-s)e^{-i\omega\tau}\times$$
$$\frac{\ln\sqrt{\frac{z^2+2z\Phi+\Phi^2+\Psi^2}{\Phi^2+\Psi^2}}+i\left(\arctan\frac{\Phi}{\Psi}-\arctan\frac{z+\Phi}{\Psi}\right)}{s(\omega-s)(-\frac{i\omega}{d}(1-\frac{z}{d})+\frac{4c_0}{a^2})-\frac{2c_0\omega}{a^2}(\omega(1-\frac{z}{d})+\frac{2zc_0i}{a^2})}dsd\omega, \tag{5.19}$$

where

$$\Phi=\mathrm{Re}\left\{\frac{s(\omega-s)(i\omega(1-\frac{z}{d})-\frac{4zc_0}{a^2})}{s(\omega-s)(-\frac{i\omega}{d}(1-\frac{z}{d})+\frac{4c_0}{a^2})-\frac{2c_0\omega}{a^2}(\omega(1-\frac{z}{d})+\frac{2zc_0i}{a^2})}\right\}, \tag{5.20}$$

and

$$\Psi=\mathrm{Im}\left\{\frac{s(\omega-s)(i\omega(1-\frac{z}{d})-\frac{4zc_0}{a^2})}{s(\omega-s)(-\frac{i\omega}{d}(1-\frac{z}{d})+\frac{4c_0}{a^2})-\frac{2c_0\omega}{a^2}(\omega(1-\frac{z}{d})+\frac{2zc_0i}{a^2})}\right\}. \tag{5.21}$$

From now on, we consider the unfocused source ($d=\infty$). The solution then reduces to

$$p_2=\frac{\beta\rho_0a^2}{8\pi}\iint_{-\infty}^{\infty}\omega^2s(\omega-s)\tilde{F}(s)\tilde{F}(\omega-s)e^{-i\omega\tau}\times$$
$$\frac{\ln\sqrt{\frac{z^2+2z\Phi+\Phi^2+\Psi^2}{\Phi^2+\Psi^2}}+i\left(\arctan\frac{\Phi}{\Psi}-\arctan\frac{z+\Phi}{\Psi}\right)}{2s(\omega-s)-\omega(\omega+\frac{2zc_0i}{a^2})}dsd\omega, \tag{5.22}$$

where

$$\Phi=\mathrm{Re}\left\{\frac{ia^2}{2c_0}\frac{s(\omega-s)(\omega+\frac{4zc_0i}{a^2})}{2s(\omega-s)-\omega(\omega+\frac{2zc_0i}{a^2})}\right\}, \tag{5.23}$$

and

$$\Psi=\mathrm{Im}\left\{\frac{ia^2}{2c_0}\frac{s(\omega-s)(\omega+\frac{4zc_0i}{a^2})}{2s(\omega-s)-\omega(\omega+\frac{2zc_0i}{a^2})}\right\}. \tag{5.24}$$

Now, we want to look at some general properties of Eq. (5.22). First, we want to get an approximate solution of Eq. (5.22) valid close to the source. If we expand the integrand in powers of z, and just keep the lowest order, it should be possible to obtain such a solution. In this way, we do not know, however, for which z-values we can expect the solution to be valid. This procedure leads to the very simple first approximation

$$p_2(\mathbf{0},\tau,z)\sim\frac{\beta\rho_0c_0z}{2}\frac{\partial}{\partial\tau}F^2(\tau) \tag{5.25}$$

for small z-values. In order to check this solution, we can compare with numerical solutions. In figure 5.1 we compare the approximate solution with a numerical solution of the problem. We comment here that the numerical solution was based on the integral

discussed in chapter 6, and not on numerical integration of Eq. (5.22) directly. The pulses in this figure are normalized to the factor

$$P_2 = \beta \rho_0 c_0^2 \left(\omega_0 a / c_0\right)^2 . \tag{5.26}$$

This is also the case for all the remaining figures in this chapter. We see that for this pulse, Eq. (5.25) is valid for $z \lesssim 0.2 \frac{\omega_0 a^2}{2c_0}$, i.e. up to about 0.2 Rayleigh distances for the carrier frequency of the pulse generated by the source. For larger z-values, the asymptotic formula overestimates the amplitude and also gives the pulse a wrong shape. The validity up to a fraction of the Rayleigh distance is not very surprising when we remember that diffraction is the only effect present besides the nonlinearity. We also note that the approximate solution Eq. (5.25) is equal to the one-dimensional solution Eq. (5.5). This is not surprising when we remember that the linear solution of this problem has no replica pulses, but just a wake which was not very notable close to the source. Therefore, the solution of the linear problem close to the source is not very different from the one-dimensional solution, and we should expect a solution close to the one-dimensional also for the quasilinear field. When we approach the Rayleigh distance of the carrier frequency, however, the diffraction has distorted the linear solution, and therefore the quasilinear solution also tends to be distorted. This happens because the generation of p_2 depends on the linear solution p_1, and also because the diffraction will have an effect on the quasilinear field directly.

We also discuss the farfield solution of Eq. (5.22). Now we expand the integrand in powers of $1/z$, and neglect contributions that are less than $\ln(z)/z$ and $1/z$. As an intermediate result, we get

$$p_2 \sim \frac{\rho_0 \beta a^4}{16\pi z c_0} \int_{-\infty}^{\infty} (-i\omega) e^{-i\omega\tau} \int_{-\infty}^{\infty} -s(\omega - s)\tilde{F}(s)\tilde{F}(\omega - s) \times \left\{ \ln \left| \frac{\omega c_0 z}{s(\omega - s)a^2} \right| + i \arctan\left(\frac{\omega c_0 z}{s(\omega - s)a^2} \right) \right\} ds d\omega. \tag{5.27}$$

At first look, it seems like we have problems in this integral when $s(\omega - s) = 0$ because of the singularity in the logarithm. However, we see that the integrand also contains a $s(\omega - s)$ -factor in the nominator. Besides, we have that $\tilde{F}(0) = 0$. This means that the integrand has no singularity when $s(\omega - s) = 0$. We now want to approximate further the logarithm and the arctan functions. First we specify the time dependency like

$$F(\tau) = F_1(\tau) \sin \omega_0 \tau, \tag{5.28}$$

where F_1 is an envelope function which varies slowly compared to the sinusoid. We then expect the solution to have similar contributions as the one-dimensional problem already discussed. This means that we expect a contribution to the frequencies close to the second harmonic of ω_0 and a lowfrequency contribution due to difference frequencies of the frequencies present in the signal. Assume now that the second harmonic term dominates the lowfrequency term. The main contribution to the integral thus comes from the region close to $\omega = \pm 2\omega_0$ and $s = \pm\omega_0$ where ω and s must have the same sign. Because the logarithm has a very small derivative when the argument is large, we can assume that ω and s in the logaritmic term are equal to these constants when z is large.

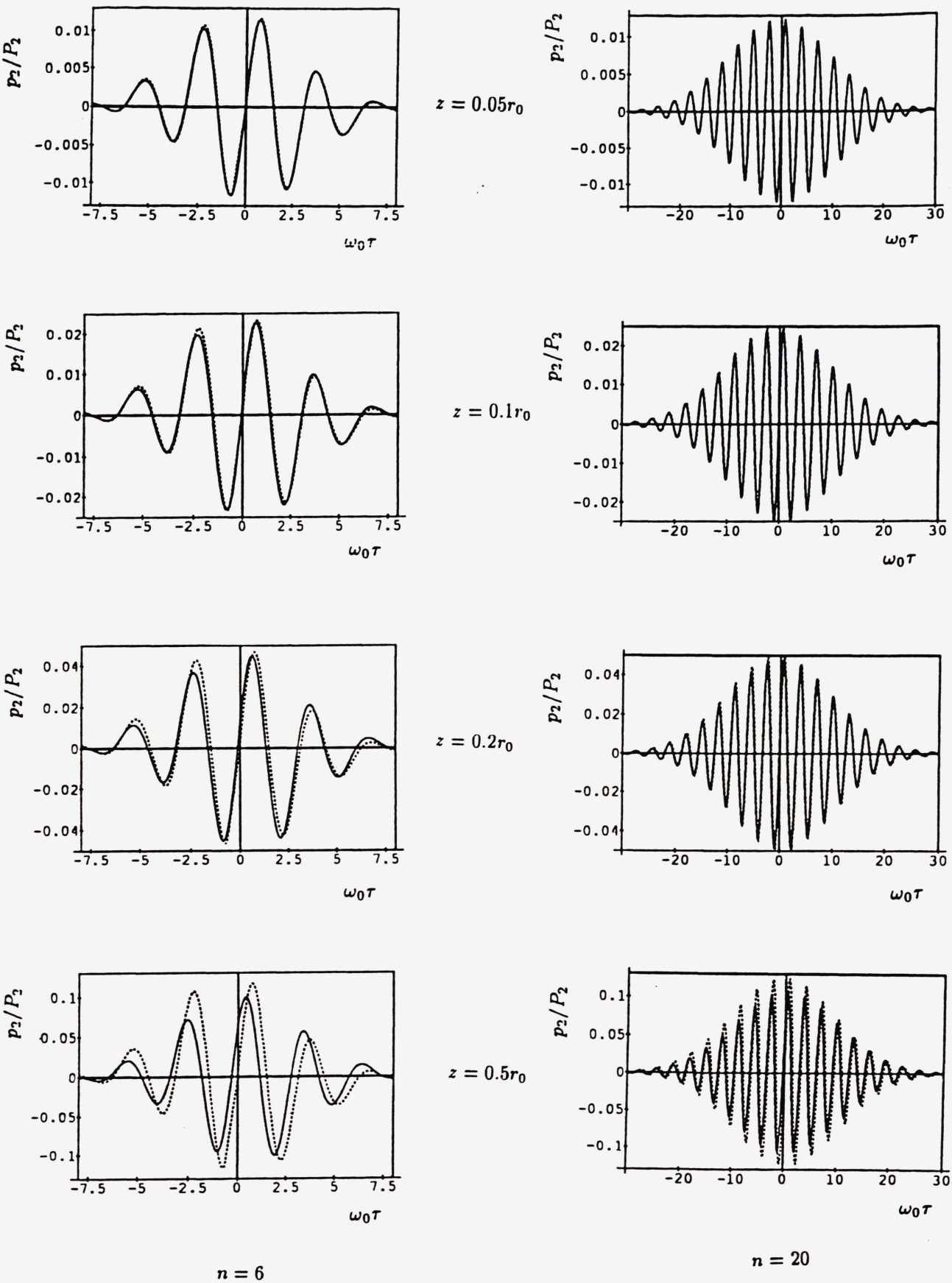

FIG. 5.1. Non-dissipative, three-dimensional, quasilinear propagation of Gaussian pulses. Comparison between a numerical solution (—) and the approximate nearfield solution (···).

In the same regions in the ω–s–plane, we can approximate the arctan by $\frac{\pi}{2}\text{sgn}(\frac{\omega}{s(\omega-s)})$ when z is large. sgn is here the signum function. Now we are able to invert one of the Fourier transforms:

$$p_2(\mathbf{0},\tau,z) \sim \frac{\rho_0\beta a^4}{8zc_0}\ln\frac{z}{r_0}\frac{\partial}{\partial\tau}\left(\frac{\partial F_1(\tau)\sin\omega_0\tau}{\partial\tau}\right)^2 - \frac{\rho_0\beta a^4}{32zc_0}\int_{-\infty}^{\infty}|\omega|e^{-i\omega\tau}\int_{-\infty}^{\infty}|s(\omega-s)|\tilde{F}(s)\tilde{F}(\omega-s)dsd\omega. \qquad (5.29)$$

We see that this farfield solution has two terms: one term in $\ln z/z$ and one term in $1/z$. The first term will dominate the solution for large z-values, but the second term is still an important correction factor. We thus expect the solution in the farfield to look almost like the time derivative of the square of the time derivative of the time dependency on the source. Compared to the first term, the correction term becomes smaller and smaller as z increases. In figure 5.2, the farfield solution is compared with a numerical solution. We see that the farfield solution including both terms above is a good approximation when $z \gtrsim 10r_0$. We see that the first term alone gives a good first idea of how the solution is, but that both terms are needed in order to get a good approximation. Even as far as at $z = 500r_0$, we see that the second term contributes to the solution.

Eq. (5.29) has both a term in $1/z$ and one term in $\ln z/z$. This is somewhat surprising. From the results of Ref. 25 and 26 it can be deduced that the quasilinear field can be approximated by $A(\tau)(B\ln z/z + C/z)$ where B and C are constants, when the source is Gaussian and monochromatic. In the case discussed here, the constant C has to be replaced by a function of τ. Therefore it is possible to observe both the $\ln z/z$ term and the $1/z$ term experimentally. This is an effect specifically due to a pulsed signal. Such effects are also found in the case of a monochromatic source when this is not Gaussian, for instance with a uniform, circular piston. It is also found as the scattered sound in the theory of scattering of sound by sound. We have thus shown that apart from the geometrical effects of using two non-collinear sources, or the actual shape of the piston, $1/z$-contributions to the solutions can be generated by the shape of the time dependency generated by the source. Such $1/z$ terms are often interpreted as nearfield effects which contribute far into the farfield.

When we compare the near- and farfield solutions of the quasilinear solutions with the similar solutions in the linear case, there is one interesting thing to be noted. The first (or zeroth) order solution in the linear nearfield has a time dependency like $F(\tau)$. In the farfield it is $F'(\tau)$. We thus see that in order to go from the linear to the quasilinear nearfield time dependency, we square and differentiate once. To go from the linear to the leading quasilinear farfield time dependency, we do exactly the same operation.

If other types of time dependencies than Eq. (5.28) are considered, we have to discuss the logarithm-term in Eq. (5.27) again. If for instance

$$F(\tau) = F_1(\tau)\frac{\sin\omega_1\tau + \sin\omega_2\tau}{2}, \qquad (5.30)$$

we would have to split up the integrand into the different contributions ($2\omega_1$, $2\omega_2$, $\omega_1+\omega_2$ and $\omega_1-\omega_2$) and discuss each of them separately.

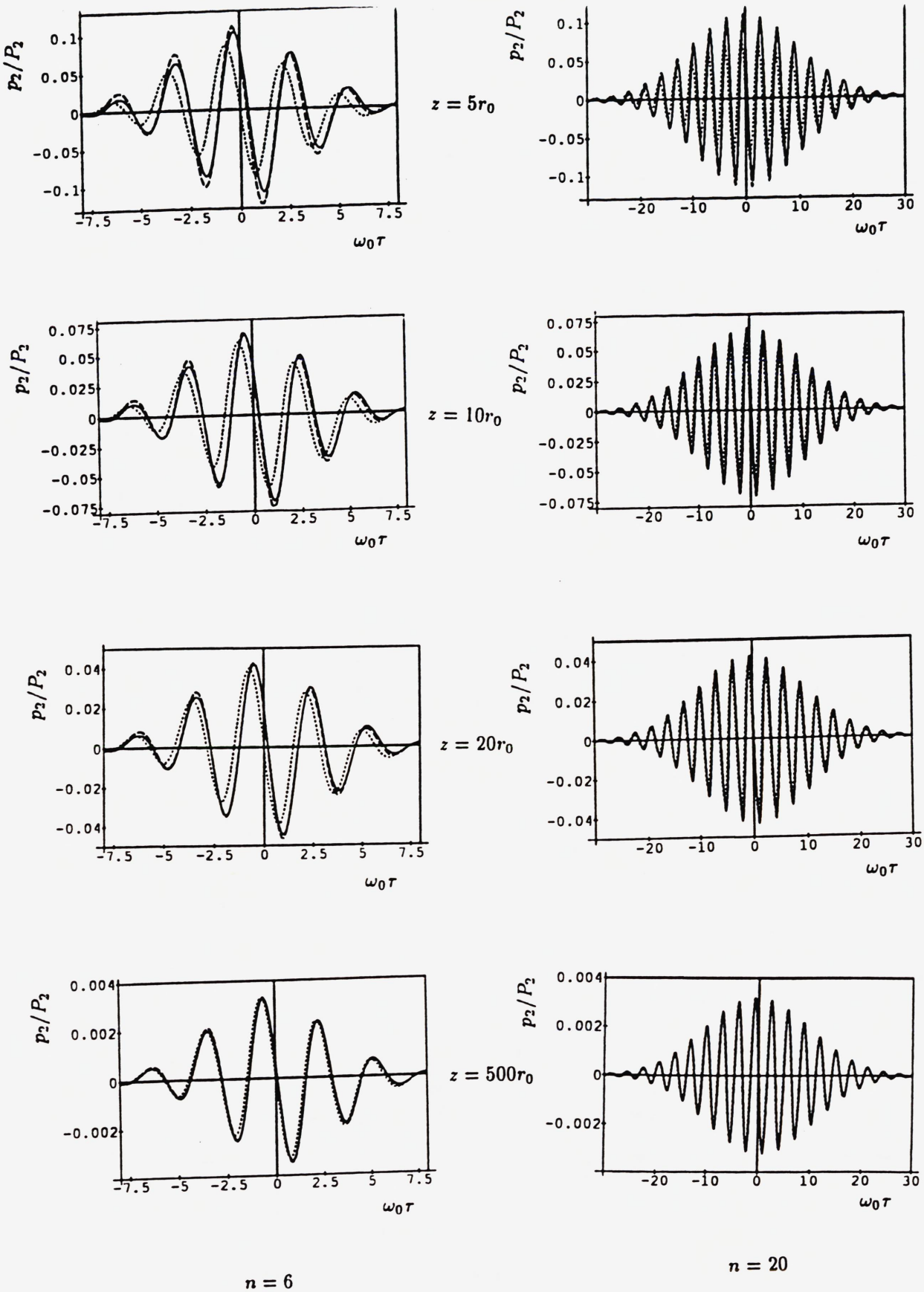

FIG. 5.2. Non-dissipative, three-dimensional, quasilinear propagation of Gaussian pulses. Comparison between a numerical solution (—) and the approximate farfield solution with one term (···) and with two terms (- - -).

5.2.2. General Sources

In section 5.2.1, we obtained asymptotic expressions for the quasilinear nearfield and farfield when the sound is generated by a Gaussian source. We will now generalize these expressions to other types of sources by a perturbation method. First, we look at the nearfield solution. We now introduce non-dimensional variables:

$$\begin{aligned} \mathbf{x} &= a\xi, \\ z &= \frac{\omega_0 a^2}{2c_0}\sigma = r_0\sigma, \\ \tau &= \overline{\tau}/\omega_0, \\ p_i &= \rho_0 c_0^2 \overline{p}_i, \qquad i = 1,2, \end{aligned} \tag{5.31}$$

where ω_0 and a are defined as usual. Introducing this into Eq. (2.16) and neglecting the absorption, gives

$$\left(\overline{\nabla}_\perp^2 - 4\frac{\partial^2}{\partial\overline{\tau}\partial\sigma}\right)\overline{p}_2 = -\beta(k_0 a)^2 \frac{\partial^2}{\partial\overline{\tau}^2}\overline{p}_1^2, \tag{5.32}$$

where $k_0 = \omega_0/c_0$ and $\overline{\nabla}_\perp^2$ is the Laplacian with respect to ξ. We now want to find a solution valid for small σ-values, and therefore expand the linear and the quasilinear pressure:

$$\overline{p}_1 = \sum_{n=0}^{\infty} \sigma^n \overline{p}_1^{(n)} \tag{5.33}$$

$$\overline{p}_2 = \sum_{n=1}^{\infty} \sigma^n \overline{p}_2^{(n)}. \tag{5.34}$$

By assuming σ small, we can introduce these expansions into Eq. (5.32) and solve the equation order by order in σ. The first order equation in σ is now

$$-4\frac{\partial}{\partial\overline{\tau}}\overline{p}_2^{(1)} = -\beta(k_0 a)^2 \frac{\partial^2}{\partial\overline{\tau}^2}(\overline{p}_1^{(0)})^2, \tag{5.35}$$

which is easily solved to get

$$\overline{p}_2^{(1)} = \frac{\beta(k_0 a)^2}{4}\frac{\partial}{\partial\overline{\tau}}(\overline{p}_1^{(0)})^2. \tag{5.36}$$

$\overline{p}_1^{(0)}$ can be found by a similar approach which gives $\overline{p}_1^{(0)} = f(a\xi)F(\overline{\tau}/\omega_0)$. We know from the linear analysis that this is a reasonable result when no replica pulses or strong wakes are present. This is the case for the Gaussian source. Going back to physical variables, we get in that case that Eq. (5.36) is identical to the nearfield solution already obtained for Gaussian sources Eq. (5.25). For sources which generate replica pulses or strong wakes, we cannot assume $\overline{p}_1^{(0)} = f(a\xi)F(\overline{\tau}/\omega_0)$, but have to include these effects in the zeroth order linear solution. For the uniform piston, a good first try for $\overline{p}_1^{(0)}$ on the acoustical axis, should be $\overline{p}_1^{(0)} = F(\overline{\tau}/\omega_0) - F((\overline{\tau} - 1/\sigma)/\omega_0)$. We thus have to expect a solution where we get squaring and time differentiation of the linear zeroth order solution, but we have to include replica pulses in this zeroth order solution.

We also want to derive the leading order farfield solution for p_2. The approach used here, is based on Ref. 27, where Hamilton, Naze Tjøtta and Tjøtta among other things found the approximative equations describing the farfield, and did a deep analysis for the case of a monochromatic source.

The analysis starts with introducing the non-dimensional variables Eq. (5.32). Further, we introduce

$$\begin{aligned} \overline{p} &= \frac{p - p_0}{\rho_0 c_0^2 \epsilon}, \\ T &= \sigma \overline{p}, \\ \mathbf{u} &= \xi/\sigma, \\ \tau_p &= \overline{\tau} - \frac{\xi^2}{\sigma}, \end{aligned} \tag{5.37}$$

where the variables are adjusted in order to fit a spherical, diverging wave. In these variables, the KZK-equation is approximated with a spherical Burgers' equation:

$$\frac{\partial T^{(0)}}{\partial \sigma} = \frac{1}{2\sigma_D \sigma} \frac{\partial}{\partial \tau_p} \left(T^{(0)}\right)^2, \tag{5.38}$$

where $\sigma_D = \frac{2c_0^2}{\beta \epsilon \omega_0^2 a^2}$ is the shock formation distance measured in Rayleigh distances. This equation is asymptotical consistent to the zeroth order in $1/\sigma$, and with $\sigma_D^{-1} \ln \sigma$ finite. We now perform a straight ahead perturbation of $T^{(0)}$:

$$T^{(0)} = T_1^{(0)} + \frac{1}{\sigma_D} T_2^{(0)} + \ldots. \tag{5.39}$$

$T_2^{(0)}$ is now related to the quasilinear approximation, and it satisfies the following equation:

$$\frac{\partial T_2^{(0)}}{\partial \sigma} = \frac{1}{2\sigma} \frac{\partial}{\partial \tau_p} \left(T_1^{(0)}\right)^2. \tag{5.40}$$

This equation can be integrated to give

$$T_2^{(0)} = \int_{\sigma_M}^{\sigma} \frac{1}{2\sigma'} \frac{\partial}{\partial \tau_p} \left(T_1^{(0)}(\sigma')\right)^2 d\sigma' + T_2^{(0)}(\sigma = \sigma_M). \tag{5.41}$$

σ_M is here a matching distance where we have to match the asymptotical farfield solution to a solution valid closer to the source. Unfortunately, we cannot use the nearfield solution discussed above in this matching. These two solutions have no region of overlap. Several ways of doing this matching is discussed in Ref. 27. We can for instance use the output of a computer program computing the quasilinear solution. This is a purely numerical approach. Alternatively, we can assume the nonlinearity so weak that we use the linear solution at the matching distance. This means that $T_2^{(0)} = 0$ at $\sigma = \sigma_M$. In this approach the generation of the quasilinear field in the nearfield has to be negligible. We will not discuss the different matching conditions any further, but proceed to the discussion of the solution in the pulsed case. The linear field $T_1^{(0)}$ can then be found by

a similar approach, or by using the results in chapter 4. Anyhow, we find that at the acoustical axis,

$$T_1^{(0)} = A\frac{\partial}{\partial \tau_p}\overline{F}(\tau_p), \tag{5.42}$$

where $A = \frac{1}{\pi a^2}\iint_{-\infty}^{\infty} f(\mathbf{x}')d\mathbf{x}'$ and $\overline{F}(\tau_p) = F(T\tau_p)$. By introducing this, we get

$$T_2^{(0)} = \frac{A^2((\overline{F}'(\tau_p)^2)'}{2}(\ln\sigma - \ln\sigma_M) + T_2^{(0)}(\sigma = \sigma_M). \tag{5.43}$$

In physical variables, this gives

$$p_2 \approx \frac{\beta\rho_0 c_0 a^4 A^2}{8z}\frac{\partial}{\partial\tau}\left(\frac{\partial F(\tau)}{\partial\tau}\right)^2\left(\ln\left(\frac{z}{r_0}\right) - \ln\left(\frac{z_M}{r_0}\right)\right) + (z_M/z)p_2(z = z_M). \tag{5.44}$$

In the case of a Gaussian source, $A = 1$ and the $\ln z/z$-part of the solution is equal to the similar part of Eq. (5.29) when we assume $F(\tau) = F_1(\tau)\sin\omega_0\tau$. We see that the $1/z$-dependent part of the solution depends on the matching distance chosen, and can therefore not be compared directly with the similar part of Eq. (5.29). Eq. (5.44) also shows that the $1/z$-dependent terms are to be expected for all types of sources, not only the Gaussian source.

The perturbation analysis in this section is done in the absence of absorption. It would also been possible to perform a similar analysis in the dissipative nearfield. The results would then have been a bit more complex in the farfield case, but they would nevertheless have confirmed the results which will be derived in the discussion of the dissipative nearfield in section 5.3.

5.2.3. A Special Case

We will now consider a special case of the quasilinear, non-dissipative, pulsed sound propagation where it is possible to derive an analytical solution not only for the near- or farfield, but uniform i z. This solution is possible when considering some special pulses. These pulses are the same as the ones described in section 4.3.3. The Fourier transforms of these pulses are rational functions in ω, and with no poles on the real ω-axis. When considering a Gaussian source and the solution on the acoustical axis, we can find approximations to the solution which are uniform in z.

We start the discussion with Eq. (5.18) where we put $d = \infty$ to get a plane source and $\mathbf{x} = \mathbf{0}$ in order to get the solution on the acoustical axis:

$$p_2 = \frac{\rho_0 c_0\beta}{4\pi}\iint_{-\infty}^{\infty}\int_0^z \frac{\omega^2 s(\omega - s)\tilde{F}(s)\tilde{F}(\omega - s)e^{-i\omega\tau}dz'dsd\omega}{s(\omega - s)(i\omega - \frac{4c_0}{a^2}(z - z')) - \frac{2z'c_0\omega}{a^2}(\omega + \frac{2zc_0 i}{a^2})}. \tag{5.45}$$

This equation describes the quasilinear solution on the acoustical axis from a plane, Gaussian source which radiates into a three-dimensional, non-dissipative medium. In the analysis above, we proceeded by integrating with respect to z'. Now, we will specify $\tilde{F}$ as the Fourier transform of a function from the class of functions described above, and then integrate with respect to s. As an example of this, we consider the time dependency

$$F(\tau) = e^{-\gamma|\tau|}\sin\omega_0\tau. \tag{5.46}$$

This is the same example as in section 4.3.3, and we will call this pulse an exponential pulse. Now, we Fourier transform this pulse, and insert it into Eq. (5.45). The s-integral can then be written

$$\int_{-\infty}^{\infty} \frac{s(\omega-s)\tilde{F}_1(s)\tilde{F}_1(\omega-s)ds}{(s-s_1)(s-s_2)}$$
$$= \frac{-8\gamma^2\omega_0^2}{\pi}\int_{-\infty}^{\infty} \frac{s^2(\omega-s)^2}{(s+\omega_0+i\gamma)(s+\omega_0-i\gamma)(s-\omega_0+i\gamma)(s-\omega_0-i\gamma)(s-s_1)(s-s_2)} \cdot$$
$$\frac{ds}{(s-\omega-\omega_0-i\gamma)(s-\omega-\omega_0+i\gamma)(s-\omega+\omega_0-i\gamma)(s-\omega+\omega_0+i\gamma)}$$

$$= \frac{-8\gamma^2\omega_0^2}{\pi} 2\pi i \text{ Res(The Integrand)}, \tag{5.47}$$

where the residue is taken at the points $s = \pm\omega_0 + i\gamma$, $s = \omega \pm \omega_0 + i\gamma$ and $s = s_1$. s_1 and s_2 are here defined by

$$s_{1,2} \triangleq \frac{\omega}{2} + \left((\frac{\omega}{2})^2 + \frac{2z'c_0\omega i}{a^2} \cdot \frac{\omega + \frac{2zc_0 i}{a^2}}{\omega + \frac{4(z-z')c_0 i}{a^2}} \right)^{\frac{1}{2}}, \tag{5.48}$$

where s_1 is defined to be the root where $\arg(\,)^{\frac{1}{2}} \in [0, \pi)$. After some algebra we get

$$\begin{aligned}
&= -\frac{2\gamma\omega_0}{\omega}\left[\frac{(\omega_0+i\gamma)(\omega-\omega_0-i\gamma)^2}{(\omega-2i\gamma)(\omega-2\omega_0)(\omega-2\omega_0-2i\gamma)(s_1-\omega_0-i\gamma)(s_2-\omega_0-i\gamma)} \right. \\
&+ \frac{(\omega_0-i\gamma)(\omega+\omega_0-i\gamma)^2}{(\omega-2i\gamma)(\omega+2\omega_0)(\omega+2\omega_0-2i\gamma)(s_1+\omega_0-i\gamma)(s_2+\omega_0-i\gamma)} \\
&+ \frac{(\omega_0+i\gamma)(\omega+\omega_0+i\gamma)^2}{(\omega+2i\gamma)(\omega+2\omega_0)(\omega+2\omega_0+2i\gamma)(s_1+\omega_0+i\gamma)(s_2+\omega_0+i\gamma)} \\
&+ \left. \frac{(\omega_0-i\gamma)(\omega-\omega_0+i\gamma)^2}{(\omega+2i\gamma)(\omega-2\omega_0)(\omega-2\omega_0+2i\gamma)(s_1-\omega_0+i\gamma)(s_2-\omega_0+i\gamma)} \right] \\
&- \frac{16i\gamma^2\omega_0^2 s_1^2 s_2^2}{((s_1+\omega_0)^2+\gamma^2)((s_1-\omega_0)^2+\gamma^2)((s_2+\omega_0)^2+\gamma^2)((s_2-\omega_0)^2+\gamma^2)(s_1-s_2)}.
\end{aligned} \tag{5.49}$$

The last term in Eq (5.49) is completely different from the other four terms. Numerical calculations show that this term is negligible when we consider relative long pulses. More specifically, this means pulses where $\omega_0 \gtrsim 4\gamma$. That means that for pulses that are not extremely short, it is a good approximation to neglect this term. We thus put Eq. (5.49) with the last term neglected, into Eq. (5.45) :

$$p_2 \approx \frac{\rho_o c_0 \beta\gamma\omega_0}{2\pi i}\int_0^z \int_{-\infty}^{\infty} \frac{\omega e^{-i\omega\tau}}{\omega + \frac{4c_0 i}{a^2}(z-z')} \cdot [\cdot]\, d\omega dz', \tag{5.50}$$

where $[\cdot]$ means that parenthesis in Eq. (5.49). We see that the z'-integral still can be evaluated analytically, so within this approximation we have reduced the numerical work to a single integral. Before we evaluate the z'-integral, however, we will take a

look at the ω-integral. The first thing to say here, is that it seems at first sight as if this integrand is a multiple-valued function (from s_1 and s_2). When looking at the terms in the parenthesis as one thing, we will nevertheless see that the roots in s_1 and s_2 are cancelled through quadration. Therefore the integrand as a function of the complex variable ω has no branch points and is an analytical function apart from poles at isolated points. We can therefore once again use the residue-theorem, this time to evaluate the ω-integral. First we note that the singularities on the real axis are removable when we look at all the integrand as one function. These singularities will therefore not contribute to the integral.

We see that the integrand has singularities at some fixed points ($\omega = \pm 2\omega_0 \pm 2i\gamma$). Besides these, there are some singularities which are functions of z and z'. These singularities are also moving from the upper to the lower halfplane, and it is difficult to calculate the contribution to the integral from these poles. These terms correspond to very short transients in the linear case. They are negligible everywhere except close to $\tau = 0$. A necessary condition for this to be fullfilled is that the absolute value of the imaginary part of the singularity is large compared to 2γ. This has at least to be fullfilled where the main contribution to the z'-integral from this singularity will be.

We assume now that this is the case here, and expect our solution not to be valid close to $\tau = 0$. We have to separate the two cases $\tau < 0$ and $\tau > 0$. When $\tau < 0$, we get:

$$p_2 \approx \frac{\rho_0 c_0 \beta \gamma \omega_0}{2\pi i} \int_0^z 2\pi i \text{Res}(\text{The Integrand}) dz', \tag{5.51}$$

where the residue is taken at the points $\omega = \pm 2\omega_0 + 2i\gamma$ and $\omega = 2i\gamma$. After some algebra this reduces to:

$$\begin{aligned} p_2 \approx\ & \rho_0 c_0 \beta \gamma^2 \frac{1}{2}(\omega_0^2 + \gamma^2) e^{2\gamma\tau} \int_0^z \frac{dz'}{\gamma(\omega_0^2+\gamma^2) + \frac{2c_0}{a^2}((z-z')\omega_0^2 + (z+z')\gamma^2) + \frac{4zz'c_0^2\gamma}{a^4}} \\ & + \frac{1}{2}\rho_0 c_0 \beta e^{2\gamma\tau} \\ & \text{Re}\left\{ e^{-2i\omega_0\tau} i(\omega_0 + i\gamma)^3 \int_0^z \frac{dz'}{(\omega_0+i\gamma)^2 + \frac{2c_0 i}{a^2}(z+z')(\omega_0+i\gamma) - \frac{4zz'c_0^2}{a^4}} \right\}. \end{aligned} \tag{5.52}$$

Now we evaluate the z'-integral easily:

$$\begin{aligned} p_2 \approx\ & \frac{\frac{1}{2}\rho_0 c_0 \beta \gamma^2 (\omega_0^2+\gamma^2) e^{2\gamma\tau} \ln \frac{\gamma(\gamma + \frac{2zc_0}{a^2})^2 + \gamma\omega_0^2}{(\omega_0^2+\gamma^2)(\gamma + \frac{2zc_0}{a^2})}}{\frac{2c_0}{a^2}(\gamma^2 - \omega_0^2) + \frac{4zc_0^2\gamma}{a^4}} \\ & + \frac{1}{2}\rho_0 c_0 \beta e^{2\gamma\tau} \text{Re}\left\{ \frac{i e^{-2i\omega_0\tau}(\omega_0+i\gamma)^3}{\frac{2c_0 i}{a^2}(\omega_0+i\gamma) - \frac{4zc_0^2}{a^4}} \right. \\ & \left. \left[\ln \sqrt{\frac{z^2 + 2\Phi_1 z + \Phi_1^2 + \Psi_1^2}{\Phi_1^2 + \Psi_1^2}} + i(\arctan \frac{\Phi_1}{\Psi_1} - \arctan \frac{z+\Phi_1}{\Psi_1}) \right] \right\}, \end{aligned} \tag{5.53}$$

where Φ_1 and Ψ_1 are defined by

$$\Phi_1 = \mathrm{Re}\left\{\frac{(\omega_0+i\gamma)^2+\frac{2zc_0i}{a^2}(\omega_0+i\gamma)}{\frac{2c_0i}{a^2}(\omega_0+i\gamma)-\frac{4zc_0^2}{a^4}}\right\},$$

$$\Psi_1 = \mathrm{Im}\left\{\frac{(\omega_0+i\gamma)^2+\frac{2zc_0i}{a^2}(\omega_0+i\gamma)}{\frac{2c_0i}{a^2}(\omega_0+i\gamma)-\frac{4zc_0^2}{a^4}}\right\}.$$

We note here that the singularity in z in the first term of Eq. (5.53) is removable so that it does not make any complications for the results. Eq. (5.53) is thus an approximative solution of the quasilinear problem Eq. (2.16) valid on the acoustical axis. The solution is valid when using a plane, Gaussian source which radiates into a non-dissipative medium, and where the time dependency is an exponential pulse. The solution is uniform in z, and valid for long pulses in the sense $\omega_0 \gtrsim 4\gamma$. Eq. (5.53) is the solution valid for negative τ-values. Unfortunately, it is not valid very close to $\tau = 0$. When τ is positive, the approach is similar and the result is:

$$\begin{aligned} p_2 \approx\ & \frac{\frac{1}{2}\rho_0 c_0 \beta\gamma^2(\omega_0^2+\gamma^2)e^{-2\gamma\tau}\ln\left|\frac{-\gamma(-\gamma+\frac{2zc_0}{a^2})^2-\gamma\omega_0^2}{(\omega_0^2+\gamma^2)(-\gamma+\frac{2zc_0}{a^2})}\right|}{\frac{2c_0}{a^2}(\gamma^2-\omega_0^2)-\frac{4zc_0^2\gamma}{a^4}} \\ & + \frac{1}{2}\rho_0 c_0 \beta e^{-2\gamma\tau}\mathrm{Re}\left\{\frac{ie^{-2i\omega_0\tau}(\omega_0-i\gamma)^3}{\frac{2c_0i}{a^2}(\omega_0-i\gamma)-\frac{4zc_0^2}{a^4}}\right. \\ & \left.\left[\ln\sqrt{\frac{z^2+2\Phi_2 z+\Phi_2^2+\Psi_2^2}{\Phi_2^2+\Psi_2^2}}+i(\arctan\frac{\Phi_2}{\Psi_2}-\arctan\frac{z+\Phi_2}{\Psi_2})\right]\right\}, \end{aligned} \tag{5.54}$$

$$\Phi_2 = \mathrm{Re}\left\{\frac{(\omega_0-i\gamma)^2+\frac{2zc_0i}{a^2}(\omega_0-i\gamma)}{\frac{2c_0i}{a^2}(\omega_0-i\gamma)-\frac{4zc_0^2}{a^4}}\right\},$$

$$\Psi_2 = \mathrm{Im}\left\{\frac{(\omega_0-i\gamma)^2+\frac{2zc_0i}{a^2}(\omega_0-i\gamma)}{\frac{2c_0i}{a^2}(\omega_0-i\gamma)-\frac{4zc_0^2}{a^4}}\right\}.$$

In order to obtain these approximative solutions, we have to evaluate the z'-integral as a Cauchy principal value integral. This seems consistent because the Fourier integrals that we have interchanged with the z'-integral must be considered as Cauchy principal value integrals from the theory of Fourier analysis. Numerical results show that the solution Eqs. (5.53) and (5.54) is very good when the pulse is not too short and when $|\tau| \gtrsim \pi/\omega_0$, as expected.

When $\gamma = 0$, we get a monochromatic onsource signal. Then Eqs. (5.53) and (5.54) both reduce to

$$p_2 = \frac{1}{4}\rho_0\beta\omega_0^2 a^2 \mathrm{Re}\left\{\frac{e^{-2i\omega_0\tau}}{1+\frac{z}{r_0}i}\left(\ln\sqrt{\frac{z^2+r_0^2}{r_0^2}}+i\arctan\frac{z}{r_0}\right)\right\}. \tag{5.55}$$

This is the same result as can be deduced from Ref. 28 to be the exact solution. It is thus a demonstration of the validity of Eqs. (5.53) and (5.54) when the pulses are long.

In Eqs. (5.53) and (5.54), there are two basic restrictions. First, when we evaluated the s-integral, we did an approximation which led to a long-pulse approximation. Next, when the ω-integral was evaluated, a new approximation made the solution not valid very close to $\tau = 0$. We therefore have to find the solution close to $\tau = 0$ in another way. One approach is then to do as elsewhere in this work. We then have to solve a double or triple integral numerically. Alternatively, we can still use the long-pulse-approximation obtained after the s-integration above. Then the z'-integral could have been evaluated before the ω-integral. Then we finally end up with only the ω-integral. This integral can be solved numerically. Thus, within the long-pulse-approximation, we can reduce the numerical work to a single integral close to $\tau = 0$, and elsewhere we have an analytical expression.

When considering the exponential pulse chosen as the time dependency, it is perhaps not so strange, that the analytical approximation breaks down close to $\tau = 0$. At $\tau = 0$, the exponential pulse is just continuously differentiable once. When keeping in mind that the farfield formula Eq. (5.29) contains a second derivative of the time dependency $F(\tau)$, we have to expect problems when $F(\tau)$ is not that smooth. Else we comment that when making nearfield approximation of Eqs. (5.53) and (5.54), we get the same result as when the exponential pulse is substituted into the general nearfield expression. The $\ln z/z$ term of the general farfield solution can also be obtained in a similar way when we use the long pulse approximation $\omega_0 \gg \gamma$. Unfortunately, this approach cannot be generalized to find the off-axis solution, or to a dissipative media. It can, however, be generalized to focused Gaussian sources. The calculations will then be similar to the ones above. It is also possible to use other, and smoother functions from the class of functions discussed above. Whether the solution then will be valid also close to $\tau = 0$, is an open question.

5.3. Three-dimensional, Dissipative Nearfield

Now, we will include dissipation in the discussion of the quasilinear solution. Here, we will just consider pulses of the type

$$F(\tau) = F_1(\tau) \sin \omega_0 \tau, \tag{5.56}$$

where $F_1(\tau)$ as usual is varying slowly compared to the sinusoid. In chapter 3 and 4, we have seen that at first, when $z < L_0$, we have to expect much of the same behaviour as in the non-dissipative case, except for an amplitude correction similar to the one used in the monochromatic theory. When $z > L_0$, we have seen that completely different behaviours are expected, and that the behaviour of the pulse is closely related to the bandwidth of the generated pulse. We will now look at the same effects in the quasilinear case. In this section, we consider the dissipative nearfield, $z < L_0$, and we postpone the discussion of the dissipative farfield, $z > L_0$, to the next section. In both these sections, we will use pulses with Gaussian envelope functions in the numerical examples. These pulses are chosen because they are narrowbanded, and therefore realistic pulses to use in physical experiments. Besides this, they are easier to treat numerically than most other realistic pulses.

In this section, we will demonstrate how Eqs. (5.25) and (5.29) can be applied in the dissipative nearfield after a minor adjustment. Most of the frequencies contributing

to the signal are close to $\omega = \pm 2\omega_0$. We therefore try to adjust the amplitudes of the asymptotical expressions by multiplying by a factor $\exp(-4z/L_0)$. The factor 4 comes from the fact that the absorption distance related to the frequency $2\omega_0$ is $L_0/4$. We thus get the following nearfield formula:

$$p_2(\mathbf{0},\tau,z) \sim \frac{\beta\rho_0 c_0 z}{2} e^{-\frac{4z}{L_0}} \frac{\partial}{\partial\tau} F^2(\tau), \quad z \ll r_0. \tag{5.57}$$

In the same way, the farfield formula will be

$$\begin{aligned} p_2(\mathbf{0},\tau,z) \sim e^{-\frac{4z}{L_0}} \Bigg(& \frac{\rho_0\beta a^4}{8zc_0} \ln\frac{2zc_0}{\omega_0 a^2} \frac{\partial}{\partial\tau} \left(\frac{\partial F_1(\tau)\sin\omega_0\tau}{\partial\tau} \right)^2 \\ & - \frac{\rho_0\beta a^4}{32zc_0} \int_{-\infty}^{\infty} |\omega| e^{-i\omega\tau} \int_{-\infty}^{\infty} |s(\omega-s)| \tilde{F}(s)\tilde{F}(\omega-s) ds d\omega \Bigg), \quad z \gg r_0. \end{aligned} \tag{5.58}$$

We now want to examine how large z can be compared to L_0 if these expressions still are to be valid.

In figure 5.3 we have put $L_0 = 0.1r_0$. The observation points chosen are $z = 0.005r_0$, $z = 0.01r_0$ and $z = 0.02r_0$. At these distances, Eq. (5.25) is valid in the non-dissipative case. We see that at $z = 0.005r_0$ and partly also at $z = 0.01r_0$, the modified nearfield formula Eq. (5.57) predicts very well the numerically calculated signal. At $z = 0.02r_0$, the nearfield formula tends to underestimate the signal. The signal now also tends to oscillate more slowly than closer to the source. This is the same tendency as was found in the linear solution. Because the non-dissipative nearfield formula is valid at observation points up to $z \approx 0.2r_0$, the deviation at $z = 0.02r_0$ is caused by the absorption alone. $z = 0.02r_0$ means here also $z = 0.2L_0$. When we remember that the absorption distance for the second harmonic $2\omega_0$ is $L_0/4$, we see that the observation point is now almost at the absorption distance of the second harmonic. It is therefore not surprising that such a simplified modelling of the absorption breaks down. We also see from figure 5.3 that different pulse-lengths seem to give the same conclusion in this case. Thus we conclude that the simplified modelling of the absorption is valid up to $z \lesssim 0.1L_0$.

The farfield approximative solution Eq. (5.58) is examined in figure 5.4. The absorption distance is here chosen to be $L_0 = 100r_0$. The conclusion is almost the same here as in the nearfield case. At $z = 20r_0 = 0.2L_0$, we see a small tendency of stretching in the numerical solution compared to the approximative solution. The amplitude is well described by the approximative solution. When $z = 50r_0 = 0.5L_0$, Eq. (5.58) underestimates the signal. Besides this, the stretching of the signal is significant, especially for the shorter pulse. This effect is not described by the approximative solution. We therefore have to expect that Eq. (5.58) is valid when $10r_0 \lesssim z \lesssim 0.3L_0$. The first restriction here comes from the farfield (diffraction) formula and the second restriction from the nearfield (absorption) formula. We see in the figure that at $5r_0$ it is not so good because of the diffraction, and at $50r_0 = 0.5L_0$, the absorption has started the changing of the waveform.

5.4. Three-dimensional, Dissipative Farfield

We now proceed to the dissipative farfield, $z > L_0$. In this region, there are several earlier models. Most of these models simplify the discussion by assuming a collimated,

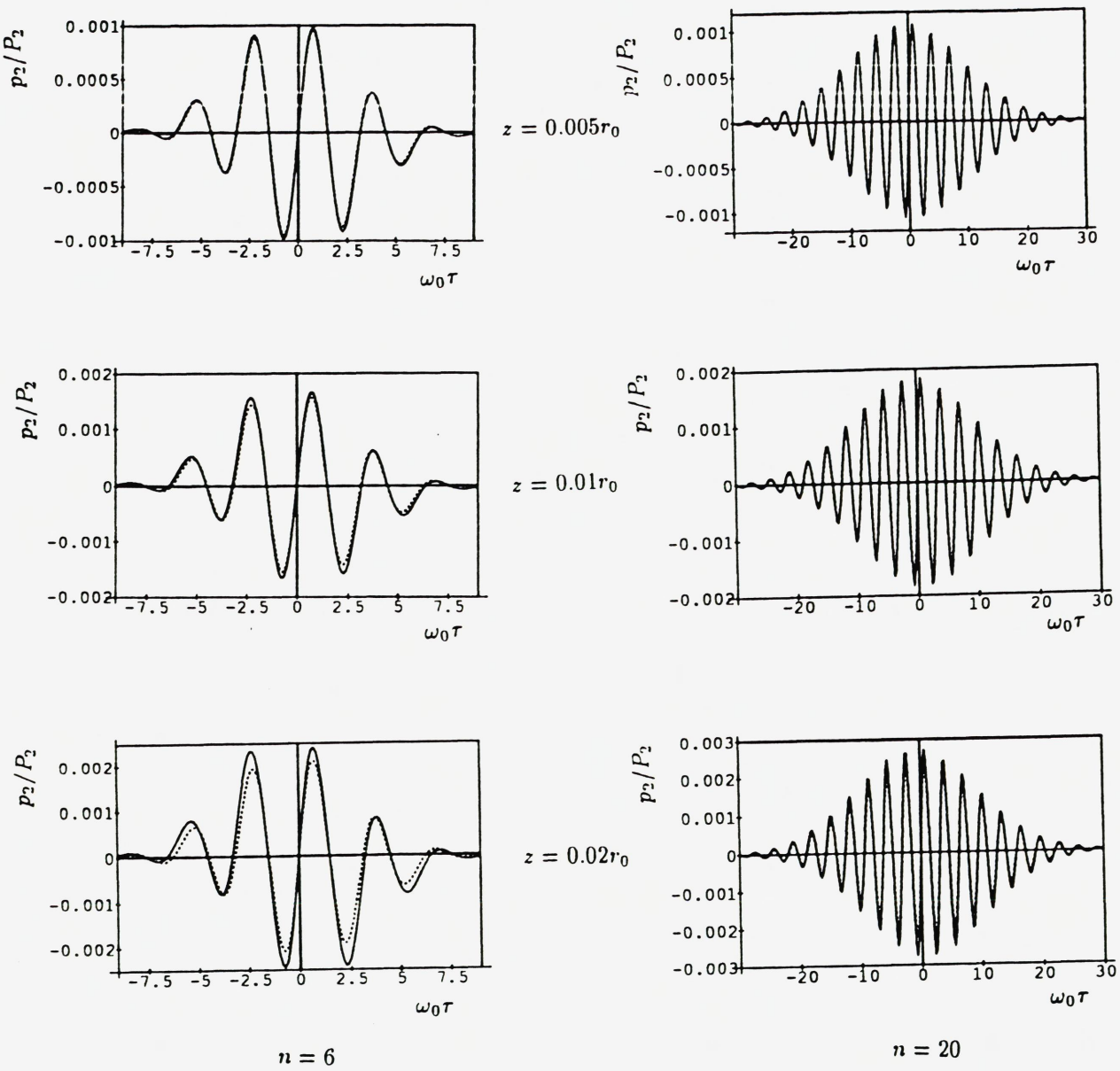

FIG. 5.3. Dissipative, three-dimensional, quasilinear propagation of Gaussian pulses when $L_0 = 0.1r_0$. Comparison between a numerical solution (—) and the approximate nearfield solution ($\cdots$).

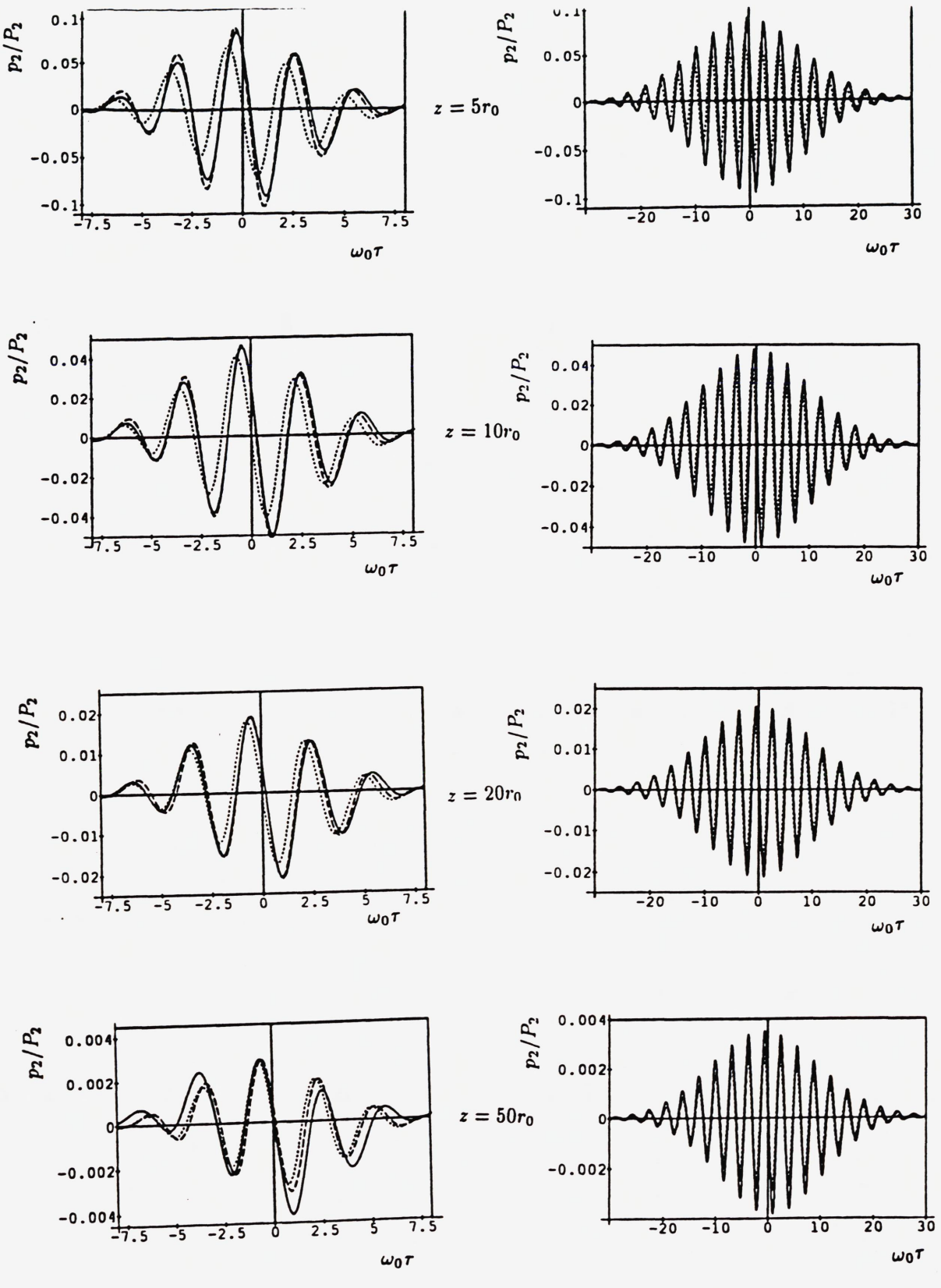

FIG. 5.4. Dissipative, three-dimensional, quasilinear propagation of Gaussian pulses when $L_0 = 100r_0$. Comparison between a numerical solution (—) and the approximate solution valid when $r_0 \ll z \ll L_0$, with one term (· · ·) and with two terms (- - -).

linear nearfield. We start this section by a brief introduction of some of them. Afterwards, we proceed to a discussion of the dissipative farfield within the present model.

5.4.1. Earlier Models

The discussion of the quasilinear, dissipative farfield of a pulsed signal dates back to Berktay[8] in 1965. Two years after Westervelt's famous paper on parametric, acoustic arrays[29], Berktay used those ideas to find a solution in this region. The model assumed a plane collimated linear solution

$$p_1 = \rho_0 c_0^2 f(\mathbf{x}) F_1(\tau) \sin \omega_0 \tau e^{-\frac{z}{L_0}}. \tag{5.59}$$

The absorption in the linear solution is treated by an exponential factor, and the diffraction is neglected. The approximation done in the modelling of the absorption can here perhaps be used because most of the quasilinear sound is generated from the linear sound field in the dissipative nearfield. We have earlier seen that the absorption behaves approximately like this there. The diffraction in the linear solution is neglected in Berktay's model. We therefore have to expect the ratio r_0/L_0 to play an important role. The idea further is now that the quasilinear field is split up in a term with frequencies close to the second harmonic, and a lowfrequency term, just like in Eq. (5.9). In the dissipative farfield, the highfrequency term is damped away by the absorption. The solution will therefore just consist of a lowfrequency term. Finally, Berktay found that

$$p_2 \sim \frac{\beta \rho_0 S L_0}{16\pi z} \frac{\partial^2 F_1^2(\tau)}{\partial \tau^2}, \tag{5.60}$$

where a minor correction of the formula according to Moffett and coworkers[30] is included. In order to do the decoupling between the high- and the lowfrequency band, it has to be assumed that the pulse in some sense is quite long. In the formula above, a uniform source with general shape was assumed. S is then defined to be the crossectional area of the collimated beam from this source. Thus for instance for a circular piston, we get $S = \pi a^2$. In the present work, we have used Gaussian sources in the numerical examples. From the definition of S, we could be led to believe that for a non-uniform source, $S = \iint f(\mathbf{x}) d\mathbf{x}$. In order to get numerical agreement between Berktay's solution and a numerical solution later, it is, however, necessary to define $S = \iint f(\mathbf{x})^2 d\mathbf{x}$ and thereby look at S more as an energy than an area.

Eq. (5.60) has later been verified experimentally by Moffett and coworkers[9, 30, 31]. The solution far away from the acoustical axis, and when the absorption is very weak, was also discussed in these works. They found that in both these cases, the signal looked like the first- and not like the second derivative of the envelope function squared. The off-axis result was first mentioned by Westervelt in Ref. 32. Several others, like Pace and Ceen[10] and Grinberg and coworkers[11], have worked more on these problems, and have among other things rederived these results. Stepanishen and Koenigs[12] later derived a formula which describes the transition from the second derivative to the first derivative of the envelope function squared when the observation point moves from the acoustical axis to a point far outside the acoustical axis.

Common to all these works is the collimated linear nearfield. Different authors have assumed the linear field in different ways, but generally, both diffraction and absorption

of the linear field are treated in an ad hoc manner. The treatment of these effects in the quasilinear field is also partly just ad hoc. Because none of these models have a consistent treatment of absorption and diffraction, the different models cannot confirm each other. From experiments we can see that they describe the reality in some cases. The limitations of these models, however, have not been discussed in the above-mentioned works. Questions left open from these works are

- How short can a pulse be before Berktay's formula breaks down?
- How does the diffraction (through the fraction r_0/L_0) affect the result?
- For what ranges of z, except that $z \gg L_0$, is Berktay's formula valid?
- When does the solution off axis look like the first derivative of the envelope function squared?

The model in this work includes diffraction and absorption in a consistent way. It can therefore be used to analyse these questions. We will try to answer them by looking at numerical results where no approximations are made except the choice of the quasilinear approximation of the KZK-equation as the mathematical model.

5.4.2. Results on the Acoustical Axis

We now want to analyse the dissipative farfield mostly by using numerical results. The solution on the acoustical axis will be discussed in this section, and the off-axis results are postponed to the next section.

As mentioned above, the pulses used will be Gaussian, and therefore relatively narrowbanded:

$$F(\tau) = e^{-\left(\frac{\omega\tau}{n}\right)^2} \sin \omega_0 \tau. \tag{5.61}$$

We will use the four values $n = 6, 20, 50$ and 100 in order to discuss the dependency of the pulse-length on the solution. First, we will study the effect of increasing z. In figure 5.5, we see a long pulse ($n = 50$) at four different different distances. The absorption is here relatively strong, with $L_0 = 0.1r_0$. Berktay's solution is therefore expected to be valid since the diffraction is not a too dominating effect in the generation of the quasilinear pulse. We see that when $z = 5L_0$, the rapid oscillations from the second harmonic-related part of the solution have not been completely damped away. Except for these small ripples, Berktay's solution predicts very well the waveform received. At $z = 10L_0$, the small ripples are damped away, and Berktay's formula provides almost perfect agreement. When z is increased more, to $100L_0$ and to $1000L_0$, this picture changes. We see now that with increasing z, the pulse tends to be stretched out and more damped compared with Berktay's solution. With z increased more, this effect is even more dominating. The explanation of this is that we now get $z = O(L_s)$, where L_s is the slow absorption distance defined from the characteristic frequency of the envelope function of the pulse. For the Gaussian pulses discussed here, a good estimate for L_s is $L_s = (n/2)^2 L_0$. When we approach this distance, the absorption starts to damp away the highest of the low frequency components of the signal. Therefore we get a similar stretching of the signal as we got in the linear case. This effect can also be given a slightly different explanation. When $z \gg L_0$, the linear part of the signal is damped away,

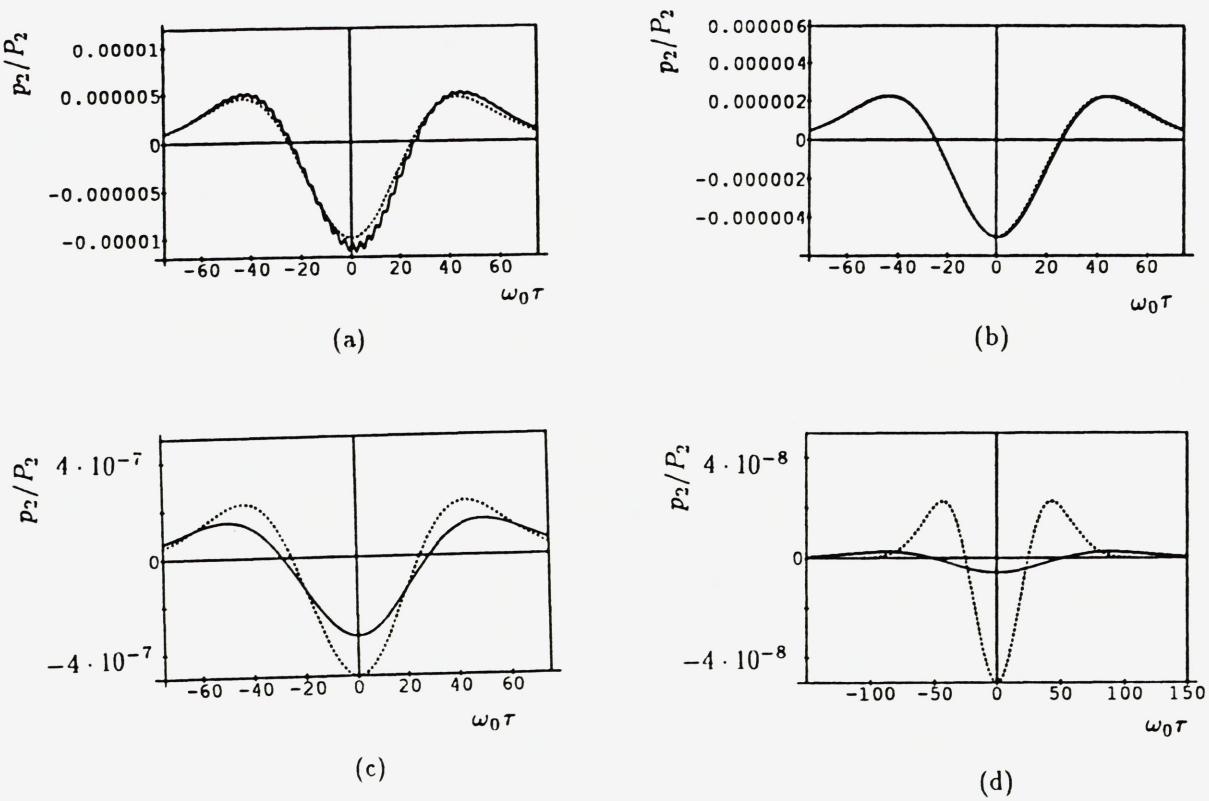

FIG. 5.5. Comparison between a numerical solution (—) and Berktay's solution (···) when z is increasing. $n = 50$, $L_0 = 0.1r_0$, $z = 5L_0$ (a), $z = 10L_0$ (b), $z = 100L_0$ (c) and $z = 1000L_0$ (d)

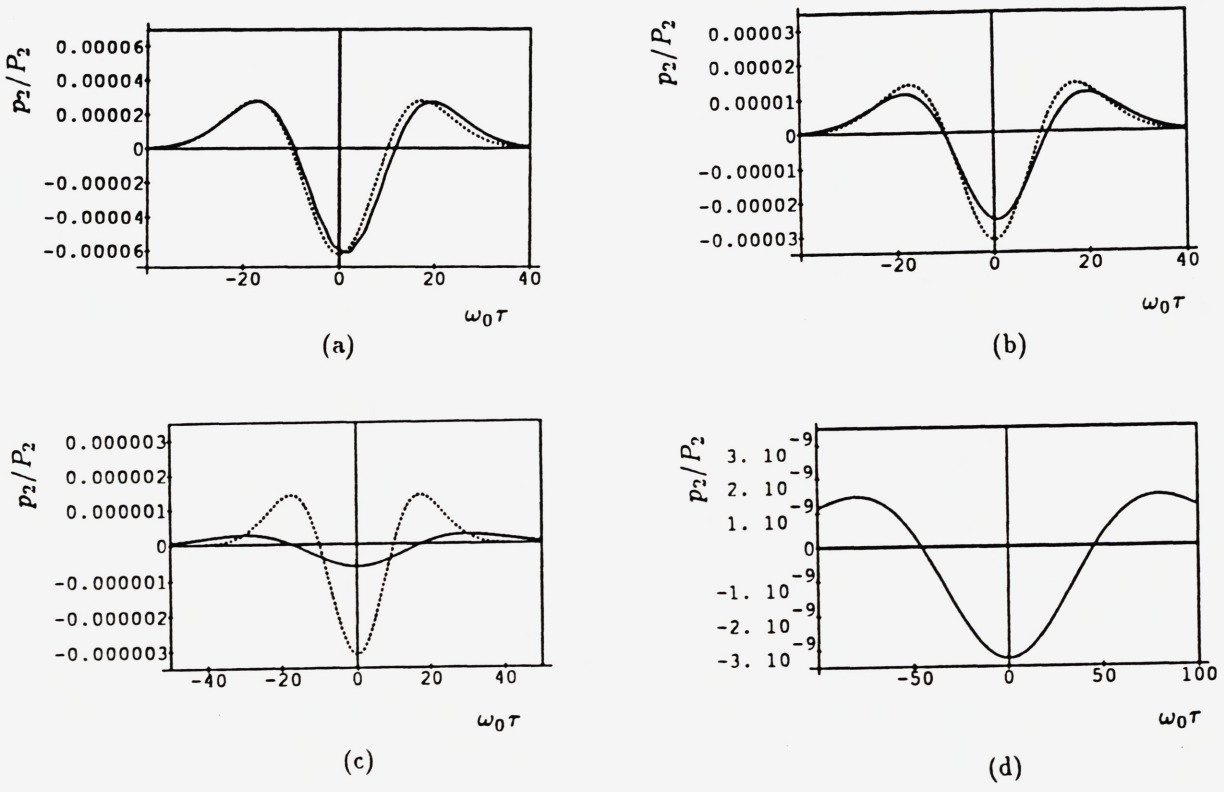

FIG. 5.6. Comparison between a numerical solution (—) and Berktay's solution ($\cdots$) when z is increasing. $n = 20$, $L_0 = 0.1r_0$, $z = 5L_0$ (a), $z = 10L_0$ (b), $z = 100L_0$ (c) and $z = 1000L_0$ (d)

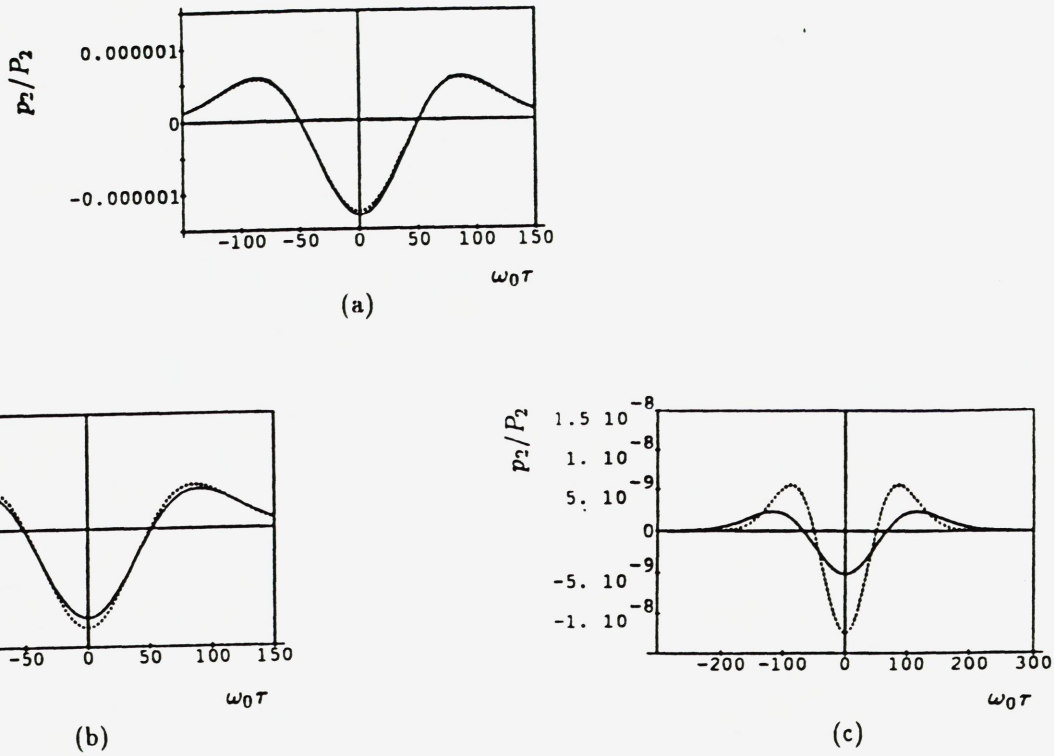

FIG. 5.7. Comparison between a numerical solution (—) and Berktay's solution (···) when z is increasing. $n = 100$, $L_0 = 0.1r_0$, $z = 10L_0$ (a), $z = 100L_0$ (b) and $z = 1000L_0$ (c)

since the Gaussian pulse is relatively smallbanded. The generation of the quasilinear field is therefore ended, and the quasilinear signal propagates like a linear signal. A low-frequent linear signal affected by the absorption tends to stretch out, according to chapter 3. Therefore Berktay's formula cannot predict the correct waveform any longer. Summing up, we can say that Berktay's formula is an intermediate formula valid when $L_0 \ll z \ll L_s$.

In figure 5.6, we see the same as in figure 5.5 except that the pulse is shorter. The conclusion is the same except that the widening of the pulse and the overestimation by Berktay's formula starts much earlier. This is because L_s now is smaller than in figure 5.5. Therefore, it confirms the conclusion that Berktay's formula is valid when $L_0 \ll z \ll L_s$. Note here that the pulse in fact starts to stretch out already at $z = 10L_0$. At $z = 5L_0$, it has not completely lost the ripples from the high frequencies. We therefore see that the pulse is now so short that Berktay's solution only predicts the signal well at the distances where the lowfrequent part dominates the signal for the first time.

Figure 5.7 is the same as figure 5.5 and figure 5.6, except that the pulse now is longer. We then see that Berktay's solution is valid for higher z-values than above, but that it finally starts failing. Figure 5.8 describes for a short pulse the transition from a highfrequent signal satisfying Eq. (5.57) to a lowfrequent signal which stretches out. We see here that Berktay's solution never predicts the correct signal. The explanation of this is that the pulse now is so short that the situation $L_0 \ll z \ll L_s$ is impossible. Therefore Berktay's solution cannot give the correct answer.

We have now analysed the validity of Berktay's solution for increasing z-value and for different pulse-lengths. Now we will consider the effect of different absorption relative

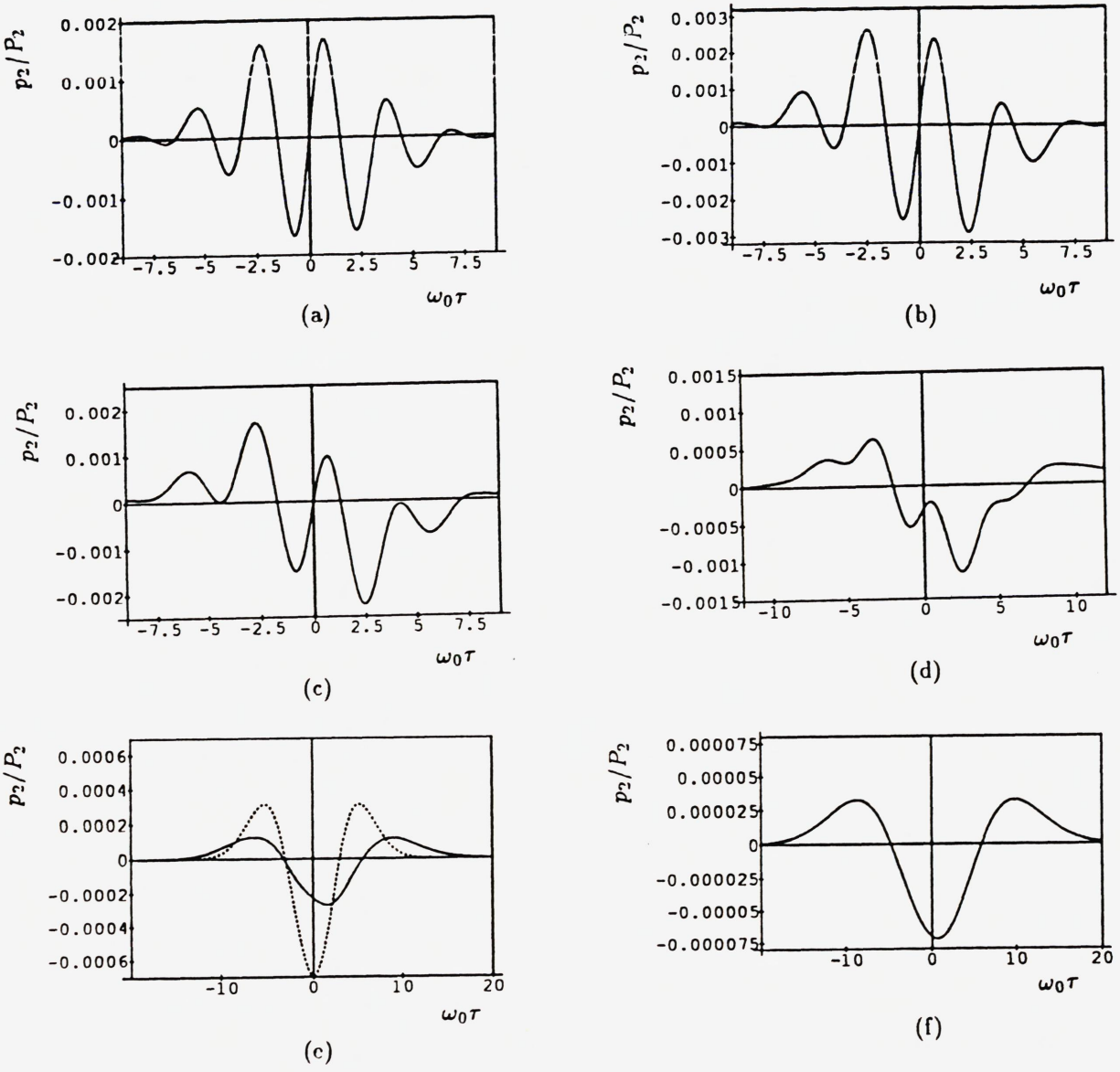

FIG. 5.8. The evolution of a short Gaussian pulse ($n = 6$) for increasing z-values (—). The dotted curve is Berktay's solution. $L_0 = 0.1r_0$, $z = 0.1L_0$ (a), $z = 0.5L_0$ (b), $z = L_0$ (c), $z = 2L_0$ (d), $z = 5L_0$ (e) and $z = 10L_0$ (f).

to the diffraction. We thus want to study the influence on Berktay's formula of the ratio L_0/r_0. In figure 5.9, the intermediate pulse is chosen. The distance $z = 10L_0$ has been chosen because Berktay's solution then was approximately valid above. We see that when the absorption is getting weaker so that the diffraction plays a more important role, the signal is not the second derivative of the envelope function squared any longer. It looks like it starts to approach the first derivative of the envelope function squared instead. This was the effect described above, and suggested by Moffett and coworkers. What is perhaps more surprising, is that Berktay's solution breaks down also when the absorption is too strong ($L_0 = 0.01r_0$). It then seems like the signal undergoes the same change as when the absorption gets very weak ($L_0 = 100r_0$). This is more difficult to explain. One would believe that the plane collimated model underlying in Berktay's formula should be very good when the absorption is so strong that the signal hardly feels the diffraction. This does not turn out to be the case here. It is perhaps easier to understand that the amplitude of the signal cannot be predicted by Berktay's solution when the absorption is very strong than to understand that the shape of the signal cannot be estimated. This is because the generation of the quasilinear solution by the linear solution does not last that long. Therefore the quasilinear solution in the farfield should have lower amplitude when $L_0 \ll r_0$ than when $L_0 = O(r_0)$. Anyway, we conclude that Berktay's formula again seems to be an intermediate formula. This time it is valid when the absorption distance is not too small or too great compared with the Rayleigh distance.

The effect of diffraction is also shown in figure 5.10. This time, a longer pulse has been chosen, and also even weaker absorption than in figure 5.9 is considered. Here, the observation point is $z = 20L_0$. It is just at this point the solution starts the damping and stretching effect not described by Berktay's solution. We know from above that Berktay's solution is approximately valid when $L_0 = 0.1r_0$. We see in this figure that when the absorption is too strong ($L_0 = 0.01r_0$), Berktay's solution is not so good any longer. We see, however, that for this long pulse, Berktay's solution is more robuste for changes in r_0/L_0 than the shorter pulse ($n = 20$). When the absorption gets very weak ($L_0 \gg r_0$), we see that the signal looks more like the first- than the second derivative of the envelope function squared. This confirms the prediction made by Moffett and coworkers.

Now, how do these results fit in with the experimental results obtained by Moffett and coworkers[30, 31, 9]? The easiest results to compare with, are the results in Refs. 30 and 31 where the pulses propagate in carbon tetrachloride. Dissipative effects are much more dominating in carbon tertachloride than in water. This means that it is possible to get the situation $z \gg L_0$ when using a relatively small tank in the experiment. In these actual experiments, $L_0 = 1.92$cm and the largest z–value used in the experiment was 42cm. The Rayleigh distance was $r_0 = 136$cm. This means that $L_0 = 0.014r_0$, which is quite strong absorption. There are two different pulses used. In Ref. 30, measurements are shown for the longer pulse. This pulse contains a little more than 40 oscillations and is therefore longer than all the pulses considered here. We therefore have to expect that Berktay's formula is approximately valid. This is because the pulses were not so much affected by the ratio r_0/L_0 when they were quite long. Besides, the largest z–distance where it was measured was about $z = 21.8L_0$. At this distance we still have $L_0 \ll z \ll L_s$. Therefore the stretching of the pulse was not observed. Therefore, it was

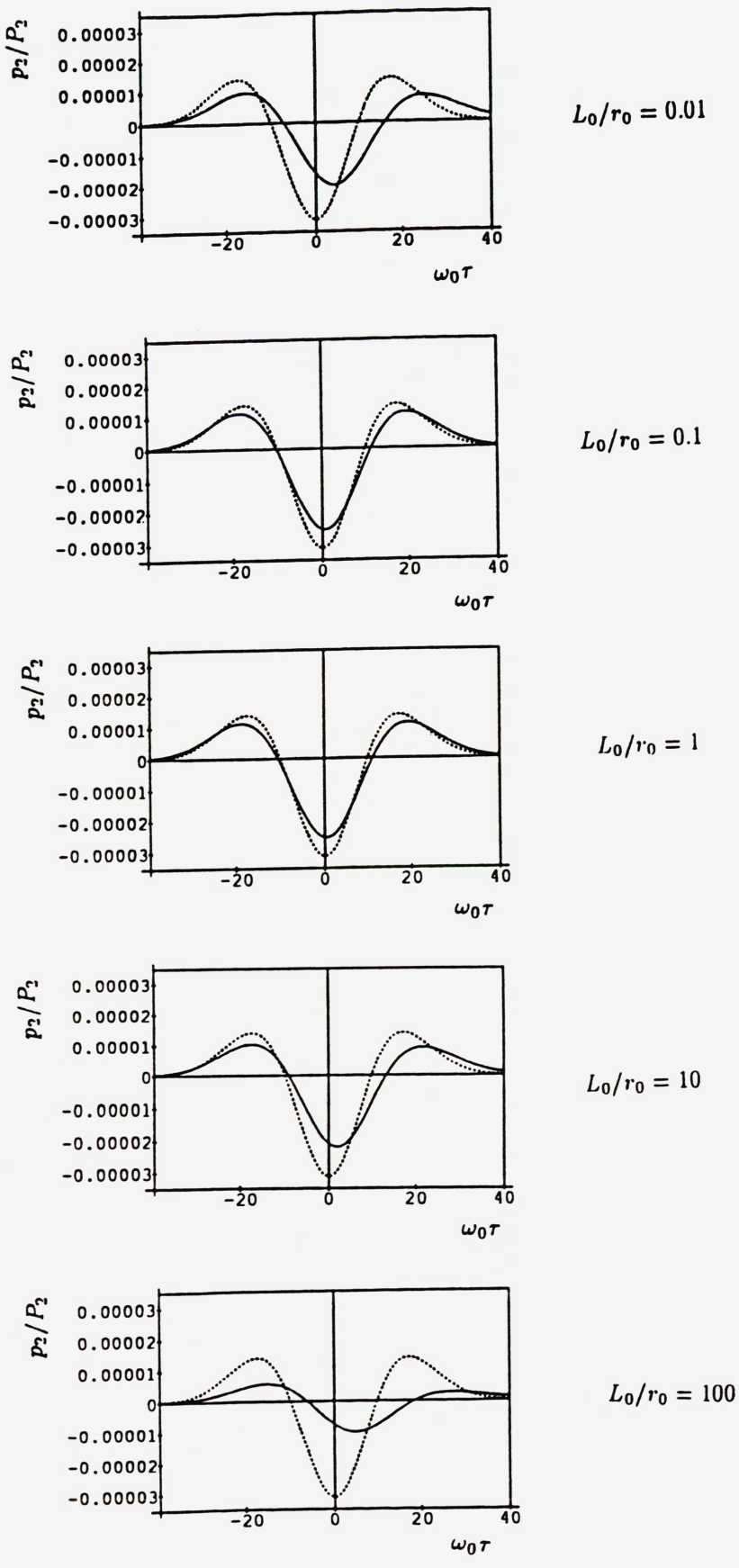

FIG. 5.9. Comparison between a numerical solution (—) and Berktay's solution ($\cdots$) for different values of L_0/r_0. $n = 20$, $z = 10L_0$.

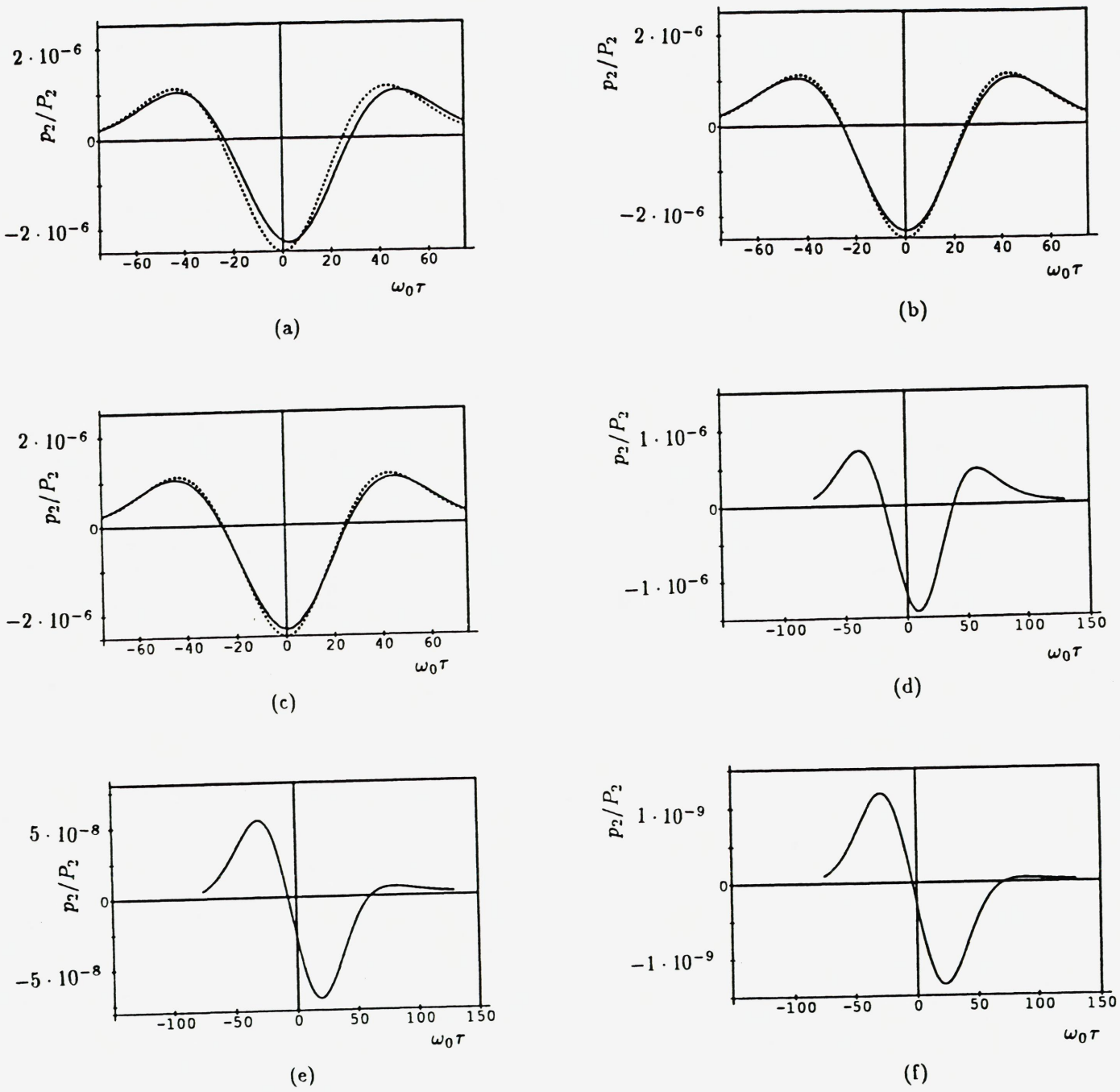

FIG. 5.10. Comparison between a numerical solution (—) and Berktay's solution (···) for different values of L_0/r_0. $n = 50$, $z = 20L_0$, $L_0 = 0.01r_0$ (a), $L_0 = 0.1r_0$ (b), $L_0 = r_0$ (c), $L_0 = 100r_0$ (d), $L_0 = 10^4 r_0$ (e) and $L_0 = 10^6 r_0$ (f).

not surprising that Moffet et. al. found that Berktay's formula predicted their measured results quite well. In Ref. 31, they used a shorter pulse with about 20 oscillations. This pulse therefore is roughly as long as the Gaussian pulse with $n = 50$. The other parameters in the experiment are the same as the ones referred above. Again, Moffett et. al. found that the results are quite well predicted by Berktay's formula. However, if we look carefully at figure 5 in Ref. 31, we see that at the end of the signal, it is a little bit stretched and damped compared with Berktay's formula. It is perhaps difficult to say if this effect is real or if it is caused by experimental errors. However, this is the same result as we found for the long pulse ($n = 50$) when $L_0 = 0.01r_0$ in figure 5.10. Therefore, this experimental result can perhaps confirm that when the dissipative effects are too strong compared to the diffraction, Berktay's solution does not predict the received signal so well any longer.

Experimental results related to this topic were also recently published by Cervenka and Alais[33]. Their experiment was performed in water, and they got $L_0 = 1.36r_0$. The measured signals were received at $z = 2.7L_0$ and then lowpass-filtered in order to throw away the rapid oscillations both in the linear and in the quasilinear solution. Therefore, that case is a bit different from the case studied in this work. It is therefore difficult to say if the results obtained here still are valid. They used two different pulses, one Gaussian and one with an envelope function like a chirp. The Gaussian pulse would correspond to an n–value somewhere between 150 and 200. We will therefore expect Berktay's formula to be valid when $z \gg L_0$. They find an agreement with Berktay's solution that is not quite as good as expected from the analysis in this work. This can perhaps be explained by the fact that they did not measure in the region where $z \gg L_0$ but instead they lowpass-filtered their signal in order to study the self-demodulation. We know from the analysis of the dissipative nearfield that if a similar approach was used there, they would not find Berktay's formula, but instead a signal proportional to $\frac{\partial F_1^2(\tau)}{\partial \tau}$ since we then also have $z \ll r_0$. We can therefore not expect Berktay's solution to predict the lowfrequent part of the signal perfectly until in the dissipative farfield ($z \gg L_0$). The other pulse used in their experiment was a pulse with an envelope function like a chirp. This means that it in fact is a series of different pulses where the next pulse is generated just after the previous one. The first pulse contains many oscillations, and the following pulses are shorter and shorter. The last pulses are so short that it is difficult to distinguish between the different pulses. They find that Berktay's formula predicts quite well what happens for the first pulses, but that it gradually starts failing when the pulses get shorter. They call this a saturation effect, but cannot explain it. From the work done here, we can say that Berktay's formula breaks down because the pulses are too short. Then we have found that Berktay's solution highly overestimates the signal. Therefore it is not surprising that they observe this saturation.

5.4.3. Results outside the Acoustical Axis

As mentioned above, several persons have predicted that the signal will look like the first derivative of the envelope function squared when the observation point is far outside the acoustical axis. These models assume that Berktay's solution is valid on the acoustical axis. In figure 5.11, we see the change in the waveform when we leave the acoustical axis. When $x = 0$, Berktay's solution is approximatively valid. We see here

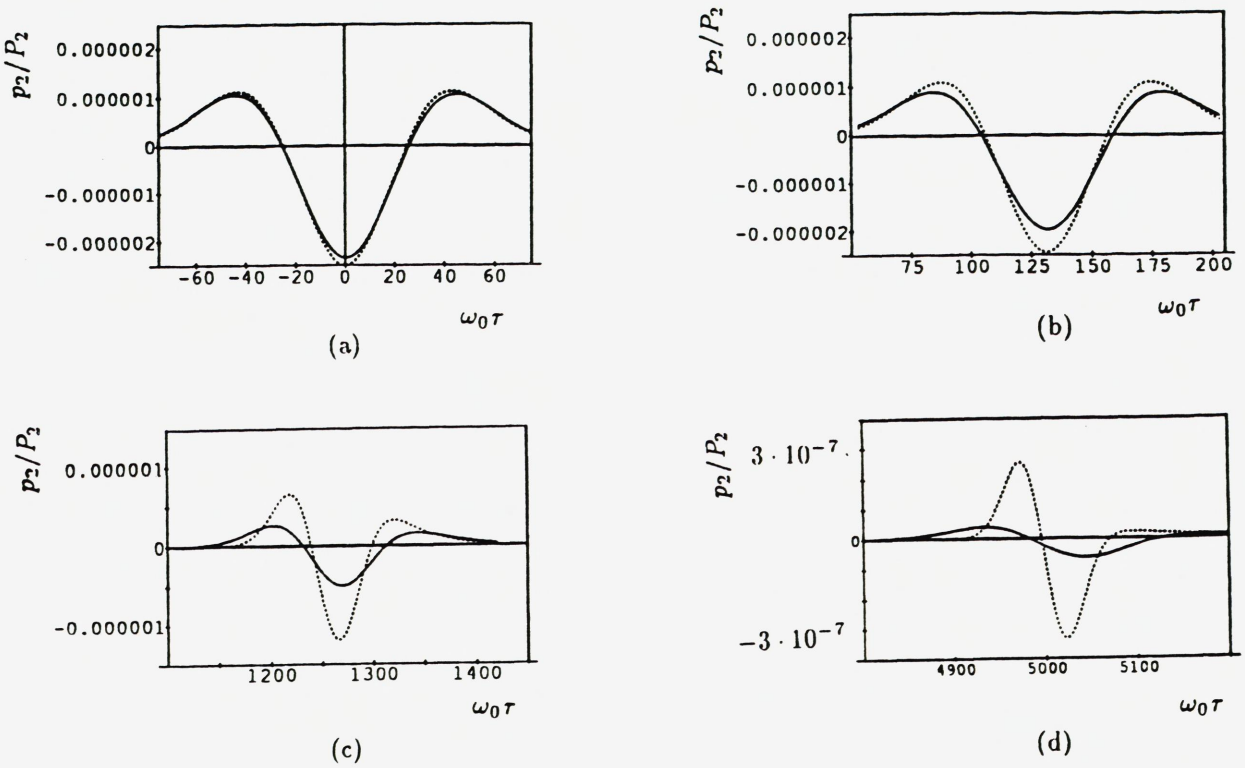

FIG. 5.11. Comparison between a numerical solution (—) and Stepanishen and Koenigs' solution ($\cdots$) for increasing x. $n = 50$, $z = 20L_0$, $L_0 = 0.1r_0$, $x = 0$ (a), $x = 16a$ (b), $x = 50a$ (c) and $x = 100a$ (d).

how the waveform approaches the first derivative of the envelope function squared when x increases. Stepanishen and Koenigs' solution is plotted in the same figure. Before plotting, we made an approximation similar to the approximations in the waveforms performed by the parabolic approximation. This is consistent with their model because they started with Westervelt's equation for the pressure, and then made a quasilinear approximation of this equation. Naze Tjøtta and Tjøtta[3] showed that this equation has the same validity as the parabolic approximation and thus the KZK-equation. We see that the numerical solution and Stepanishen and Koenig's solution describe the shape of the solution in about the same way. The arrival times of the two solutions are slightly different. Most discrepancy is there, however, in the prediction of the amplitude, where the solution of Stepanishen and Koenigs clearly overestimates the numerical solution. This is perhaps not very surprising. The solution of Stepanishen and Koenigs does not include different directivity functions due to different sound sources. Their predictions were made for uniform sources. It is therefore not surprising to find a difference in directivity when using a non-uniform source like the Gaussian.

Figure 5.12 shows a similar change from on-axis to off-axis observation point as figure 5.11. The difference is now that $L_0 = 100r_0$. This means that at the acoustical axis, Berktay's solution is not valid. Despite this, the signal looks like the first derivative of the envelope function squared when the observation point is far outside the acoustical axis. It thus seems like the signal will look like the first derivative of the envelope function squared when the observation point is far outside the acoustical axis. Both when Berktay's solution is valid on the acoustical axis, and when it is not valid, this

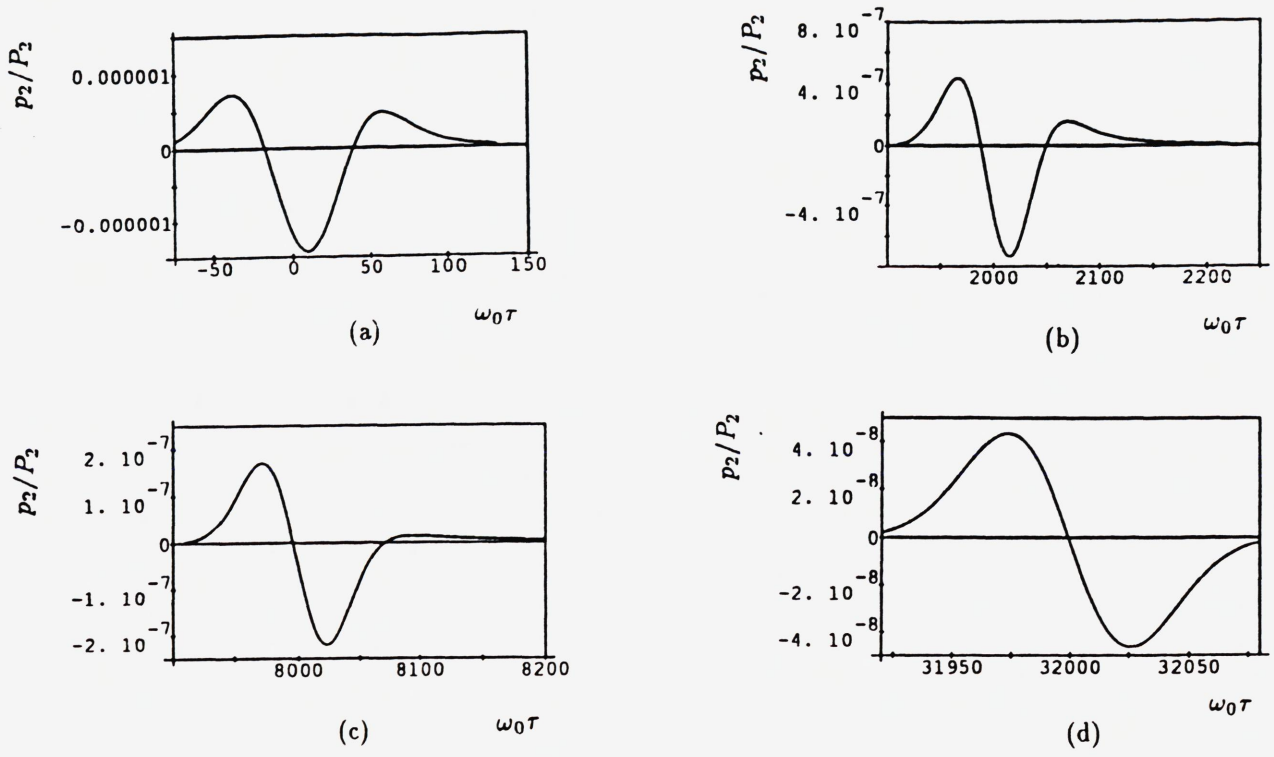

FIG. 5.12. Off-axis solution for increasing x. $n = 50$, $z = 20L_0$, $L_0 = 100r_0$, $x = 0$ (a), $x = 2000a$ (b), $x = 4000a$ (c) and $x = 8000a$ (d).

seems to be the case.

5.5. General Remarks

We have now discussed the quasilinear, pulsed sound propagation with special emphasis on the sound generated by a Gaussian source. The method presented makes it possible to calculate the quasilinear sound pressure both in the absence of dissipative effects, in the dissipative nearfield and in the dissipative farfield. Asymptotical expressions are presented for the case of no absorption, both for Gaussian and more general sources. The transition from the dissipative nearfield to the dissipative farfield is discussed, and earlier models for the sound propagation in the dissipative farfield are analyzed. The analysis is made for Gaussian sources. Therefore probably some of the results about the interaction between diffraction and dissipation have to be modified when using other types of sources. There is, however, no reason to expect qualitatively different results in the dissipative farfield when using for instance a uniform circular piston instead of a Gaussian source.

The time dependency in the analysis above has been

$$F(\tau) = F_1(\tau)\sin\omega_0\tau, \tag{5.62}$$

where $F_1(\tau)$ is a slowly varying envelope function compared with the sinusoid. Both the numerical and the asymptotical discussion could also have been done for other types of time dependencies. We can for instance use a time dependency like

$$F(\tau) = F_1(\tau)\frac{\sin\omega_1\tau + \sin\omega_2\tau}{2}, \tag{5.63}$$

where the two frequencies ω_1 and ω_2 are relative high, but quite close to each other. We then get a pulsed version of the parametric array, where frequencies close to the sum and difference frequencies $\omega_2 \pm \omega_1$ are generated together with the frequencies close to each second harmonic, and the very low frequencies. This leads to various regions where the pulse changes form depending on what frequencies are still present in the signal and what frequencies which are damped away. This means that the asymptotical and numerical models can be used for quite general time dependencies.

Chapter 6

Numerical Solution of Integrals

Now, we will describe how the integrals present in this work have been solved numerically. Many of the integrals presented above are Fourier integrals, at least in one of the integration variables. One of these integrals will be discussed in detail. This is Eq. (2.20) which describes the quasilinear sound field from a pulsed Gaussian source which radiates into a dissipative fluid. The source can be plane or weakly curved. This integral has been chosen because it was the most difficult one, and because many of the other integrals in the present work can numerically be treated as special cases.

6.1. Integral on Non-dimensional Form

We thus want to consider the numerical calculation of the integral

$$p_2 = \frac{\beta\rho_0 c_0}{4\pi}\iint_{-\infty}^{\infty}\int_0^z \omega^2 s(\omega-s)\tilde{F}(s)\tilde{F}(\omega-s)e^{-i\omega\tau-\frac{D\omega^2}{2c_0^3}z}\times \frac{\exp\left(\frac{Ds(\omega-s)}{c_0^3}z'\right)}{s(\omega-s)(i\omega(1-\frac{z}{d})(1-\frac{z'}{d})-\frac{4(z-z')c_0}{a^2})-\frac{2z'c_0\omega}{a^2}(\omega(1-\frac{z}{d})+\frac{2zc_0 i}{a^2})}\times \exp\left[\frac{-i\omega\mathbf{x}^2\left(s(\omega-s)(\frac{2}{a^2}+\frac{i\omega}{2dc_0}(1-\frac{z'}{d}))+\frac{z'\omega}{a^2}(\frac{2c_0 i}{a^2}-\frac{\omega}{d})\right)}{s(\omega-s)(i\omega(1-\frac{z}{d})(1-\frac{z'}{d})-\frac{4(z-z')c_0}{a^2})-\frac{2z'c_0\omega}{a^2}(\omega(1-\frac{z}{d})+\frac{2zc_0 i}{a^2})}\right]dz'dsd\omega.. \tag{6.1}$$

First, we have to introduce non-dimensional variables, coordinates and parameters in this integral. We first introduce a charateristic angular frequency ω_0, which in the case of several characteristic frequency scales, should be chosen as the highest characteristic frequency present. We then define Rayleigh distance and absorption distance in the usual way:

$$r_0 = \frac{\omega_0 a^2}{2c_0}, \tag{6.2}$$

$$L_0 = \frac{2c_0^3}{D\omega_0^2}. \tag{6.3}$$

Next, we define the non-dimensional variables, coordinates and parameters which are used in the numerical work:

$$\omega = \omega_0\overline{\omega},$$

$$
\begin{aligned}
s &= \omega_0 \overline{s}, \\
\widetilde{F}(\omega) &= \overline{\widetilde{F}}(\overline{\omega}), \\
\tau &= \overline{\tau}/\omega_0, \\
z &= r_0 \overline{z}, \\
z' &= r_0 \overline{z}', \\
x &= a\overline{x}, \\
L_i &= r_0/L_0, \\
d_i &= r_0/d,
\end{aligned}
\tag{6.4}
$$

where

$$
x = |\mathbf{x}| \tag{6.5}
$$

as usual. This means that L_i is the Rayleigh distance measured in absorption distances. This quantity is 0 if there is no absorption. Similarly, d_i is the Rayleigh distance measured in focal distances, which means that a plane source has $d_i = 0$. z and z' are now scaled to the Rayleigh distance, and the transverse coordinate x is scaled to the source radius a. The frequency variables and the time coordinate are all scaled to the fast characteristic frequency ω_0. We now introduce the above-mentioned quantities in the integral Eq. (6.1). For simplicity, we neglect the overlining in the non-dimensional quantities:

$$
p_2 = \frac{\beta\rho_0 c_0^2}{8\pi}\left(\frac{\omega_0 a}{c_0}\right)^2 \iint_{-\infty}^{\infty}\int_0^z \omega^2 s(\omega-s)\widetilde{F}(s)\widetilde{F}(\omega-s)e^{-i\omega\tau - L_i(\omega^2 z - 2s(\omega-s)z')} \times \frac{\exp\left[\frac{-i\omega x^2(s(\omega-s)(2+i\omega d_i(1-zd_i))+\omega z'(i-\omega d_i))}{s(\omega-s)(i\omega(1-zd_i)(1-z'd_i)-2(z-z'))-z'\omega(\omega(1-zd_i)+zi)}\right] dz'dsd\omega}{s(\omega-s)(i\omega(1-zd_i)(1-z'd_i)-2(z-z'))-z'\omega(\omega(1-zd_i)+zi)}. \tag{6.6}
$$

To reduce the numerical work, it is important to make use of any symmetries in the integrand. In this case, the integrand $G(\omega, s, z')$ has two important symmetries when we assume that $\widetilde{F}$ is the Fourier transform of a real function. These symmetries are

$$
G(-\omega, -s, z') = G(\omega, s, z')^*, \tag{6.7}
$$

$$
G(\omega, \omega - s, z') = G(\omega, s, z'), \tag{6.8}
$$

where $*$ means the complex conjugate. This means that we can rewrite the integral Eq. (6.6) as

$$
p_2 = \frac{\beta\rho_0 c_0^2}{2\pi}\left(\frac{\omega_0 a}{c_0}\right)^2 \int_0^{\infty}\int_{\omega/2}^{\infty}\int_0^z \mathrm{Re}\left\{\omega^2 s(\omega-s)\widetilde{F}(s)\widetilde{F}(\omega-s)e^{-i\omega\tau - L_i(\omega^2 z - 2s(\omega-s)z')} \times \frac{\exp\left[\frac{-i\omega x^2(s(\omega-s)(2+i\omega d_i(1-zd_i))+\omega z'(i-\omega d_i))}{s(\omega-s)(i\omega(1-zd_i)(1-z'd_i)-2(z-z'))-z'\omega(\omega(1-zd_i)+zi)}\right] dz'dsd\omega}{s(\omega-s)(i\omega(1-zd_i)(1-z'd_i)-2(z-z'))-z'\omega(\omega(1-zd_i)+zi)}\right\}. \tag{6.9}
$$

This integral can be solved numerically in several ways. Here we will describe two ways of doing it. The first approach uses an integration routine called DCUHRE (formally called ADMINT)[34]. This was the way most of the results presented in chapter 5 have been computed. This routine is, however, not very good on the integration domain present in the integral above. When the work on this dissertation was almost finished, a new integration routine (DCUTET) had been developed[35]. This routine was better on the present problem, and therefore we also give a short introduction to the use of this routine.

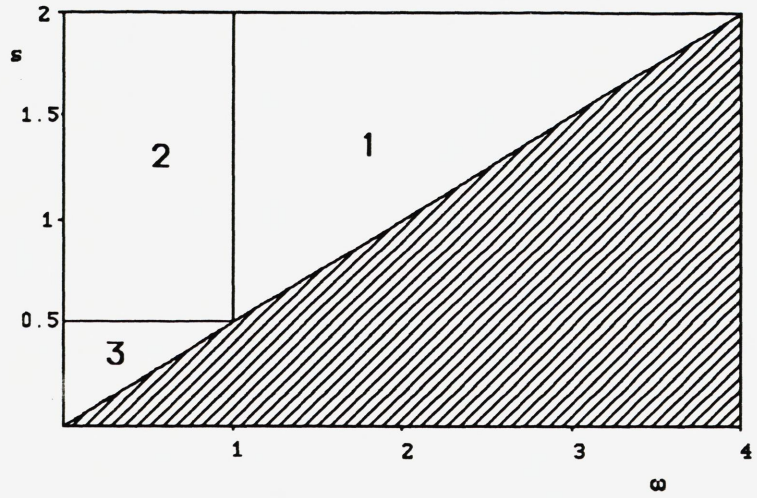

FIG. 6.1. Integration domain and the different integration sections projected into the ω-s-plane.

6.2. Numerical solution, first approach

As mentioned above, the integral in Eq. (6.9) was solved by using DCUHRE. This is an adaptive integration routine for solving multiple integrals (up to 15 dimensions) of vector functions over a finite hyperrectangle. We see at once that Eq. (6.9) does not have this structure for two reasons. First, the integration domain is infinite, and then the projection of the integration domain into the ω -s -plane is an (infinite) triangle and not a rectangle as required by DCUHRE. The perhaps simplest way to overcome this, is to extend the integrand to the region $\omega > 0$, $s > 0$ by defining it as zero outside the integration domain. Then we can use DCUHRE on the integral when we truncate the integration domain at some large values of ω and s. This is not a good way of doing it, because we in this way introduce a discontinuity in the integrand. The adaptive routine will then evaluate very carefully around the discontinuity in order to obtain the desired error estimate. This will be very timeconsuming.

An alternative to this process is to introduce the transformation $s = \omega s_1$ and integrate with respect to ω and s_1. This will transform the integration domain over to an infinite hyperrectangle. We can then proceed by truncating this infinite domain so that we get a finite hyperrectangle. There are, however, some reasons for not using this method. We know from the definition of $\widetilde{F}(\omega)$ that this function often has maximums somewhere close to $\omega = \pm 1$. This means that two regions in the integration domain will be specially important. This is the region around $\omega = 2$, $s = 1$ and the region around $\omega = 0$, $s = 1$. The first region gives the contribution to the terms similar to second harmonics and sum frequency, while the last one gives the contributions similar to the difference frequency of a parametric array, as described in chapter 5. This latter contribution is the one important for instance when discussing Berktay's solution. The transformation indicated above sends the area around $\omega = 0$, $s = 1$ to infinity. It is therefore inconvenient to use that transformation when the low frequencies corresponding to Berktay's solution are discussed.

A solution of this problem is shown in figure 6.1, where we introduce a borderline at $\omega = 1$. We then use the transformation on the region $\omega > 1$ (region 1). The other

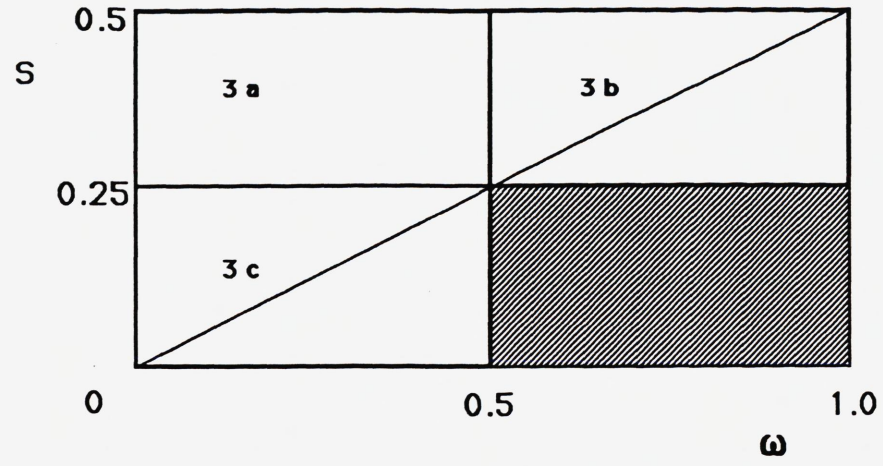

FIG. 6.2. Integration section 3 divided into 3 sub-sections.

region will be divided into two regions: $s > 1$ (region 2) and $s < 1$ (region 3). We have thus infinite hyperrectangles in section 1 and 2, while section 3 still is a triangular region in the ω, s -plane. The main contribution to the integrand will come from either section 1 or section 2 (or both), while section 3 just will be a small correction. The idea is now to compute section 3 after the main contribution to the integral has been found. As shown in figure 6.2, section 3 is divided into 3 new sections: $\omega < 0.5$ and $s > 0.25$ (3a), $\omega > 0.5$ (3b), $\omega < 0.5$ and $s < 0.25$ (3c). Section (3a) is a hyperrectangle and can therefore be calculated. Sections 3b and 3c are extended to hyperrectanguler sections by letting the integrand be 0 outside the actual region. These two sections can be calculated with a larger errorbound than the main contribution because we here are just calculating a small correction to that main contribution. Therefore, this algorithm will not be as time-consuming as the one mentioned first in this section.

The algorithm thus starts with finding out if the main contribution to the integral comes from section 1 or section 2. This is determined by the ratio z/L_0. If this ratio is less than one, most of the rapid oscillations with frequencies around $\omega = 2$ still are present and will dominate the solution. It is therefore natural to look for the main contribution in section 1. If $z/L_0 > 1$, most of the rapid oscillations are damped away, and the solution will be dominated by the low frequencies. The main contribution is therefore expected to be in section 2. Section 1 is now truncated at a reasonable high s-value, and section 2 at reasonable high s_1 and ω–values. The truncation values used in most of the computations are $\omega = 3$ and $s = s_1 = 1.5$. Further, section 2 is divided into section 2a which contains the region of section 2 where $\omega < 1/2$, and section 2b which contains the rest of section 2. When section 2 contains the main contribution, we will look for that in section 2a which contains the lowest frequencies. These regions are illustrated in figure 6.3, where s on the vertical axis is for the region $\omega < 1$ and s_1 for the region $\omega > 1$. The algorithm can thus be described

- Read the desired parameters, and the relative errorbound required in the integration.
- Decide the truncation values used in ω, s and s_1
- Determine whether the main contribution comes from section 1 or section 2a.

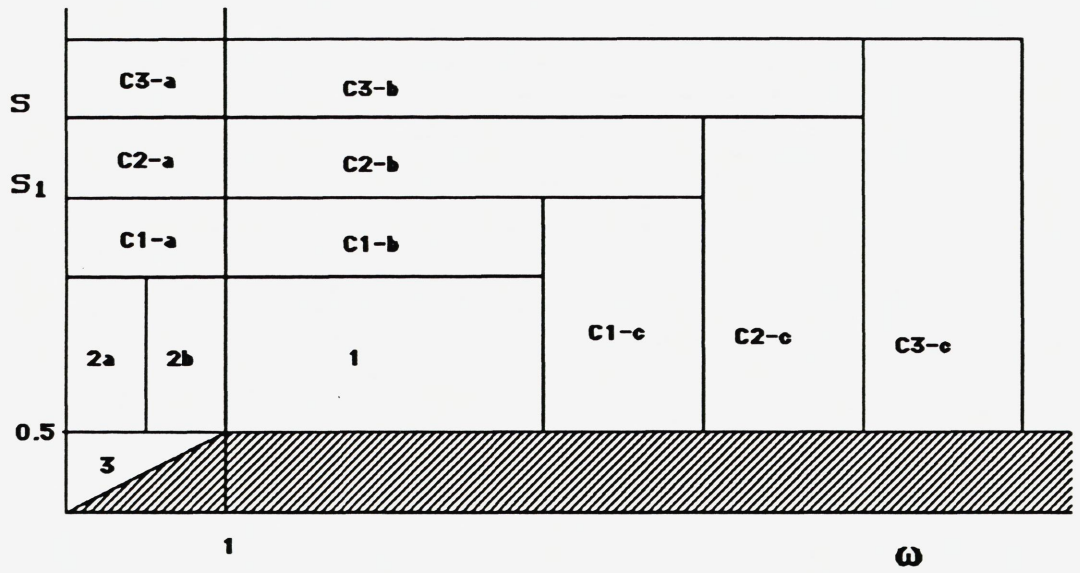

FIG. 6.3. All integration sections in the computation.

- Calculate the main contribution with the desired relative errorbound.
- Calculate section 2b and either section 2a or 1 (the one which not contains the main contribution). The relative errorbound is the required one, and the absolute errorbound is the prescribed errorbound multiplied with the absolute value of the value of the integral of the regions already calculated.
- Calculate section 3a, 3b and 3c with the same type of errorbound as in the calculation of section 2b.

By using the absolute error bound in this way, we do not calculate small corrections to the integral with a greater accuracy than necessary. If we for instance require three significant numbers in the answer, it is not necessary to calculate a contribution which will just be a correction to the last significant number, with 3 significant numbers. Now, we have hopefully got a good estimate of the integral. However, there can be significant contributions to the integral in the regions which are not discussed above. Therefore we will calculate the integral also in some correction regions C1, C2, ... which are illustrated in figure 6.3. The algorithm of the computation of these corrections is as follows:

- Calculate the sections C1-a,b and c. The relative errorbound is the required one, and the absolute errorbound is the prescribed errorbound multiplied with the absolute value of the value of the integral of the regions already calculated.
- If the correction computed does not make a significant change in the computed integral, then quit. Else, compute new corrections (C2, C3, ...) until the corrections are not significant.

When the Gaussian pulses were used, an Alliant fx/8 using one processor used typically 20 minutes of CPU time to calculate one curve with 150 points when using this algorithm. This problem is very good for parallel processors. This means that for instance 8 processors will reduce the computer time with a factor between 7 and 8. Besides this, the code can be optimized further than done in the version described above, by using the fact that most of the integrand can be calculated once for all the τ-values that are desired.

6.3. Numerical solution, second approach

We will now shortly mention the differences in the algorithm by using the integration routine DCUTET instead of DCUHRE. DCUTET is an adaptive integration routine which computes triple integrals over a collection of general tetrahedrons. The error estimate is for all the tetrahedrons together. This means that the triangular region in the $\omega - s$-plane does not constitute any problems. We can cover all the contributions for $s < s_0$ for some s_0 with tetrahedrons. We call this the main contribution to the integral. This main contribution can now be calculated by just one call of DCUTET. Afterwards, corrections are calculated in a similar way as with DCUHRE. This means that the problem with the triangular region in the DCUHRE integration is gone. In this way, time can be saved, and a safer errorbound can be obtained.

Chapter 7

Summary, Conclusions and General Remarks

In this work, we have discussed the pulsed sound propagation within the parabolic approximation. The discussion has included both linear and weakly nonlinear results. The effects of absorption and diffraction have been studied, both separately and together.

In chapter 3, we found that in the linear case, the solution in the dissipative farfield is strictly dependent on the actual pulse shape, and especially on the bandwidth of the generated pulse. If the pulse is a sinusoid oscillating inside a slowly varying envelope function, there are two characteristic absorption distances present. The fast absorption distance was defined from the high frequency of the sinusoid, and is thus similar to the absorption distance in the monochromatic case. Besides this, we had to introduce a slow absorption distance related to the bandwidth of the actual pulse, and thus also related to the characteristic frequency of the envelope function. It was shown that before the fast absorption distance, the signal will be damped much like a monochromatic signal. When the observation point is larger, the behaviour is strictly dependent on the actual bandwidth of the envelope function. Far beyond the slow absorption distance, the exponential damping of the pulse is replaced by z^{-1} for the maximum amplitude, and by $z^{-3/2}$ for the energy of the signal when we are using a one-dimensional model. The actual amplitude of the signal was shown to depend on the content of the very low frequencies in the generated signal, as expected.

The linear, non-dissipative three-dimensional case was discussed in chapter 4. It was shown that the parabolic approximation is valid in the pulsed case as long as the observation point is not too far from the acoustical axis or too close to the plane sound source. The actual critical values depend both on the generating source and on the generated pulse. For a uniform, circular piston, we can generally say that similar restrictions are imposed in order to guarantee the validity of the parabolic approximation, as the ones imposed when using a monochromatic signal. Close to the source, we found that when $z = O(a(\omega_0 a/c_0)^{1/3})$ or larger, the parabolic approximation is valid. We also found similar validity conditions as in the monochromatic theory when we discussed the validity outside the acoustical axis in the farfield. Next, we discussed the farfield more in detail when using a pulsed signal. It was shown that the signal ahead of the plane source looks like the time derivative of the signal generated by the source. It was also shown how this signal outside the acoustical axis splits up into two contributions. We

then get a smeared version of the generated pulse which comes from the nearest point on the edge of the sound source, and the negative of another smeared version of the generated pulse which comes from the furthest point on the edge of the source. We also showed how the directivity changes when the pulse-length was varied. When the pulse gets shorter, the sidelobes in the beam pattern gradually disappear. Focusing effects were then built into the results, and it was shown how the results for a plane source are directly applicable in the focused case. For instance, it was shown that in the focal plane, the sound field looks like the sound field in the unfocused, non-dissipative farfield. The results with only absorption and with only diffraction were then put together. It was among other things shown how the one-dimensional results were directly applicable in some three-dimensional cases.

The first correction to the linear solution due to nonlinear effects was discussed in chapter 5. It was here presented a way to calculate the sound pressure both in the dissipative nearfield and in the dissipative farfield. In this calculation, it was assumed that the generating source had a Gaussian onsource amplitude distribution. Besides the nonlinearity, the model accounted consistently both for diffraction and dissipation. Asymptotical results were presented for the case of no absorption and for the dissipative nearfield. These results gave short formulas which could be used to estimate the quasilinear solution in the diffractional nearfield ($z \ll r_0$) and in the diffractional farfield ($z \gg r_0$). In the dissipative farfield, earlier models were discussed and compared to this new model. It was shown that the earlier models were valid in some parameter regions: The observation point had to be between the fast and the slow absorption distance, the pulse had to be quite long, and the Rayleigh distance r_0 and the fast absorption distance L_0 had to be of about the same order of magnitude.

To conclude, we have presented a model which describes the linear and weakly nonlinear sound propagation from a pulsed sound source. As stated above, the model is applicable when the nonlinearity is not too strong. In addition, we have neglected effects like dispersion and inhomogeneity, and have got a non-causal model in the dissipative case. This non-causality is related to the parabolic approximation which is underlying in this work. The parabolic approximation imposes new restrictions on the model with respect to observation points and parameter regions. In order to discuss pulsed signals in a model where the parabolic approximation is not present, and where the absorption, diffraction and nonlinearity are consistently accounted for, we would have to use the same general model as in Refs. 36, 37, 5 and 38, except that dissipative effects also would have to be included. This model would then have to be used for the pulsed problem. This is a very complex model, and the numerical calculations would have been very difficult and time consuming.

In this work, we have just considered the weakly nonlinear propagation of a pulsed sound beam, and the work is done within the parabolic approximation. A natural next step in this work, is to consider the effect that stronger nonlinearity causes on a pulsed sound signal. This means that we cannot use the quasilinear approximation of the KZK-equation, but instead have to solve the complete KZK-equation. There are different ways to do this. One possible algorithm is to solve the KZK-equation by a finite difference method. For a monochromatic onsource time dependency, this was first done by Aanonsen and presented in Ref. 39. His algorithm was later on improved in several ways, and generalized to the case of a bifrequent source and to weakly focusing sources. Contri-

butions to this work were made by several authors, and more details and references will be found for instance in Ref. 40. This algorithm has also been used for multifrequent onsource time dependencies in order to study a pulsed sound signal. This is reported for instance by Neighbors and Bjørnø[41] and by Baker and Humphrey[42]. Later on, also Berntsen, Frøysa, Naze Tjøtta and Tjøtta[43] will publish on this topic. Hamilton and Lee[44] have used a different difference algorithm to solve the same problem. They solve the problem in the time domain instead of in the frequency domain.

Common for these two approaches of solving the complete KZK-equation for a pulsed signal, are the problems in describing the diffractional nearfield in a proper way. If replica pulses or strong wakes are present, Refs. 43 and 44 both show that the algorithm will not describe satisfactorily the solution on the acoustical axis when $z < 0.3r_0$. The reason for this is that the difference algorithm propagates the solution with finite steps in the z–direction. Besides, the Laplacian has also been discretized. Therefore we need some propagation distance in order to bring the information of what happens at the discontinuous edge of a piston to the acoustical axis. When using a Gaussian source, we can expect this problem to be much smaller because there then are no replica pulses or very strong wakes present in the solution. Suggestions have been made about what should be done to overcome this problem, but until now, nothing has been done to try these ideas. A possible solution could be to use a wide angle version of the parabolic approximation close to the source. In the linear case, such equations are derived for instance by Vefring and Mjølsnes[45]. These equations have a wider range of validity than the parabolic approximation used in this work. Therefore there is a hope that by solving this equation close to the source, we can improve the solution in the nearfield. Unfortunately, consistent wide angle equations are not known in the nonlinear case. We therefore have to solve the linear wide angle equation up to a certain range, and then switch to the KZK-equation. Alternatively, we can replace the linear part of the KZK-equation by the wide angle approximation and solve the nonlinear equation that then appears. However, this has not been proved to be a consistent equation which accounts for diffraction, dissipation and nonlinearity.

It is also possible to find solutions in the case of strong nonlinearity in another way. In Ref. 46, Coulouvrat showed how it is possible to find uniform solutions of the KZK-equation when knowing the quasilinear approximation. This was done by the method of renormalization, and the solution described both the generation of shock waves and the decay of these waves. His analysis was done for a Gaussian onsource amplitude distribution and a monochromatic onsource time dependency. He also neglected dissipative effects. Coulouvrat and the present author have just started an attempt to generalize this method to also include pulsed sound beams. The linear and the quasilinear solutions obtained in this dissertation will be one of the starting points for this analysis. Later on, the results can be generalized so that they are valid also for other onsource amplitude distributions.

Appendix A

Boundary Conditions for Weakly Curved Sources

We will now derive the consistent boundary conditions for curved sources in the parabolic approximation. It will be based on Ref. 47 where the results in Ref. 48, 49 and 50 are discussed further and generalized to pulsed sources.

The curved source is located at the surface $S : z = g(\mathbf{x})$. When we assume that the boundary condition is separable, we get

$$P(\mathbf{x}, g(\mathbf{x}), t) = p_0 + \rho_0 c_0 v_0 f(\mathbf{x}) F(t), \tag{A.1}$$

where t is the physical time and $P(\mathbf{x}, z, t) = p(\mathbf{x}, z, \tau)$ is the physical pressure. The governing equation is

$$\left(\nabla_\perp^2 - \frac{2}{c_0}\frac{\partial^2}{\partial\tau\partial z} + \frac{D}{c_0^4}\frac{\partial^3}{\partial\tau^3}\right) p = -\frac{\beta}{\rho_0 c_0^4}\frac{\partial^2}{\partial\tau^2}(p - p_0)^2, \tag{A.2}$$

and the boundary condition formulated for $p_1(\mathbf{x}, z, \tau)$ will be

$$p(\mathbf{x}, g(\mathbf{x}), \tau) = p_0 + \rho_0 c_0 v_0 f(\mathbf{x}) F(\tau + \frac{g(\mathbf{x})}{c_0}). \tag{A.3}$$

Now we wish to formulate an equivalent boundary condition in the plane $z = 0$, because we then can solve the problem in the same ways as we solve the plane problem. If we assume that $g(\mathbf{x})$ is not too large, we may expand Eq. (A.3) around $z = 0$, and get:

$$p(\mathbf{x}, g(\mathbf{x}), \tau) = p(\mathbf{x}, 0, \tau) + g(\mathbf{x})\left(\frac{\partial}{\partial z} p(\mathbf{x}, g(\mathbf{x}), \tau)\right)_{z=0} + \cdots. \tag{A.4}$$

When $g(\mathbf{x})$ is not "too large", we thus get the approximate boundary condition at $z = 0$:

$$p(\mathbf{x}, 0, \tau) = p_0 + \rho_0 c_0 v_0 f(\mathbf{x}) F(\tau + \frac{g(\mathbf{x})}{c_0}). \tag{A.5}$$

This means that we assume that the propagation from the plane $z = 0$ to the surface $z = g(\mathbf{x})$ is a plane wave propagation. This assumption is not strange when we remember that the parabolic approximation assumes that the propagation is almost a plane wave

in the z-direction. The variations in the pressure in the z-direction apart from the plane wave motion is assumed to be on the scale of Rayleigh distances. This means, however, that we cannot choose the curved surface $g(\mathbf{x})$ quite general. We can also look at this as introduction of a "curved" retarded time $\tau_c = t - (z - g(\mathbf{x}))/c_0$ instead of the "plane" retarded time $\tau = t - z/c_0$. The physical meaning of this new retarded time is quite intuitive and is also commented in section 4.4. We will now discuss the validity of the equivalent plane source boundary condition in more details.

The neglected term in Eq. (A.4) is of relative order $\delta/r_{\omega_{\min}}$ where δ is the maximum depth of the source, and $r_{\omega_{min}}$ is the Rayleigh distance of the lowest characteristic frequency, ω_{min}, actually present in the signal on the source. Thus, the approximation is justified whenever

$$\frac{\delta}{a} \ll \frac{\omega_{min} a}{2c_0}. \tag{A.6}$$

Remember now that $\frac{\omega_{min} a}{c_0}$ is assumed large in the derivation of the KZK-equation, or equivalent in the parabolic approximation. This means that the condition is not very restrictive. Among others, we can have $\delta = O(a)$.

Consider now the case of a spherical cap located in a plane and infinitely compliant baffle, in more details. In this case, $g(\mathbf{x})$ can be written

$$g(\mathbf{x}) = d - \sqrt{d^2 - \mathbf{x}^2} \quad , x < a. \tag{A.7}$$

The curvature radius is here d, and we define the aperature angle of the source to be 2α. This means that $\delta = d - \sqrt{d^2 - a^2} = 2d \sin^2(\alpha/2)$. This means that Eq. (A.6) now will be

$$\frac{2c_0}{\omega_{min} a} \tan\frac{\alpha}{2} \ll 1. \tag{A.8}$$

If the source is weakly focused in the sense that $\alpha \ll 1$, we can approximate

$$g(\mathbf{x}) = d - \sqrt{d^2 - \mathbf{x}^2} \approx \frac{\mathbf{x}^2}{2d}. \tag{A.9}$$

The conditions for the validity of this approximative boundary condition are

$$d \gg a \qquad \text{and} \qquad d \gg \frac{c_0}{\omega_{min}}. \tag{A.10}$$

These conditions are not very restrictive either. When using the parabolic approximation, we have a priori supposed that the transverse variation close to the source is on the scale a. Thus we have to require that $d = O(r_0)$ or greater. This is a condition similar to the other similarity conditions stating that for instance $L_0 = O(r_0)$ which is supposed in the derivation of the parabolic approximation[3]. We know from that analysis that even if r_0 and L_0 asymptotically are of the same order, the ratio r_0/L_0 can have a relative large numerically value, and the model will still give reasonable output. Similar, numerical calculations where d is quite a bit smaller than r_0 give reasonable results. Therefore, it is natural to believe that the focal distance d asymptotically have to be of the same order as the Rayleigh distance. This is a measure of the balance between the two effects of focusing and spherical spreading. They are taken into account in the same order of approximation. Numerically, d can still be quite a bit smaller than r_0. Naze Tjøtta,

Tjøtta and Vefring[51] have also performed an analysis of the validity of the boundary condition of a focused sound source. We refer to that work for more exact limitations of this model.

Finally, we will see why we cannot use the similar approach if we do not assume a parabolic approximation. If we then tried to get an equivalent plane source by the similar approach, we would have got this expansion:

$$P(\mathbf{x},0,t) = P(\mathbf{x},g(\mathbf{x}),t) - g(\mathbf{x})\left(\frac{\partial P}{\partial z}(x,z,t)\right)_{z=g(\mathbf{x})} + \cdots. \tag{A.11}$$

The first term on the right hand side is known, but now we cannot say much about the remaining terms. We find some information by taking the transverse gradient of Eq. (A.1):

$$\left(\nabla_\perp P + \frac{\partial P}{\partial z}\nabla_\perp g(\mathbf{x})\right)_{z=g(\mathbf{x})} = \rho_0 c_0^2 F(t)\nabla_\perp g(\mathbf{x}). \tag{A.12}$$

Now, since both $\nabla_\perp P$ and $\partial P/\partial z$ are unknown on the surface S, we need more information, i.e., we need to know the normal derivative of P on S. However, we cannot give both P and its normal derivative on S. We are thus back to the same problem as we meet when we are trying to use the Kirchhoff–Helmholtz equation for a curved boundary. We are able to bypass this problem when we make the parabolic approximation because $\partial P/\partial z$ a priori is negligible compared to $\nabla_\perp P$.

REFERENCES

[1]E. A. Zabolotskaya and R. V. Khokhlov, "Quasiplane waves in the nonlinear acoustics of confined beams," *Sov. Phys. Acoust.* **15**, 35–40 (1969).

[2]V. P. Kuznetsov, "Equations of nonlinear acoustics," *Sov. Phys. Acoust.* **16**, 467–470 (1971).

[3]Jacqueline Naze Tjøtta and Sigve Tjøtta, "Nonlinear equations of acoustics with applications to parametric acoustic arrays," *J. Acoust. Soc. Am.* **69**, 1644–1652 (1981).

[4]J. Naze Tjøtta and S. Tjøtta, "An analytic model for the nearfield of a baffled piston transducer," *J. Acoust. Soc. Am.* **68**, 334–339 (1980).

[5]J. Naze Tjøtta and S. Tjøtta, "Interaction of sound waves. Part III: Two real beams," *J. Acoust. Soc. Am.* **83**, 487–495 (1988).

[6]P. R. Stepanishen, "Transient Radiation from Pistons in an Infinite Planar Baffle," *J. Acoust. Soc. Am.* **49**, 1629–1638 (1971).

[7]J. Naze Tjøtta and S. Tjøtta, "Nearfield and farfield of pulsed acoustic radiators," *J. Acoust. Soc. Am.* **71**, 824–834 (1982).

[8]H. O. Berktay, "Possible Exploitations of Non-linear Acoustics in Underwater Transmitting Applications," *J. Sound. Vib.* **2**, 435–461 (1965).

[9]Mark B. Moffett and Peter Mello, "Parametric acoustic sources of transient signals," *J. Acoust. Soc. Am.* **66**, 1182–1187 (1979).

[10]N. G. Pace and R. V. Ceen, "Time domain study of the terminated transient parametric array," *J. Acoust. Soc. Am.* **73**, 1973–1978 (1983).

[11]I. E. Grinberg, B. K. Novikov, and V. I. Timoshenko, "Parametric array in the self-demodulating regime," *Sov. Phys. Acoust.* **30**, 118–120 (1984).

[12]P. R. Stepanishen and P. Koenigs, "A time domain formulation of the absorption limited transient parametric array," *J. Acoust. Soc. Am.* **82**, 629–634 (1987).

[13]K.-E. Frøysa, J. Naze Tjøtta and S. Tjøtta, "Linear and Nonlinear Propagation of a Pulsed Sound Beam," Proceedings of 13th International Congress on Acoustics, Belgrade, Yugoslavia, edited by P. Pravica, **1**, 145–148 (1989).

[14]K.-E. Frøysa, "Weakly Nonlinear Propagation of a Pulsed Sound Beam," in *Frontiers of Nonlinear Acoustics,* proceedings of the 12th ISNA, edited by M. F. Hamilton and D. T. Blackstock, Elsevier Applied Science, London and New York (1990).

[15]K.-E. Frøysa, J. Naze Tjøtta and S. Tjøtta, "Finite amplitude effects on the propagation of a pulsed sound beam in a dissipative fluid," *J. Acoust. Soc. Am.* Suppl. 1, **85**, S5 (1989).

[16]K.-E. Frøysa, "Linear Soundpropagation from a Pulsed Source," thesis for the Cand. Scient. Degree, Department of Mathematics, University of Bergen, Bergen, Norway (1987) (in Norwegian).

[17]N. S. Bakhvalov, Ya. M. Zhileikin and E. A. Zabolotskaya, "Nonlinear Theory of Sound Beams," American Institute of Physics, Translation Series, New York (1987).

[18]N. Bleistein and R. A. Handelsman, "Asymptotic Expansions of Integrals," Dover Publications, Inc., New York (1986).

[19]D. S. Jones, "Generalized Functions," McGraw-Hill, London (1966).

[20]M. Daltveit, "Parabolic Approximation in relation with a pulsed piston," thesis for the Cand. real. Degree, Department of Mathematics, University of Bergen, Bergen, Norway (1982) (in Norwegian).

[21]Fritz Oberhettinger, "Tabellen zur Fourier Transformation," Springer Verlag, Berlin, Göttingen, Heidelberg (1957).

[22]Carl M. Bender and Steven A. Orszag, "Advanced Mathematical Methods for Scientists and Engineers," McGraw-Hill International Book Company (1978).

[23]Corinne M. Darvennes, Mark F. Hamilton, Jacqueline Naze Tjøtta and Sigve Tjøtta, "Effects of absorption on the interaction of sound beams, with applications to scattering of sound by sound," to be published in *J. Acoust. Soc. Am.*

[24]Jacqueline Naze Tjøtta, James A. TenCate and Sigve Tjøtta, "Effects of boundary conditions on the nonlinear interaction of sound beams," to be published in *J. Acoust. Soc. Am.*

[25]G. S. Garrett, J. Naze Tjøtta, and S. Tjøtta, "Nearfield of a large acoustic transducer, Part III: General results," *J. Acoust. Soc. Am.*, **75**, 769–779 (1984).

[26]J. Berntsen, J. Naze Tjøtta, and S. Tjøtta, "Nearfield of a large acoustic transducer, Part IV: Second harmonic and sum frequency," *J. Acoust. Soc. Am.* **75**, 1383–1391 (1984).

[27]M. F. Hamilton, J. Naze Tjøtta, and S. Tjøtta, "Nonlinear effects in the farfield of a directive sound source," *J. Acoust. Soc. Am.*, **78**, 202–216 (1985).

[28]M. F. Hamilton, J. Naze Tjøtta, and S. Tjøtta, "Noncollinear interaction of two sound beams from displaced Gaussian sources, with application to parametric receiving arrays," *J. Acoust. Soc. Am.* **82**, 311–318 (1987).

[29]P. J. Westervelt, "Parametric Acoustic Array," *J. Acoust. Soc. Am.* **35**, 535–537 (1963).

[30]M. Moffett, P. J. Westervelt, and R. T. Beyer, "Large-amplitude pulse propagation — A transient effect," *J. Acoust. Soc. Am.* **47**, 1473–1474 (1970).

[31]M. Moffett, P. J. Westervelt, and R. T. Beyer, "Large-amplitude pulse propagation — A transient effect. II," *J. Acoust. Soc. Am.* **49**, 339–343 (1971).

[32]P. J. Westervelt, in *Nonlinear Acoustics*, Proceedings of the 1969 Symposium held at Applied Research Laboratories, edited by T.G. Muir, 165–181 (1970).

[33]Pierre Cervenka and Pierre Alais, "Fourier formalism for describing nonlinear self-demodulation of a primary narrow ultrasonic beam," *J. Acoust. Soc. Am.* **88**, 473–481 (1990).

[34]J. Berntsen, T. O. Espelid and A. Genz, "An Adaptive Algorithm for the Approximate Calculation of Multiple Integrals," To appear in *ACM Trans. Math. Software*

[35]J. Berntsen, R. Cools and T. O. Espelid, "An Algorithm for Automatic Integration over a collection of 3-dimensional Simplices" Submitted for publication in *ACM Trans. Math. Software*

[36]J. Naze Tjøtta and S. Tjøtta, "Interaction of sound waves. Part I: Basic equations and plane waves," *J. Acoust. Soc. Am.* **82**, 1425–1428 (1987).

[37]J. Naze Tjøtta and S. Tjøtta, "Interaction of sound waves. Part II: Plane wave and real beam," *J. Acoust. Soc. Am.* **82**, 1429–1435 (1987).

[38]J. Berntsen, J. Naze Tjøtta, and S. Tjøtta, "Interaction of sound waves. Part IV: Scattering of sound by sound," *J. Acoust. Soc. Am.* **86**, 1968–1983 (1989).

[39]S. I. Aanonsen, T. Barkve, J. Naze Tjøtta and S. Tjøtta, "Distortion and harmonic generation in a finite amplitude sound beam," *J. Acoust. Soc. Am.* **75**, 749–768 (1984).

[40]Erlend H. Vefring, "Nonlinear propagation and interaction of collinear sound beams," Report No. 86 (Dr. Scient. dissertation), Department of Mathematics, University of Bergen, Bergen, Norway (1989).

[41]T. H. Neighbors and L. Bjørnø, "Focused Finite-Amplitude Ultrasonic Pulses in Liquids," in *Frontiers of Nonlinear Acoustics*, proceedings of the 12th ISNA, edited by M. F. Hamilton and D. T. Blackstock, Elsevier Applied Science, London and New York (1990).

[42]A. C. Baker and V. F. Humphrey, "Nonlinear propagation of short ultrasonic pulses in the focused fields," in *Frontiers of Nonlinear Acoustics*, proceedings of the 12th ISNA, edited by M. F. Hamilton and D. T. Blackstock, Elsevier Applied Science, London and New York (1990).

[43]J. Berntsen, K.-E. Frøysa, J. Naze Tjøtta and S. Tjøtta, unpublished paper to be submitted for publication in *J. Acoust. Soc. Am.*

[44]Yang-Sub Lee and Mark F. Hamilton, "A time domain computer algorithm for solving the KZK equation," *J. Acoust. Soc. Am.* Suppl. 1, **88**, 4PA10 (1990)

[45]Erlend H. Vefring and Svein Mjølsnes, "A parabolic wave equation based on a rational-cubic approximation," *J. Acoust. Soc. Am.* **87**, 619–623 (1990).

[46]F. Coulouvrat, "An analytical approximation of strong nonlinear effects in bounded sound beams," Submitted for publication in *J. Acoust. Soc. Am.*

[47]Jacqueline Naze Tjøtta, private communication.

[48]Bernard G. Lucas and Thomas G. Muir, "The field of a focusing source," *J. Acoust. Soc. Am.* **72**, 1289–1296 (1982).

[49]Bernard G. Lucas, Jacqueline Naze Tjøtta and Thomas G. Muir, "Field of a parametric focusing source," *J. Acoust. Soc. Am.* **73**, 1966–1971 (1983).

[50]Bernard G. Lucas and Thomas G. Muir, "Field of a finite-amplitude focusing source," *J. Acoust. Soc. Am.* **74**, 1522–1528 (1983).

[51]Jacqueline Naze Tjøtta, Sigve Tjøtta and Erlend H. Vefring, "Effects of focusing on the nonlinear interaction between two collinear finite amplitude sound beams," To appear in the March 1991 issue of *J. Acoust. Soc. Am.*